An-Najah National University

Faculty of Graduate Studies

PEROVSKITE-BASED FILM ELECTRODES FOR WATER PURIFICATION WITH SOLAR ENERGY

By

Tamara Basem Qasem Zorba

Supervisors

Prof. Hikmat S. Hilal

Prof. Shehdeh Jodeh

This Thesis is Submitted in Partial Fulfillment of the Requirements for the Degree of PhD of Chemistry, Faculty of Graduate Studies, An-Najah National University, Nablus - Palestine.

2023

PERVOSKITE-BASED FILM ELECTRODES FOR WATER PURIFICATION WITH SOLAR ENERGY

By

Tamara Basem Qasem Zorba

This Thesis was Defended Successfully on 8/10/2023 and approved by

Prof. Hikmat S. Hilal
Supervisor

Signature

Prof. Shehdeh Jodeh

Co-Supervisor

Signature

Dr. Wadie Sultan
External Examiner

Signature

Dr. Mohyeddin Assali
Internal Examiner

Signature

Prof. Othman Hamed
Internal Examiner

Signature

An-Najah National University

Faculty of Graduate Studies

PEROVSKITE-BASED FILM ELECTRODES FOR WATER PURIFICATION WITH SOLAR ENERGY

By
Tamara Basem Qasem Zorba

Supervisors

Prof. Hikmat S. Hilal

Prof. Shehdeh Jodeh

In accordance with An-Najah National University Deans Council Regulations for the award of Doctor of Chemistry, the following papers have been published after their extraction from the dissertation:

Perovskite Nano-Powder and Nano-Film Catalysts in Mineralization of Aqueous Organic Contaminants through Solar Simulated Radiation.

Dedication

I dedicate this thesis

To my daughters (Merna and Marah) who endured my absence and being busy for a long time.

To my newborn (Zain El-Din), who suffered harsh conditions with me during my research work and writing the thesis while I was pregnant with him. I'm sorry, my baby.

To my mother and father, I hope you will be proud of me.

To my brother (Tamer), who helped me with designs and technological matters.

To my brother (Ahmad) and sisters (Diala & Hanadi) for their continuous support for me.

To my dear husband (Mohammad), without whom I would not have reached here.

To myself that endured difficulties, fatigue, stress and exhaustion until she arrived here.

Acknowledgments

Praise be to Allah, who enabled me to complete my thesis.

I would like to thank with full gratitude and appreciation my supervisors, Prof. Hikmat S. Hilal and Prof. Shehdeh Jodeh for their guidance, support, advice and suggestions.

I also would like to thank the technical staff at the Department of Chemistry at An-Najah National University. Special thanks are due to my friends who supported me. I acknowledge

Help from Prof. Tae Woo Kim, Korea Institute of Energy Research, Korea for help with XRD and SEM measurements, and from Prof. Hikmat S. Hilal, for originally suggesting film photo catalysis in batch and continuous flow photo degradation reactions.

Declaration

I, the undersigned, declare that I submitted the thesis entitled:

PEROVSKITE-BASED FILM ELECTRODES FOR WATER PURIFICATION WITH SOLAR ENERGY

I declare that the work provided in this thesis, unless otherwise referenced, is the researcher's own work, and has not been submitted elsewhere for any other degree or qualification.

Student's Name: Tamara Basem Zorba

Signature: Tamara

Date: 8-10-2023

List of Contents

List of Tables

List of Figures

List of Appendices

PEROVSKITE-BASED FILM ELECTRODES FOR WATER PURIFICATION WITH SOLAR ENERGY

By

Tamara Basem Qasem Zorba

Supervisors

Prof. Hikmat Hilal

Prof. Shehdeh jodeh

Abstract

Drinking water contamination with various materials, including organic compounds and dyes, is a major global challenge. It is essential to reclaim contaminated water by safe, practical and affordable methods. There are many methods, among which photocatalytic degradation of organic contaminants is a new and effective strategy. In photodegradation, people normally use nanoparticles of semiconducting metal oxide materials, with wide band gaps. These materials showed efficiency to use the UV fraction (5%) of the oncoming solar radiations. However, the nanoparticles are difficult to isolate from the water after treatment. In this study, new methods are described to find solutions to this technical difficulty. Two perovskites, manganese titanate ($MnTiO_3$) and zinc titanate ($ZnTiO_3$) were prepared as nano-powders and glass-supported nano-films and characterized by XRD, SEM, XPS, SEM and others. The materials were then used as catalysts in photodegradation of methylene blue (a model dye contaminant) in water under solar simulated radiations. The effect of different reaction conditions on the photodegradation process was investigated to examine performances of both catalysts in their powder and film forms. Batch and continuous flow reactions were investigated using the film form to examine the suitability of the process at future commercial scales. The findings demonstrate the contaminant was eliminated and completely mineralized in less than six hours using both powder and film catalysts. The films demonstrated greater catalytic effectiveness than the powders in both perovskite mixtures. The $MnTiO_3$ system showed higher efficiency than the $ZnTiO_3$ in both powder and film forms. Both batch and continuous flow reactions showed similar efficiency in methylene blue removal by catalysts film forms of each perovskite. Water contaminated with different concentrations of methylene blue can be treated with both perovskite catalyst systems, but to avoid catalysts separation difficulties, using the film forms is strongly recommended. The results confirm the potential for using both perovskite catalysts at larger-scale water purification in the future, as both exhibited high efficiency especially in the continuous flow process.

Keywords: Zinc titanate; manganese titanate; methylene blue photodegradation; solar simulated radiation

Chapter One

Introduction

1.1 Overview

Contamination refers to the introduction of any hazardous objects, harmful or undesirable, a biological system or a chemical product, into the environment. Contamination can harm ecosystems, human health, and the general health of organisms, which can result in disease outbreaks, poisoning, and environmental degradation [1]. Environmental pollution can occur in the air, such as smoke from industrial activities or exhaust fumes from transport vehicles. It also occurs in soil where heavy metal, chemical or hazardous material random dumping can lead to soil contamination. Pollution also occurs in water, which may result from oil spills, agricultural runoff, or uncontrolled dumping of untreated home or industrial wastewaters. Surface and groundwater pollution is one of the disputed platforms, which are due to several sources, the most significant of which are industrial development, agricultural practices, incorrect waste disposal, and natural occurrences [2].

According to recent studies, water pollution causes the deaths of about 14,000 cases per day [3]. Water pollution can contain harmful parasites, viruses, bacteria, chemicals, or heavy metals that pose health risks when consumed. This can harm aquatic ecosystems, resulting in the loss of biodiversity, disruptions in the food chain, diseases, and death of living organisms. Additionally, industries that depend on clean water, including agriculture, tourism, and fisheries, can be negatively impacted by water pollution sources, which can lead to large financial losses and decreased output [3].

One of the most important sources of water pollution, whether surface or groundwater, is dyes. Dyes are considered toxic colored organic compounds. Worldwide, there are more than 100,000 commercially produced dyes at large industrial scale, such as cosmetics, textiles, food, medicine, plastics, printing, etc. [4-6]. These industries produce huge amounts of dyes, as more than 15% of these dyes are released into water resources [7, 8]. They pollute the water and make it unsuitable for environmental and human consumption, with many environmental problems due to toxicity and stability to biodegradation. They may cause various types of human cancer [9]. Dyes can also be toxic to aquatic life, such as algae, fish, and other organisms by lowering oxygen levels in aquatic bodies. By preventing sunlight from penetrating they may disrupt the food chain, they may upset the ecosystems natural equilibria. Some dyes have the potential to pollute the environment for a very long period [9-11]. Methylene blue is an example of widely spread hazardous dye contaminants.

1.2 Methylene blue and removal methods

Methylene blue (with the IUPAC name [7-(dimethylamino)phenothiazine-3-ylidene]-dimethylazanium chloride) is an aromatic heterocyclic dye, having molecular formula $C_{16}H_{18}ClN_3S$ and molecular weight 319.851 g/mol. It has a net positive charge [12, 13] and the counter negative charge is the negative Cl^-. The structure, model and resonance of the methylene blue are shown in Figure (A.1 in Appendix A) [14, 15].

Methylene blue is a green, odorless powder, that is highly water soluble, but turns blue when dissolved in water. It is widely used in various applications such as textile, silk, cotton, wool, leather and paper industries [16, 17]. It is considered a toxic substance and has many side effects, especially at contact with the skin and eyes or when swallowed or inhaled. Methylene blue can cause the so-called methemoglobinemia, a disorder where red blood cells are less able to transport oxygen [18]. Methemoglobinemia symptoms that include cyanosis, shortness of breath, fast heartbeat, wooziness, headache, and dizziness. It can also increase the risk of serotonin syndrome which is characterized by agitation, disorientation, fast heartbeat, high blood pressure, dilated pupils, tremors, and stiffness of the muscles. Additionally, methylene blue may cause allergy responses in certain people who are susceptible to it that may cause itching, rash, disorientation, swelling, and breathing difficulties, together with intestinal issues including nausea, vomiting, and discomfort in the abdomen [18-20]. All of these toxic effects are often linked with abuse, overdose, or combinations with other pharmaceuticals. Therefore, methylene blue must be used as directed. The toxicity of methylene blue was studied and it was noted that the level of non-noticeable harmful limit was $25\ mg\ kg^{-1}$ [21]. Literature highlighted the necessity of removing methylene blue and other organic dyes from water. In fact, methylene blue is commonly used as a model contaminant in water treatment research.

Different effective methods are used to remove methylene blue and other dyes from wastewater. Physical methods include filtering, adsorption and coagulation. Biological methods include using of microbes and enzymes, biodegradation and biosorption. Chemical methods include electro-Fenton, ozonation and photocatalysis [22, 23]. Despite the effectiveness of these methods, they have their own disadvantages. For example, physical methods such as filtration do not effectively remove dyes with large concentrations because they use relatively large particles and thus do not remove or capture all dye molecules. In addition, they produce secondary waste products that need additional processing and special disposal. Filtration procedures produce filter blocks that contain the adsorbed contaminant. The proper processing and disposal of these waste byproducts can be difficult and may call for extra treatment procedures, which would raise the process overall complexity and costs [24]. Similarly, coagulation, frequently produces significant amounts of residuals during the process. The residues could contain coagulant substances like aluminum or iron salts that might bring new pollutants into the water or produce dangerous byproducts during the chemical processes. Furthermore, coagulation frequently calls for the use of costly chemicals like ferric chloride or aluminum sulfate. Adsorption may also take large amount of energy and resources when utilizing activated carbon or ion exchange resins [25,].

Biological methods, such as bioremediation or biodegradation can be successful in eliminating methylene blue and other dyes from wastewater, but they have some disadvantages. When compared to some physical or chemical treatment techniques, biological treatments might be too slow [26]. The dye biodegradation may take days, weeks, or even longer, depending on the concentration, the environmental conditions, and the specific microbial strains. Additionally, biological approaches may be sensitive to a variety of environmental conditions, including temperature, pH, and oxygen availability, which affect microbial activity and decrease the effectiveness of dye removal. Furthermore, biodegradation is not appropriate for high dye concentrations in wastewater [27].

Some chemical methods could need energy-consuming equipment like ultraviolet (UV) lights or ozone generators. But they can be cost-effective compared to other dye removal methods, especially when dealing with high dye concentrations. Chemical methods soundly balance between cost and effectiveness. Chemical methods have more advantages than other methods, as they are highly effective in removing dyes from wastewater even at low concentrations, with sound dye removal rates [28]. Chemical methods also can be applied to a large variety of dyes. They yield faster treatment processes, which is particularly advantageous when handling big amounts of wastewater. Moreover, chemical methods can make it easier to recover or reuse dyes from wastewater, which can be advantageous for both the economy and the environment by reducing the demand for new dye production and the volume of wastewater that has requiring treatment [29]. The most recently used and highly effective chemical method is photocatalysis because it has more advantages than electro-Fenton and ozonation. Electro-Fenton is an advanced oxidation technique that has been used to remove dyes from wastewater. Despite its benefits, it still has disadvantages. The electrochemical cell requires a significant amount of energy to run, which increases cost, especially at large-scale applications [30]. Also, because the catalyst might be consumed or deactivated throughout the treatment process, it needs to be replaced periodically, which further increases costs. Compared to other wastewater treatment methods, electro-Fenton systems may be more difficult to design, run, and maintain, which increases the risk of maintenance problems and operational mistakes [31]. Ozonation is another efficient technique for removing dyes from wastewater, but has disadvantages such as the production of byproducts. When organic compounds in the wastewater are exposed to ozone, during the ozonation process, dangerous byproducts such as ketones, aldehydes and organic acids may be produced. These byproducts may even be more toxic than the original dyes themselves. In addition, ozone has a short half-life and degrades quickly in water making difficult to store or transport. Thus, it must be produced on-site, which increases costs and complexity of the process. Moreover, ozonation systems can be difficult to build, run and manage [32].

1.3 Photocatalysis

Photocatalysis is one of the most important contemporary techniques for the transformation of dangerous chemical molecules from the water and air into harmless components. It is used in wastewater treatment from organic pollutants such as methylene blue and other dyes. by using a photocatalyst substance. Semiconductors, like titanium dioxide (TiO_2), are commonly used as catalysts. Light energy is commonly used to induce chemical processes [33]. Some advantages of photocatalysis for methylene blue removal include high efficiency, excellent performance and the ability to effectively degrade the aqueous dye at high rates. Photocatalysis applies to a large variety of dyes, including various kinds and chemical structures. Additionally, because photocatalysis uses sun radiations or other artificial light sources as the energy input, under air oxygen, it is considered environmentally friendly. Because no additional chemicals or reagents are needed, less hazardous materials are used in the treatment process and do not consume intensive energy. most importantly, the photocatalyst itself is typically stable and non-toxic so the process is a green technology [34]. Through photocatalysis, dyes may be completely mineralized and transformed into more simple and non-toxic byproducts like carbon dioxide and water. This makes sure that the dye contaminants are completely removed without yielding other dangerous and harmful byproducts. In many cases, the photocatalyst substance can be easily recovered and reused several times, which lowers operational expenses. In the long term after the treatment process, the photocatalyst is a cost-effective option since it can be recycled or separated from the treated water for further cycles. It is a simple method and can work at normal pressure and temperatures [35]. As the photocatalyst normally involves semiconductor materials, the next section describes these materials.

1.3.1 Semiconductor photocatalysis

- **Semiconductors**

A semiconductor is a solid substance with electrical conductivity that is between those of insulators and conductors. Semiconductors may be manufactured from many different elements, including silicon, gallium, germanium, arsenide, and many more, they often have crystalline structures. The mobility of electrons within a semiconductor crystal lattice structure controls the material characteristics. Under specific conditions, the electrons in a semiconductor can jump from one energy level to another, which allows them to move and conduct electricity [36, 37].

To distinguish between insulators, semiconductors, and conductors, the energy band gap (E_{bg}) concept needs to be understood. The energy difference between the lower edge of the conduction band (CB) and the upper edge of the valence band (VB) is known as the energy band gap (E_{bg}). Conductors have zero band gap energy, insulators typically have huge band gaps exceeding 4 eV and semiconductors typically have smaller band gaps than 4 eV. Additionally, in semiconductors, the maximum level of energy-filled band, or valence band (VB), is filled with electrons and corresponds to the highest occupied molecular orbital (HOMO). The conduction band (CB), which is an empty band, corresponds to the lowest unoccupied molecular orbital (LUMO) [33, 38]

- **Types of semiconductor materials**

Semiconductors may be broadly divided into two major categories: intrinsic semiconductors and extrinsic (doped) semiconductors [39].

1. Intrinsic Semiconductors: Intrinsic semiconductors are pure semiconductors with no added impurities. Silicon (Si) and germanium (Ge) are the typical types of intrinsic semiconductors. These substances have four valence electrons in their HOMO level, meaning they have a four-valence electron structure. These free electrons and holes behave as charge carriers in semiconductor pure state. When the semiconductor is excited with a photon of enough energy (hv more than E_{bg}), an electron moves from the valence band to the conduction band, and hole (also known as a vacancy) is left in the conduction band. In this kind of semiconductor, the quantity of excited electrons equals the number of holes.

2. Extrinsic (Doped) Semiconductors: In order to produce extrinsic semiconductors, impurity atoms must be deliberately added to the intrinsic semiconducting material. Doping is used to increase the material electrical conductivity [40]. There are two doping types:

a. N-type (Negative-type) Semiconductor: N-type semiconductors are produced by incorporating impurity that are rich with electrons, and can donate electrons to the crystal. Phosphorus (P), is often utilized as a dopant to make N-type semiconductors. The dopant atoms contain a total of five valence electrons each, and when they take the place of a few host atoms, one more electron becomes accessible for conduction, leading to an excess of negatively charged electrons serving as the majority carriers. The Fermi level is closer to the conduction band in n-type.
b. P-type (Positive-type) Semiconductor: Impurity atoms with fewer valence electrons than the host material are added to produce p-type semiconductors. Boron (B) is a

typical dopant used to make p-type semiconductors. When the dopant atom replaces a host atom, it takes an electron and creates a "hole" in the crystal valence band. The hole serves as a positively charged carrier. The boron dopant atoms only contain three valence electrons. The Fermi level is closer to the valence band in p-type. Figure (A.2, in Appendix A) shows the mechanisms for producing charged carriers in semiconductors.

- **Semiconductors photocatalysis**

Semiconducting materials are used in the semiconductor photocatalysis method to capture light energy and induce chemical processes. The semiconductor material behaves as a photocatalyst. When excited by incident photons, of enough energy, the semiconductor particle has electron-hole pairs. The excited electrons and holes can take part in a variety of redox reactions, making the conversion of light energy into chemical energy. Metal oxides, such as zinc oxide (ZnO), titanium dioxide (TiO_2), and tungsten trioxide (WO_3), are commonly used semiconductor materials for photocatalysis. These materials have appropriate energy band structures that enable effective charge separation and light absorption [36].

There are multiple advantages to photocatalysis by semiconductors, such as efficient light absorption. A semiconductor has a bandgap that enables it to absorb a photon throughout a broad range of wavelengths, including visible light, depending on its value. This characteristic makes it possible for catalyst to use more of the solar spectrum for the reaction of photocatalysis, which increases the process' overall efficiency. Semiconductors' bandgaps can be altered by changing their composition or structure. This tunability enables researchers to customize the photocatalyst for particular applications by optimizing the bandgap to correspond with the solar spectrum and enhancing the efficiency of absorption. For photochemical stability, under photochemical conditions, semiconductors often remain stable, enabling them to endure continuous light exposure without significantly degrading. This stability guarantees the photocatalyst's longevity and continuous functioning throughout time. Semiconductors also have intrinsic catalytic activity, which allows them to take part in chemical processes on their own without the need for external co-catalysts. Thus, the photocatalytic system is made simpler and less expensive as a result of this characteristic. Moreover, photocatalysis employing semiconductors is a renewable and sustainable process since it uses sunshine or solar-simulated light as the energy source. Unlike conventional catalysts, it does not rely on limited or non-renewable resources and can support environmentally friendly and green technology. Overall, semiconductors are extremely beneficial for effective and long-lasting photochemical reactions due to their strong light absorption capabilities, stability, catalytic activity, and tunability [37, 41].

- **Continuous flow photocatalytic**

In continuous flow photocatalytic systems, the reactor is designed to allow a continuous flow of reactants and a steady supply of light to maintain a constant reaction rate. In these processes, the procedures include the continual addition of reactants into the reactor, where they come into contact with a photocatalyst while being under the influence of light. As the reaction develops, the products are then continually collected. A continuous flow photocatalytic reactor architecture might change based on the particular application and specifications. Compared to conventional batch photocatalysis, it has many benefits, including increased scalability, better control over reaction conditions, better product separation from reactants, and the capacity to conduct lengthy reactions without often restarting [42].

The following are some applications for continuous flow photocatalysis. Continuous flow photocatalysis has been successfully accomplished for several organic transformations. It makes it possible to synthesize complex compounds with better yields and selectivity. Due to this, the technology has found applications in the synthesis of natural products, pharmaceuticals and fine chemicals. It can also be employed to turn solar energy into chemical fuels, like methanol or hydrogen, through CO_2 reduction or water splitting. These processes are necessary for the generation and storage of renewable energy. Additionally, continuous flow photocatalysis is employed for the purification and treatment of water. Utilizing photocatalysts like titanium dioxide (TiO_2), the organic contaminants may be degraded and water sources can be cleaned. Organic dyes, herbicides, and pharmaceutical residues may all be effectively broken down by photocatalysts by constantly pumping polluted water through a reactor under UV radiation [43]. In case of TiO_2, the UV radiation is needed because the TiO_2 has a wide band gap of ~3.2 eV which corresponds to wavelengths shorter than 387 nm, i.e. in the UV range.

- **Main steps in the photocatalytic process**

A typical photocatalytic process involves the following steps [44, 45]:

The first step is light absorption: the photocatalyst absorbs photons from the incident radiations (UV or visible light sources) with a suitable energy that is higher than the band gap of the photocatalyst. In order to produce the reactive species needed for the photocatalytic processes. Where light promotes electrons (e^-) in the semiconductor to be excited from the valence band (VB) to the conduction band (CB).

The second step is charge separation: the photogenerated electrons and holes become spatially separated within the semiconductor material due to its internal electric field. A positive hole (h^+) in the valence band (VB) and an electron (e^-) in the conduction band (CB) are generated as electron-hole pairs.

The third step is redox reaction: The separated electrons and holes can take part in a variety of redox reactions with adsorbed species on the catalyst surface or in the solution that surrounds it. For instance, the holes can oxidize a reducing agent whereas the electrons can reduce an oxidizing agent.

The fourth step is Electron Transfer: the electrons involved in reduction reactions can be transferred to target molecules, such as pollutants, to start the degradation or conversion process. As a consequence, organic substances degrade into smaller, less dangerous components or are completely mineralized, then water is cleaned.

The last step is hole reactions: the holes left behind in the valence band can interact with water molecules or hydroxyl ions (OH^-) For the formation of highly reactive hydroxyl radicals (•OH), which are powerful oxidizing species. These hydroxyl radicals can also aid in the degradation of the contaminants. These mechanisms are explained in Figure (A.3, in Appendix A) [46] and equations (1.1-1.5). The effectiveness of the degrading process may be assessed using techniques like UV-Vis spectroscopy.

The mechanism is described as follows [47].

$$\text{Catalyst} + h\nu \longrightarrow e^- + h^+ \tag{1.1}$$

$$e^- + O_2 \longrightarrow O_2^{\bullet -} \tag{1.2}$$

$$O_2^{\bullet -} + H_3O^+ \longrightarrow {}^{\bullet}OH + HO_2^{\bullet} + H_2O_2 \quad (1.3)$$

$$h^+ + H_2O \text{ or } OH^- \longrightarrow {}^{\bullet}OH + H^+ \quad (1.4)$$

$$^{\bullet}OH + \text{dye} \longrightarrow \text{degradation of dye} \quad (1.5)$$

over the last few decades, nano-semiconductors have been employed in a variety of environmental purifications processes as mentioned earlier such as TiO_2, ZnO, etc. but recently perovskite has attracted significant attention as semiconductor photocatalysts [48, 49].

1.4 Perovskites

The perovskite name was given to the mineral by a Russian scientist named Lev Aleksevich von Perovski, and researcher Gustav Rose made the first discovery of perovskite in the Ural Mountains of Russia in 1839. The substance $CaTiO_3$ was given this name to identify it with a general repeating structure of ABX_3. Later, perovskite was used to describe any materials having a similar structure [50, 51].

Perovskites represent one of the most promising substances for the 21st century. Recently perovskite structures have attracted wide scientific interest in modern technology and science, where it has achieved great progress in energy storage and special interest in water treatment due to their wonderful chemical and physical properties. They have, specifically, low manufacturing costs, rigid structural activity, simplicity, electrical stability and connection, adaptability, thermal stability, and ease of processing under ambient settings, tunable band gap, and long lifetimes. Perovskites also have semiconducting behaviors. Moreover, they have great capacity for broad and powerful light absorption. Perovskite materials can therefore be used in photocatalysis applications. It was discovered that perovskite structures had better photocatalytic activity than several compounds containing transition metals [52, 53].

There are two types of perovskites: First, halide perovskites with the formula ABX_3, second, inorganic oxide perovskites having the formula ABO_3, where A and B are cations and B is smaller than A, X is halide and O is oxygen. As seen in Figure (A.4, in Appendix A), perovskite has cubic symmetry, with the A-cations lying in the middle of the cube and being 12-fold coordinated, and the B-cations being octahedrally coordinated with six oxygen anions [54].

Perovskite oxide materials (ABO_3) have received a lot of interest recently from researchers. That is due to their distinctive chemical, physical and structural characteristics, including their high stability, semi-conducting qualities, great photocatalytic activity, and structural tunability. Perovskites have been extensively studied in photocatalysis, degradation of organic pollutants, and water purification, whether under ultraviolet or visible light. Oxide perovskites are better than halide perovskites in water purification from organic contaminants [55].

Many perovskite compounds are employed as photocatalysts. The first perovskite material to be discovered and used in the photocatalysis and degradation of contaminants is $CaTiO_3$, which was effectively employed to degrade the pollutants methyl blue, rhodamine, and brilliant green under ultraviolet light [56]. Then, perovskite compounds based on titanium demonstrated better contaminant photodegradation [57]. After that, researchers were drawn to ferrites-based perovskites ($AFeO_3$) because they were less expensive and had a smaller bandgap than titanium-based perovskites. For instance, pure $BiFeO_3$ demonstrated 69% photodegradation of methyl blue under the sunshine [58].

Perovskites made of tantalite have also been reported to degrade water contaminants. The sodium tantalite ($NaTaO_3$) exhibited photocatalytic degradation characteristics as a result of its exceptional photochemical stability. Because of the material broad bandgap, the $NaTaO_3$ based photocatalytic system efficiency is considerably low. Its effectiveness is nevertheless increased by nonmetals doping. By employing sunlight as an irradiation source and a nitrogen-based sodium tantalite photocatalyst, methyl blue is claimed to be photodegraded by this process with 95.21% loss [59]. Thereafter the researchers focused on titanate perovskites.

Titanate perovskites ($ATiO_3$ structure) have been investigated for use in photocatalytic processes for many years, they are attractive substances for photocatalytic processes due to their great resistance to photo corrosion in aqueous solutions, excellent photostability, and high thermal stability. With an energy band gap (E_{bg}) value of more than 3.0 eV for the majority of titanate perovskites, these materials exhibit excellent photocatalytic abilities when exposed to UV radiations, with high efficiency [60]., Manganese titanate and zinc titanate particularly showed promising results in the field.

Various preparation techniques were reported for the synthesis of perovskite powders with various sizes. For example, halide perovskite is made using the hydrothermal method, while perovskite oxides are made using the solid phase synthesis technique and the sol-gel method. Hydrothermal processes can control particle size morphology and crystallinity of materials, where high pressure and temperature are used to precipitate perovskite crystals. Wang et al. prepared $LaCrO_3$ perovskite oxide by this method [61]. But this method has several disadvantages such as slow reaction kinetics, high energy consumption and formation of impurities.

Solid phase synthesis is a traditional method for producing perovskite oxides which involve uniformly combining two or more different metal salts and pressing the resulting mixture into sheets. But this method is generally more suitable for small-scale material production and needs a lot of energy and specialized equipment. Also, the temperature variations cause heterogeneity within the synthetic perovskite material. Yuan et al. prepared the perovskite oxide by solid phase method [61].

Sol-gel method is done by hydrolysis or alcoholysis organometallic compounds or inorganic metal salts as precursors to form sol and is finally condensed to form a gel. After heat treatment, the necessary oxide powder is obtained. The commonly utilized gels include citric acid, polyvinyl alcohol, ethanol, and ammonia, etc. Taguchi et al. produce $LaCoO_3$ with tiny particle sizes by using a gel from ethylene glycol and citric acid [62].

Sol-gel method was used here to synthesize perovskite powders because it has a number of benefits. The Sol-gel technique is a simple and cost-effective method for perovskite synthesis since it uses inexpensive precursors and does not need expensive machinery. Additionally, the sol-gel process enables the creation of a homogenous solution or gel, which makes it easier for precursors to be distributed evenly. As a result, perovskite films with a mostly uniform composition are created. It can be applied to various substrates, including glass, plastics, and flexible substrates. It also allows to control the film thickness during deposition. Other benefits make the sol-gel process extremely producible on a large scale and appropriate for producing perovskite compounds at an industrial scale [63].

1.4.1 Manganese titanate

Manganese titanate ($MnTiO_3$), is an inorganic semiconductor material, that belongs to the family of perovskite oxides. It is considered the most stable oxide perovskite and exhibits intriguing chemical and physical characteristics. This makes it suitable for various applications due to its energy gap value [55]. Applications of manganese titanate include electroceramics, electronic equipment such as capacitors, varistors, and multilayer ceramic capacitors. Materials based on manganese titanate are suited for these applications because of their favorable dielectric characteristics, high dielectric constant, and low dielectric loss [64]. Also, manganese titanate is used in gas sensors, especially for the detection of dangerous gases including carbon monoxide and nitrogen dioxide. The perovskite materials are useful for gas sensing applications because they have great sensitivity and selectivity towards particular gases [65]. Additionally, manganese titanate can be used in energy storage systems like lithium-ion batteries. Due to its large capacity and strong electrochemical capabilities, it has been investigated as an electrode material [66].

Manganese titanate has shown potential as a catalyst in various reactions, including the decomposition of organic pollutants and the oxidation of hydrocarbons. That is due to its unique surface properties and redox behavior, which make it suitable for these catalytic applications especially photocatalysis. It has lately shown promising photocatalytic activity [67]

Manganese titanate nanoparticles can be used in the degradation of organic contaminants in water and air for their significant absorption in wide wavelength ranges due to their relatively wide bandgap. The surface properties of manganese titanate have an impact on the photocatalytic activity by providing active sites for adsorption and interaction through the generation of electron-hole pairs and then the participation of electron-hole pairs in redox reactions, which facilitates various photocatalytic processes [68]. Additionally, manganese titanate photocatalysis is also an interesting topic to study because of its distinct crystal structure and resistance to strong photo-corrosion in aqueous solutions. This makes it more efficient than traditional photocatalysts [69]. Manganese titanate has strong photostability, which allows it to maintain its photocatalytic activity under intense light conditions for a lengthy period of time without significant degradation. This is essential for long-term photocatalytic applications, as it can maintain its structural and catalytic qualities, guaranteeing its efficacy throughout time. Also, it has low toxicity, which essential for applications in water or air purification, where the discharge of dangerous compounds might have a negative impact on the environment and human health [70]. Recently, Alkaykh et al prepared manganese titanate nanoparticles and used them as photocatalysts for methylene blue photodegradation under sunlight irradiation [67].

1.4.2 Zinc titanate

Zinc titanate ($ZnTiO_3$) is an inorganic semiconductor perovskite that is composed of titanium dioxide and zinc oxide. The usage of zinc titanate in a variety of applications in various fields is made possible by its many intriguing properties [71]. Some of its noteworthy applications as Gas Sensors, zinc titanate is used as a detecting material in gas sensors as it is sensitive to some gases, such as nitrogen dioxide (NO_2), carbon monoxide (CO), and hydrogen sulfide (H_2S), due to its special electrical and surface properties. This makes it effective for identifying harmful gases and keeping track of the air quality in industrial and natural environments [72]. Additionally, zinc titanate is used for producing ceramic capacitors, which serve as essential components for electronic devices because it is a dielectric material, with a high resistivity. It helps to increase the stability and energy storage capacity of these capacitors, making it suitable for applications where electrical insulation is required [73]. Zinc titanate is also used in energy storage applications. It is being investigated as a potential electrode material for lithium-ion batteries and supercapacitors with high capacity due to its electrochemical properties and unique crystal structure [74].

Zinc titanate is used as a catalyst in several chemical processes. It is appropriate for many uses including methanol production, gas purification, and the removal of volatile organic compounds from industrial pollutants because it has outstanding catalytic activity and stability. Moreover, due to its special properties, zinc titanate displays photocatalytic activity when exposed to ultraviolet (UV) light. It can be utilized for environmental applications such as water purification, air purification, and the degradation of organic contaminants, such as dyes and pharmaceuticals, in wastewater treatment [75].

Several features make zinc titanate an attractive photocatalyst for a variety of applications such band gap energy, where zinc titanate has a relatively wide band gap energy which places it in the UV light range, this property allows it to absorb UV light efficiently and produce electron-hole pairs. These electron-hole pairs can take part in a variety of chemical reactions, making zinc titanate useful for photocatalytic applications [76]. It can also maintain its structural integrity and catalytic activity over prolonged exposure to light. This property is important for practical applications that require continuous or long-term operation. Also, it can continue to function as a catalyst even after prolonged exposure to radiations for practical applications that need long-term or continuous operation, which is a crucial feature. In addition, zinc titanate is stable, non-toxic, and environmentally friendly [77]. Recently, Chen et al prepared zinc titanate nanopowder catalyst to photodegrade many organic pollutants [75].

All the important and unique properties of zinc titanate and manganese titanate are being considered here in our aspiration to photodegrade methylene blue in water.

1.5 Perovskite films

Perovskite films are thin films composed of perovskite materials with particular crystal structures. A thin film of perovskite material is deposited on a suitable substrate, such as conductive oxide or glass. Different methods can be used to make perovskite films including drop-casting, spin-coating, or Dr. blade, spray pyrolysis, vapor deposition, and others. The procedure entails depositing a precursor solution onto a substrate and then undergoing to annealing or drying, to transform it into a crystalline perovskite layer. Perovskite films have received a lot of attention recently and have demonstrated excellent potential for a variety of applications [78].

Perovskite films have attracted a lot of interest recently and have demonstrated considerable potential for a variety of applications, due to their unique features, including a high absorption coefficient, adjustable bandgap and extended carrier diffusion lengths. Some of these applications are solar cells. The field of photovoltaics has undergone a revolution because of perovskite films. It may be utilized to create effective, affordable solar cells. Where high power conversion efficiencies that are equivalent to conventional silicon-based solar cells have been attained using perovskite solar cells. Perovskite based solar cells are simple, low-cost, with high-efficiency and flexible production methods. The films can be deposited on a variety of rigid or flexible substrates [79]. Perovskite films can also be employed in light-emitting devices (LED). High color purity and adjustable emission wavelengths have been attained by researchers by adding perovskite materials into the LED construction. Compared to conventional LEDs, perovskite LEDs have the potential to be more energy-efficient and offer a wider color spectrum [80]. Furthermore, perovskite films are proven to have great properties in photodetectors, as they can be employed as active layers to enable high response, little noise and short reaction times. In image sensors, optical communication, and environmental monitoring, perovskite film-based photodetectors have been found useful [81]. Another important application of perovskite films is detection of X-rays and gamma rays. Therefore, the films can be used in security screening, nuclear research and medical imaging, where the effective conversion of high-energy photons into electrical impulses is possible by their high atomic number of elements [82].

Recently, perovskite films, they have attracted a lot of interest in the field of photocatalysis due to its distinctive optical and electrical characteristics. Perovskite films have demonstrated significant promise as effective photocatalysts based on a group of substances with the same crystal structure. One example of perovskite film photocatalysis is the degradation of organic water contaminants like methylene blue, using $BiVO_4$ material [83]. The field of perovskite film photocatalysis is still developing quickly, and research is currently being done to solve the problems with stability, scalability, and long-term performance. Nevertheless, perovskite films provide unique properties that make them promising future candidates for developing solar-driven chemical processes and applications for environmental remediation due to their special properties [84].

The method used to prepare perovskite films here is Doctor Blade. Doctor blade coating is a widely used method in the manufacturing field, for creating thin films or coatings on a variety of substrates. It includes spreading a liquid or viscous substance on a flat surface using a blade or scraper known as Doctor's blade. The doctor blade is often composed of a flexible material, such as plastic or metal, and is pushed onto the substrate while being held at an appropriate angle. The liquid substance is dropped or pumped onto the substrate throughout the coating process, and the doctor blade is then used to move over the surface and level the liquid into uniform thin layer. The regulated pressure and angle of the blade aid in regulating the final film thickness. The blade pushes extra material away to provide a precise and uniform thickness of the coating. Doctor blade coating has several advantages, including ability to create thin, homogeneous and uniform coatings with high control over thickness and smoothness. It is a flexible technique appropriate for a variety of materials and substrates. Additionally, it is a rapid method that may effectively and quickly create thin films. It causes less waste of the solution during deposition and not costly [85]. Figure (A.5, in Appendix A) summarizes the method of Doctor Blade [86].

1.6 Objectives

The major goal of this research was originally to find economic and safe processes (photodegradation) to purify water and remove organic contaminants like methylene blue from it by using non-toxic and affordable semiconducting materials (zinc titanate and manganese titanate). All technical goals were accomplished in this work, as follows:

1. Prepare zinc titanate and manganese titanate powders
2. Characterize zinc titanate and manganese titanate powders using photoluminescence spectra, UV-visible absorption spectrophotometry, X-ray diffraction, scanning electron microscopy and X-ray photoelectron spectroscopy.
3. Use the prepared zinc titanate and manganese titanate powders in the photodegradation of aqueous methylene blue under solar simulated light.
4. Study several reaction parameters such as (contaminant concentration, catalyst loading, effect of pH) on the efficiency of catalyst powders
5. Prepare zinc titanate and manganese titanate films

6. Use the prepared zinc titanate and manganese titanate films in the photodegradation of methylene blue in water under solar simulated light.
7. Study several reaction parameters such as (contaminant concentration, catalyst loading, effect of pH) on the efficiency of catalyst films
8. Compare the result of the zinc titanate powder and film efficiency in the degradation of methylene blue.
9. Compare the result of the manganese titanate powder and film efficiency in the degradation of methylene blue.
10. Compare the result of the zinc titanate and manganese titanate efficiency in the degradation of methylene blue.
11. Study the photodegradation kinetics of zinc titanate and manganese titanate.
12. Study the continuous flow rate for zinc titanate and manganese titanate and compare with batch systems.
13. Study the recovery and reuse of zinc titanate and manganese titanate (powders and Films).
14. Study the effect of pH on photodegradation of zinc titanate and manganese titanate (powders and films) and see where complete photodegradation of contaminant can be reached.
15. Calculate the actual efficiency of zinc titanate and manganese titanate, either powders or films, in terms of turnover number, turnover frequency and quantum yield at all different reaction parameters.

1.7 Novelty of this work

Only little study on zinc titanate powder and manganese titanate powder to degrade photocatalytically was conducted. Chen et al [75] used zinc titanate as photocatalysts in organic pollutant photodegradation. Alkaykh et al. [67] synthesized manganese titanate nanoparticles and employed them as photocatalysts in order to accelerate the photodegradation of methylene blue. To our knowledge these two perovskites were not widely described as nano-powder photocatalysts in methylene blue photodegradation.

Perovskite zinc titanate thin films were prepared earlier [87], but were not used in water purification to our knowledge. For the first time, the degradation of aqueous organic contaminants will be attempted using the films as photocatalysts in this work.

Perovskite manganese titanate thin films were not previously prepared except by Emrick et al., where manganese titanate layers were placed on ZnO and Mo films, which were placed on substrates [88]. The full report has not been published as a journal article. The manganese titanate deposition process also involved the use of a laser. Therefore, the present study is unique in two ways. First, we will deposit the perovskite onto a substrate devoid of any Mo or ZnO mediator layers. Second, we'll employ simple preparatory techniques (sol-gel method) for the powders. As a result, our approach will prevent additional preparatory steps, avoid additional resistance, and reduce production costs, particularly those related to expensive Mo metal. Also, the novelty here is to use of manganese titanate film for the first time in photocatalysis of aqueous organic contaminant photodegradation.

Comparisons between the efficiency of film catalysts and their powder in photodegradation of methylene blue is described here for the first time, to our knowledge. This is necessary to determine if these two perovskites are useful in future water purification applications

Recovery and reuse of the catalyst (powders and films), for practical purposes, is another novel aspect of the present study. Additionally, using the film catalysts in continuous flow reaction processes allows researchers to assess the viability of perovskites for future water purification applications. To our knowledge, no similar results were described in the literature. Hence, all objectives have been achieved here for the first time.

1.8 Basic assumptions of the study

The present study, is made to achieve its objectives, based on the following assumptions:

a. The two perovskite powders have band gap values close to 3.2 eV. Therefore, they can be excited by UV radiations, and can be used as photocatalysts in methylene blue degradation under solar simulated radiations. This is because 5% of solar simulated radiations are in the UV region. These radiations can be sufficient for photodegradation. This assumption has been tested here.
b. Removal of photocatalyst after use in water purification is difficult. This is because

the powder involves nano-particles, which are not easy to recover. This assumption has been tested here as described in the recovery and reuse study here. Therefore, using films of the perovskites should make recovery and reuse of the catalyst much easier for practical purposes. It is assumed here that the film catalyst systems will be recovered and reused with no significant loss of efficiency. This assumption has been tested here.

c. As the catalyst powder keep flowing in the reaction mixture, the particles at the reaction mixture surface will screen radiations and prevent them from reaching other catalyst sites in the reaction mixture bulk. Using film catalysts will solve this problem, as radiations may reach most catalyst sites at the film surface, if the reaction mixture depth is kept soundly small. Therefore, it is assumed here that the film catalysts will have much higher efficiency than the powder catalyst counterparts. This assumption is tested here.
d. Any difference between the band gap values between the two perovskites, will have effect on its catalytic efficiency in methylene blue photodegradation. This assumption will be tested here, by measuring band gap values for the two perovskites. The catalytic efficiencies for the two perovskites will be measured and correlated with band gap values, as described here.
e. Based on values of point of zero charge (P_{ZC}) for the two perovskites, and based on methylene blue dye behavior variation with solution pH value, it is possible to find the optimal pH range for methylene blue photodegradation to occur. These assumptions have been tested here.
f. If the perovskite catalysts effectively function in the film form, in batch reaction systems, they will also effectively function in the continuous flow experiments. This assumption has been tested here.

Chapter Two

Materials and Methods

2.1 Materials

Manganese chloride tetrahydrate $MnCl_4.4H_2O$ and titanium isopropoxide, were purchased from Sigma Aldrich Co. Nitric acid, acetic acid and sodium hydroxide were purchased from Frutarom Co. Zinc chloride was purchased from Chem. Samul. These materials were used in the synthesis of manganese titanate and zinc titanate. The contaminant methylene blue was purchased from Sigma Aldrich. Microscopic glass slides were used for films. Salt, acids, bases and organic solvents were purchased from Sigma Aldrichin pure forms.

2.2 Equipment

2.2.1 UV-Visible spectrophotometer

A Shimadzu UV spectrophotometer was used to measure all spectra (solid state and solutions). Methylene blue concentrations in solutions were measured using the calibration curve. The band at 664 nm was used for this purpose.

2.2.2 Solar simulated light

Irradiation was made using a 250 W halogen solar simulator lamp (HLX64657). The radiation intensity at the reaction mixture was measured by a Lux meter, with 100000 Lux (equivalent to 0.014 w/cm^2). Figure (A.6, in Appendix A) describes the natural solar radiation at the solar simulated spectra [54,55].

2.2.3 Lux meter

A light intensity meter (Lx-102) was used to determine the light intensity that reaches the contaminated water under study in the photo-catalytic purification experiments. The Lux unit was converted to w/cm^2 units.

2.2.4 Centrifuge

To separate contaminated liquids from solid materials, a Centrifuge Scientific Ltd model 1020 D.E was employed, at 500 rpm speed.

2.2.5 pH meter

The reaction mixture pH was measured and controlled using a Jenway 3510 pH meter as desired.

2.2.6 Mercury thermometer.

The reaction mixture temperature was measured with a mercury thermometer.

2.3 Preparation of solutions

- Methylene blue stock solution: to prepare the stock solution, 0.100 g of methylene blue was dissolved in 100 ml of distilled water, to yield a concentration of 1000 parts per million. The stock solution was used to prepare various concentrations of methylene blue (5, 10, 20, 40, 60, and 80 ppm).
- To adjust the pH of the catalytic reaction mixtures, diluted solutions of both sodium hydroxide and hydrochloric acid (0.05 M) were prepared.

2.4 Catalyst preparation

2.4.1 Preparation of manganese titanate powder

Nanoparticles of manganese titanate ($MnTiO_3$) were prepared using the sol-gel technique as described before [67]. (9.0 g, 0.033 mole) g of manganese chloride tetrahydrate ($MnCl_4.4H_2O$) was dissolved in 150 mL distilled water. Nitric acid HNO_3 (1.8 mL), acetic acid CH_3COOH (24.0 mL), and titanium isopropoxide $Ti\{OCH(CH_3)_2\}_4$ (15.0 ml) were then added. The system was kept under stirring (12 h at 50 ℃), and the resultant colloidal suspension was evaporated at 80 ℃. The resultant powder was then rinsed with water, dried and heated for 6 hours at 900 ℃.

2.4.2 Preparation of zinc titanate powder

Sol-gel method was used to synthesize zinc titanate ($ZnTiO_3$) nanoparticles as described earlier [89]. Using a heated magnetic stirrer at 70 °C for 3 hours, (50 mL, 48 g, 0.17 mole) of titanium isopropoxide $Ti\{OCH(CH_3)_2\}_4$ was added to (23.17 g, 0.17 mole) of zinc chloride ($ZnCl_2$). By gradually adding 2 M of sodium hydroxide to the mixture (drop by drop), the pH was adjusted to 12, and the agitated solution was kept at 70 °C for two hours. Then the resultant gel was separated, repeatedly rinsed with ionized water until neutral, dehydrated at 110 °C, and then calcined for three hours at 600 °C.

2.4.3 Preparation of catalyst films

Glass substrates were washed with soap and distilled water before being immersed in diluted HCl solution (10% v/v) for 1 hour in an ultrasonic cleaning bath before coating with the films. The glass substrates were then rinsed with distilled water and immersed in acetone for 1 hour using an ultrasonic cleaning bath. Finally, the substrates were rinsed with distilled water and then dried with a stream of nitrogen.

Different techniques were examined to fix the perovskite films on the glass substrates such as spray pyrolysis, drop casting and Dr. Blading. The best technique was Dr. Blading and it was adopted here. The perovskite powder was mixed with triton X, acetylacetone and distilled water in a 2:1:1:1 ratio and fixed on glass. The perovskite was used in certain quantities and thicknesses. After that, the resultant perovskite/glass was heated for one hour at 500 °C.

2.5 Catalyst characterization

Zinc titanate and manganese titanate powders used in the photodegradation experiments and that were used to form the films were characterized by, photoluminescence spectra, UV-visible absorption spectrophotometry, X-ray diffraction, scanning electron microscopy and X-ray photoelectron spectroscopy.

2.5.1 Photoluminescence (PL) spectra characterization

A Perkin-Elmer (LS50) photoluminescence Spectrometer was used to study the maximum emission of perovskite, small amount of each powder was suspended in distilled water and placed in a quartz cell. The PL spectra were then measured, vs. distilled water baseline.

2.5.2 UV-visible spectra characterization

UV-Visible spectra were measured for zinc titanate and manganese titanate powders. Each powder was individually dissolved in distilled water and placed in a quartz cell with a little quantity. Then, the wavelength of maximum absorption was measured.

2.5.3 X-ray diffraction (XRD) characterization

XRD patterns have been measured on a PANalytical X'Pert PRO X-ray diffractometer, with Cu Kα rays utilized to determine the size of the perovskite particles. The analysis was conducted at the Korean Institute of Energy Research in Daejeon, South Korea.

2.5.4 Scanning electron microscopy (SEM) characterization

SEM was measured on a Field Emission SEM (FE-SEM, JEOL JSM-6700F) to determine the morphology of the perovskite. The analysis was performed in South Korea at the Korean Institute of Energy Research in Daejeon.

2.5.5 X-Ray photoelectron spectroscopy (XPS)

AMulti Lab 2000 spectrometer with a micro-focusing monochromated Al K (1486.6 eV) X-ray source was used to analyze solid samples using XPS. The measurement was carried out at the Korean Institute of Energy Research in Daejeon, South Korea.

2.5.6 Surface Area Measurement

The method of acetic acid adsorption was used to evaluate the specific surface area of manganese titanate and zinc titanate [90]. According to Langmuir isotherm, five dry-clean large test tubes were used. Each tube was charged with 0.10 g of manganese titanate, followed by 20 ml of acetic acid with molarities ranging from 0.015 to 0.15 M.

To achieve equilibrium at 25°C, the test tubes were covered and shaken in a thermostat for an hour. All samples were filtered individually and titrated with standardized (0.10 M) sodium hydroxide with KHP using a phenolphthalein indicator.

For different acetic acid concentrations at equilibrium (C), the total number of moles of acetic acid adsorbed onto one gram of adsorbent (N) was calculated. Using Langmuir adsorption isotherms, C/N versus C was plotted according to the equation (2.1):

$$\frac{C}{N} = \frac{1}{N_m b} + \frac{1}{N_m} C \tag{2.1}$$

The number of moles of acetic acid per one gram of manganese titanate required to form a monolayer (Nm) was calculated from the slope (1/ Nm). Then the monolayer molecules of acetic acid per one-gram adsorbent were calculated. The surface area of the adsorbent was determined by multiplying the cross-sectional area of one acetic acid molecule by the number of molecules per gram of adsorbent (which is $2.1*10^{-19}$ m^2 $molecule^{-1}$) [91]. For zinc titanate, the same procedure was followed.

2.5 Photo-catalytic experiments

Methylene blue photodegradation experiments were conducted using various types of perovskite**.**

2.6.1 Photo-catalytic batch experiments using Powders

In 100 mL beakers with known loading of the perovskite photocatalyst powder and the contaminant methylene blue concentrations, photodegradation reactions were conducted. In a thermostatic beaker that was magnetically stirred, the catalytic experiments were carried out and followed. The beaker was dipped in a water bath at a constant temperature to prevent temperature changes, and the reaction mixture was continually magnetically swirled to guarantee proper catalyst distribution throughout the mixture. Throughout the reaction, the temperature was monitored and, as necessary, the water bath was adjusted to maintain a consistent temperature. On the top of the photocatalytic mixture, solar simulated light radiations with an intensity of 100,000 Lux (about equivalent to that of sunlight) were shed in a perpendicular direction.

For catalytic experiments, the standard temperature was 25 °C, and the standard pH was 7. When studying the effect of pH in some experiments, the pH was managed by adjusting it as necessary by adding drops of diluted NaOH or HCl solutions.

Small aliquots were syringed out of the reaction vessel periodically after one hour at different reaction times and then centrifuged for 6 minutes at 500 rpm. After that, a quartz cell was carefully filled with the resulting clear solution. UV/Visible spectrophotometry was used to measure the absorbance values for sample aliquots obtained at various times.

2.6.2 Photo-catalytic batch experiments using films

Photodegradation reactions using photocatalyst films were performed inside beakers containing known concentrations of methylene blue, and perovskite films with a known amount of powder that were fixed on the film by taking the weight of the film before and after fixation. The film's gross area was 4 cm^2.

The film was placed in the middle of the beaker bottom, and direct light with an intensity of 100,000 Lux was shed perpendicularly onto the top of the reaction mixture. As in the case of powder experiments, the temperature was measured throughout the reaction time and kept constant by manipulating the water bath.

Sample aliquots were taken as the reaction progressed, placed in the spectrometer quartz cell, and the absorbance values were determined using UV/Visible spectrophotometry at various times. For these trials, the default pH was 7, and the default temperature was also 25 °C. The photo-catalytic experiments system apparatus arrangement using catalyst powder and film are shown in Figure (A.7, in Appendix A).

2.6.3 Continuous flow photocatalytic experiments

Under the simulated solar lamp radiation, the glass dish with the perovskite film was placed. Methylene blue solution (80 ppm) was allowed to flow over the perovskite film catalyst by the connection of a burette with a control valve that connected to the inlet tube of the dish. The outlet tube of the glass dish was connected to the beaker to collect the methylene blue flowing through the dish.

Sample aliquots were taken and placed in the spectrometer quartz cell. The absorbance values for sample aliquots, collected at various times, were determined using UV/Visible spectrophotometry at room temperature and pH during the continuous flow rate process. The apparatus arrangement is shown in Figure (A.8, in Appendix A).

2.6 Control Experiments

- Methylene blue solution (100 ml, 40 ppm) was added to the reactor in the absence of any catalyst and stirred for 60 minutes in the presence of light. The amount of methylene blue remained constant over time when exposed to direct, simulated solar light. This indicates that in the absence of a catalyst, methylene blue does not photodegrade.

- In another control experiment, manganese titanate powder (0.1 g) and methylene blue solution (100 ml, 40 ppm) were mixed in the dark for 60 minutes. With time, the absorption spectra were measured. The fact that the contaminant's content remained constant indicates that manganese titanate photodegradation did not take place in the dark. A similar experiment was conducted using 0.1 g of zinc titanate in 100 ml of 40 ppm methylene blue solution in the dark, also the concentration of the contaminant remained constant.
- Only small methylene blue concentration loss was observed due to adsorption on the perovskite surfaces in the control experiments. Therefore, in other photocatalytic experiments, any loss in methylene blue concentrations is due to photodegradation behaviors.

2.8 Methylene blue Calibration curve

According to Figure (A.9, in Appendix A), methylene blue absorbs in the visible region with a maximum absorption wavelength of 664 nm. The spectrum is similar to the previously reported methylene blue value of 664 nm [92].

To construct the calibration curve, different concentrations of methylene blue (5, 10, 20, 40, 60 and 80 ppm) were prepared. The electronic absorption spectra were measured for different concentrations at 664 nm. A Calibration curve was constructed by measuring the absorbance of methylene blue concentration, at room temperature and pH 7, as shown in Figure (A.10, in Appendix A).

2.9 Photocatalytic degradation of methylene blue

The effect of methylene blue concentration, Perovskite loading and pH on photo-degradation reaction, were all studied here.

2.9.1 Effect of contaminant concentration

To investigate the effect of methylene blue concentrations on the photo-degradation process, various initial concentrations (5, 10, 20, 40, 60, and 80 ppm) of the dye were prepared. Every concentration of methylene blue was mixed with 0.10 g of perovskite powder, then placed in a beaker and stirred in a water bath under simulated light (with light intensity 100000 Lux, similar to natural sunlight intensity) for 60 minutes at 25 ℃ and pH 7. Every 15 minutes, a little sample of the perovskite and methylene blue reaction mixture was extracted, centrifuged, and then measured for absorbance. For technical reasons, the aliquot was diluted 10 times before measurement. That was to match the measurement with the linear calibration curve. Re-multiplication by 10 was then made to find remaining concentration with time.

For perovskite films, the same various methylene blue concentrations were prepared and placed in a beaker. The film was then placed in the middle of the beaker in a water bath under simulated light for 60 minutes at the standard temperature and pH. Every 15 min., a little amount of the solution was collected separately, and the absorbance was then measured similarly.

2.9.2 Effect of perovskite powder loading

To investigate the effect of catalyst concentration on the photo-degradation process, various loading of perovskite (0.05, 0.10, 0.15, and 0.20 g) were utilized. Each quantity of perovskite was mixed with a 100 ml solution of methylene blue (40 ppm), added to a beaker, and stirred for 60 minutes at at 25 ℃ and pH 7. This was done under simulated sunlight. Every 15 min, a little portion of the reaction liquid was removed separately, centrifuged, and measured for absorbance as described earlier.

In order to create perovskite films, different film thicknesses were prepared, with one layer being equivalent to 0.10 g, two layers being equivalent to 0.15 g, and three layers being equivalent to 0.20 g of perovskite powder. The films were then placed in the center of the beaker in a water bath under simulated light that had an intensity similar to that of natural sunlight for 60 min. at 25 ℃ and pH 7. Every 15 min, a little amount of the solution was collected separately, and the absorbance was then calculated as described earlier.

2.9.3 Effect of pH

The process of photo-degradation was investigated at various pH levels (3.5, 7.0, 8.5, and 11.0). A small amount of the reaction mixture was taken individually every 15 min and then centrifuged and measured for absorbance as described earlier. The solutions were prepared using 50 ml of methylene blue solution (40 ppm) and 0.10 g of perovskite powder for each pH value. This mixture was placed in a beaker with stirring under simulated solar light for 60 min. Drops of sodium hydroxide or hydrochloric acid were added to adjust the pH value.

Different pH values were also generated for perovskite films as powder. For each pH value, the film was put in the center of the beaker in a water bath under simulated light for 60 min. A tiny amount of solution aliquot was taken separately every 15 min., and the absorbance was then measured.

2.10 Recovery of perovskite powder and Film

Perovskite powder and film recovery were studied at room temperature. After one hour of photodegradation of the methylene blue, the powder was filtered, washed with distilled water, dried and weighed. Likewise for the film, the film was weighed after the methylene blue had photodegraded for an hour after being washed with distilled water and dried.

2.11 Nitrate ions measurement

The measurement of nitrate ions: taken 1.0 ml of working solution, diluted with 10 mL distilled water then added (0.2 mL, 1.0 M) of HCl. By deducting Abs (220 nm) –2(Abs 275 nm) from the net absorbance values, the net absorbance has been calculated. The nitrate ion concentration was measured to confirm the photodegradation of the methylene blue contaminant.

2.12 Photodegradation kinetics

The reaction kinetics were calculated to find out how the contaminant concentration affected on the reaction progress. Utilizing the well-known initial rate method using the equation, Rate = k [conc of contaminant]^x [conc of catalyst]^y, plots of ln(initial rate) vs. ln(initial conc) were constructed for both forms of perovskites powder and film.

2.13 Calculations

For each effect under study, values for contaminant degradation percentage, contaminant quantity consumed, turnover number (T.N.), turnover frequency (T.F.), and quantum yield (Q.Y.) were calculated. Table (2.1) shows how these values were calculated.

Table 2.1

How to calculate contaminant %degradation, turnover number, turnover frequency and quantum yield

* Percent Degradation =

[(Initial concentration – Final concentration)/Initial concentration] *100%

*Turnover Number (T. N.)=
No. of moles of consumed contaminant /No. of gram of catalyst

*Turnover Frequency (T. F.)=TurnoverNumber(TN) /Time (min)

*Quantum Yield (Q.Y.) = Turnover Frequency / incident photons *(100/5)

E (J) = Incident power per unit area X Total area (cm^2) X Exposure time(s)

$E(J)=nh\upsilon = nhc/\lambda$ (Plank′s equation)

$n = J / h\upsilon$

Where:

M.wt of Methylene blue = 319.85 g/mol

M.wt of $MnTiO_3$ = 150.8 g/mol

M.wt of $ZnTiO_3$ = 242.64 g/mol

Time = 60 min.

$c = 3x10^8$ m/s

$h = 6.62\times10^{-34}$ J·s

Chapter Three

Results

3.1 Photocatalyst characterization results

3.1.1 Photoluminescence (PL) spectra

The photoluminescence spectra of zinc titanate and manganese titanate powders were measured as shown in Figure (3.1). Zinc titanate has a 352 nm emission peak in the photoluminescence spectrum while manganese titanate has a 403 nm emission peak at room temperature. Using the formula E_{bg} (eV) = 1240/max (nm) [93] the band gap values were calculated as 3.52 eV for zinc titanate and 3.08 eV for manganese titanate.

Figure 3.1

Photoluminescence emission spectra for (a) zinc titanate, (b) manganese titanate

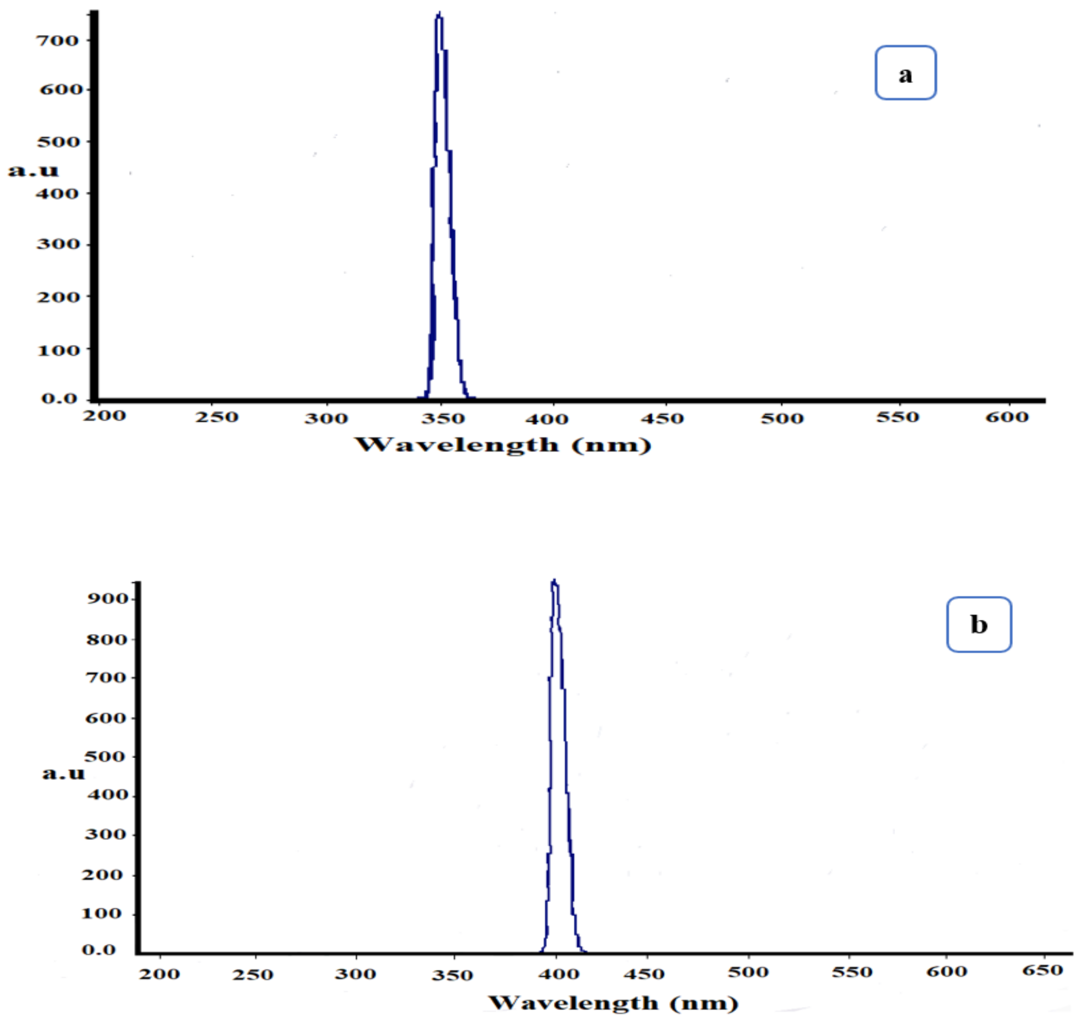

3.1.2 UV-visible spectra characterization

UV-visible spectra for zinc titanate and manganese titanate powders were measured as shown in Figure (3.2). The spectrum for zinc titanate showed maximum absorbance at 338.8 nm, whereas the spectrum for manganese titanate showed maximum absorbance at 388.5 nm.

Figure 3.2

Electronic absorption spectra were measured for (a) zinc titanate, (b) manganese titanate, the spectra were measured as aqueous suspensions

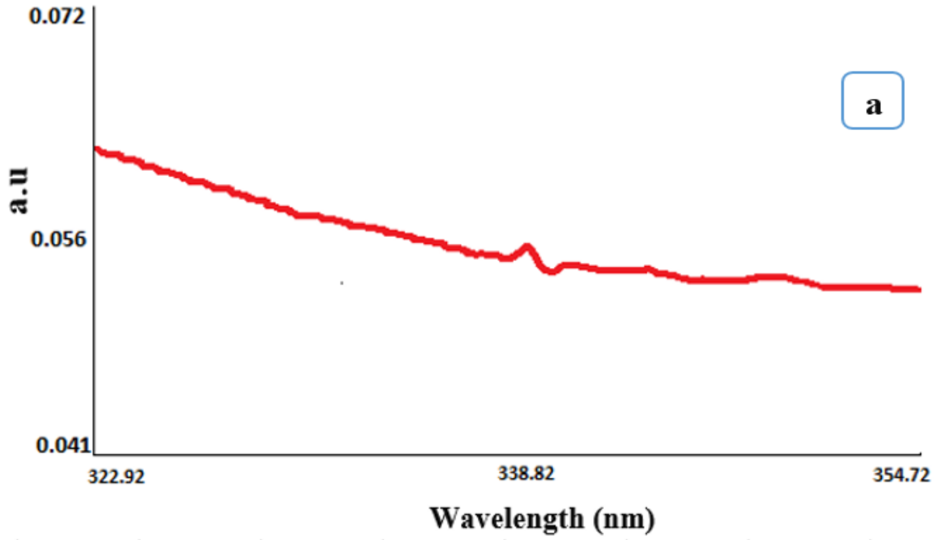

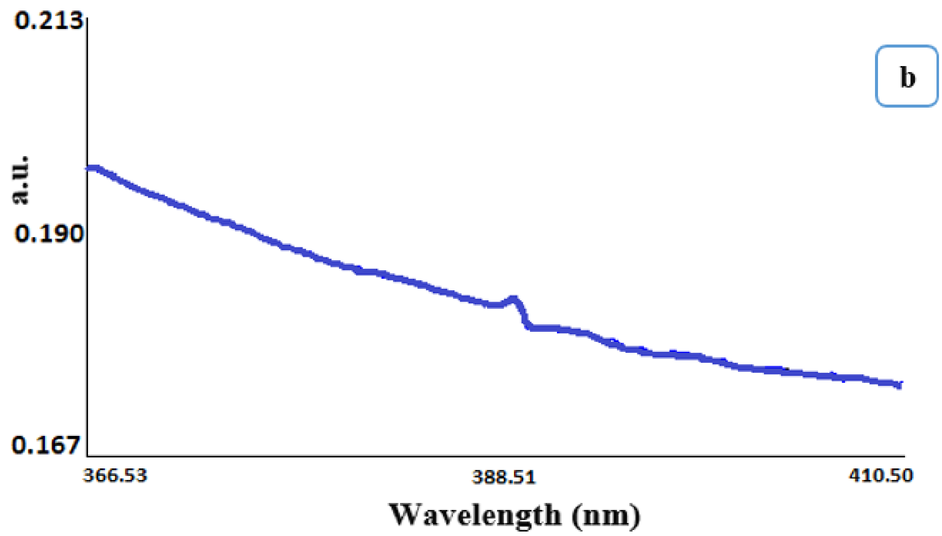

3.1.3 Scanning Electron Microscopy (SEM) Analysis

SEM spectra for zinc titanate and manganese titanate powders were measured as shown in Figure (3.3). Figures (3.3, a) show the manganese titanate powder with average sizes ~300 nm and Figures (3.3, b) show the zinc titanate powder with average sizes ~250 nm. Manganese titanate powder exists in agglomerates of nearly plate shapes but zinc titanate powder exists in agglomerates of nearly spherical shapes. Also, smaller particles are mixed in each agglomeration. Whereas in film form Figures (3.3, c and d) demonstrate that the zinc titanate film has sparsely packed agglomerates of more spherical shapes. But in the manganese titanate layer, the agglomerates had flatter forms and more homogeneity.

Figure (3.3, e and f) shows the perovskite films' cross-sectional micrographs, The average thickness of both films is not uniform. Based on SEM film thickness data, the total quantity of zinc titanate in the monolayer films is $2.3x10^{-3}$ g while the total quantity of manganese titanate in the monolayer films is $1.8x10^{-3}$ g.

Figure 3.3

SEM micrographs measured for perovskites in their various forms. Powder forms a) zinc titanate and b) manganese titanate; Film forms c) zinc titanate and d) manganese titanate; Cross-sectional films e) zinc titanate and f) manganese titanate

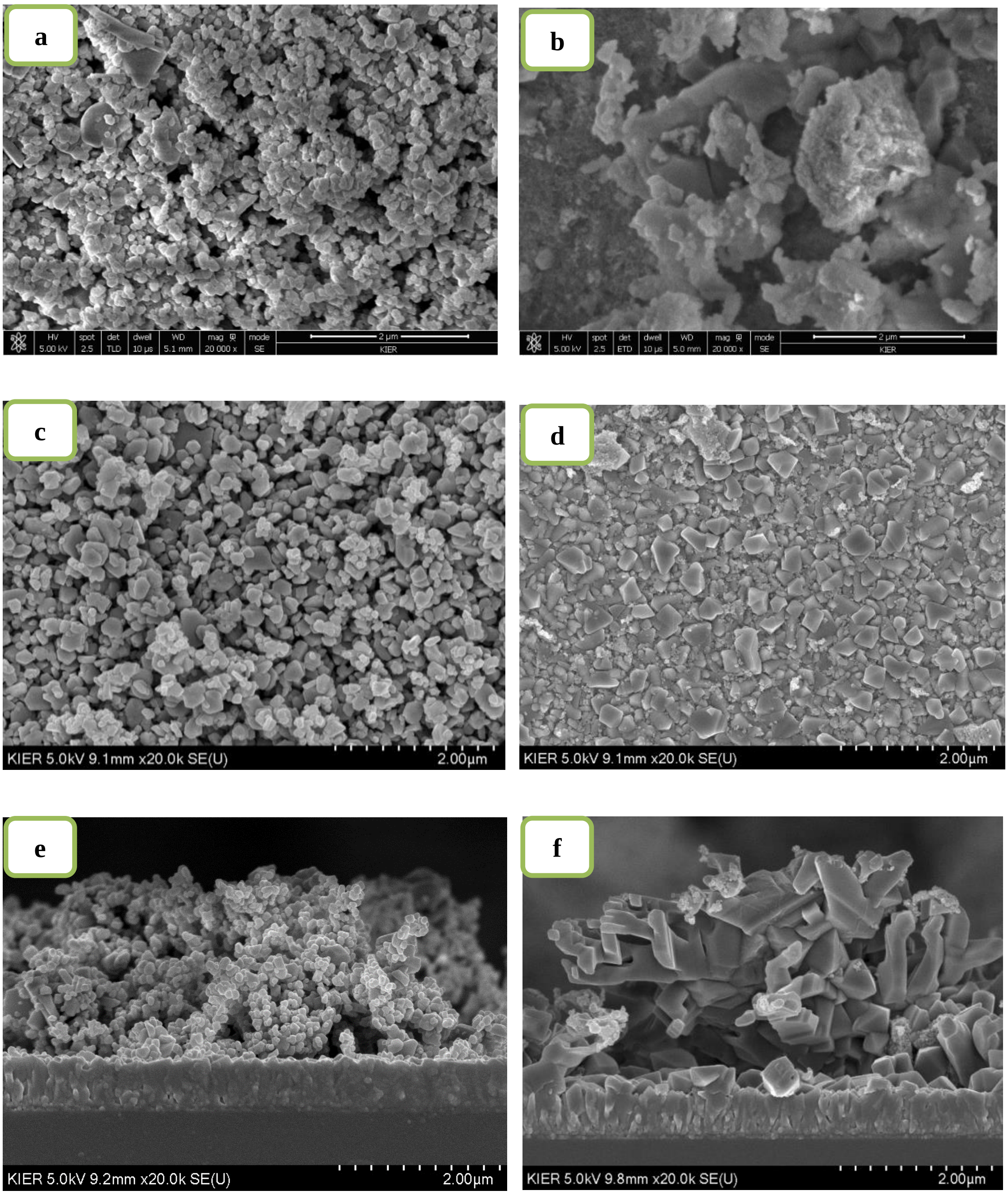

3.1.4 XRD Analysis of Perovskites

The X-ray diffraction (XRD) measurement was carried out at room temperature for zinc titanate and manganese titanate, Figure (3.4, a) shows the XRD of zinc titanate and Figure (3.4,b) shows the XRD of manganese titanate.

Figure (3.4, a) shows peaks for zinc titanate powder with reflections at 2theta (31.1°, 33.0°, 35.5°, 40.5°, 53.6°, 57.0°and 62.0°). These peaks corresponded respectively, with reflections of (201), (220), (311), (400), (422), (511) and (440). Whereas Figure (3.4, b) shows peaks for manganese titanate with reflections at 2theta (32.0°, 34.6°, 40.9°, 47.8°, 52.3°, 54.7°and 63.1°). These peaks corresponded respectively, with reflections of (104), (111), (113), (024), (116), (018) and (300).

Figure 3.4

XRD patterns measured for a) zinc titanate, b) manganese titanate

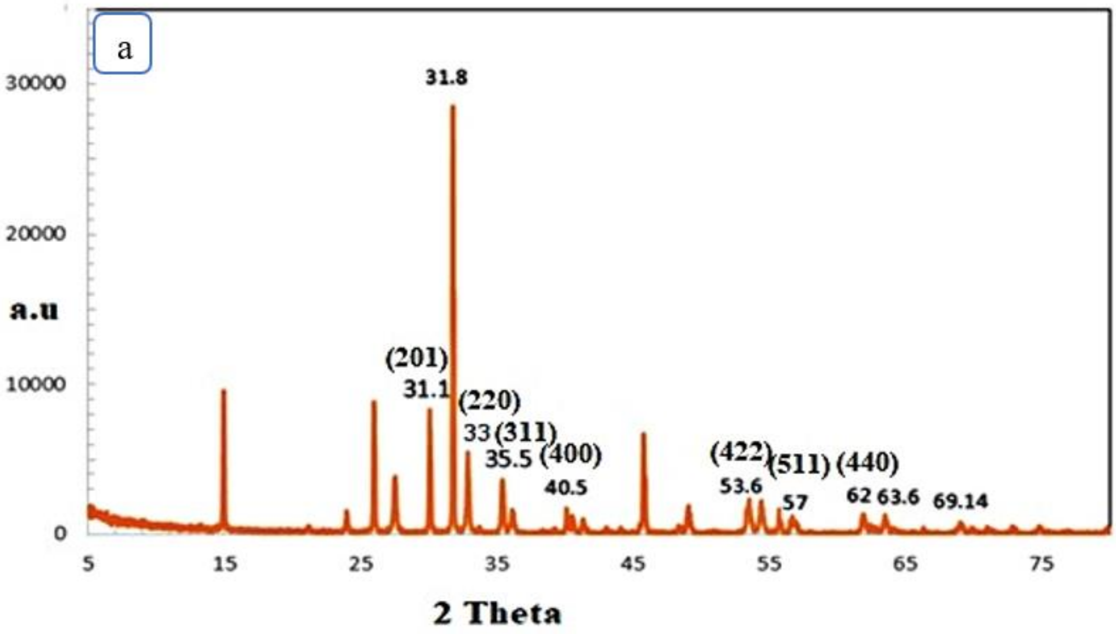

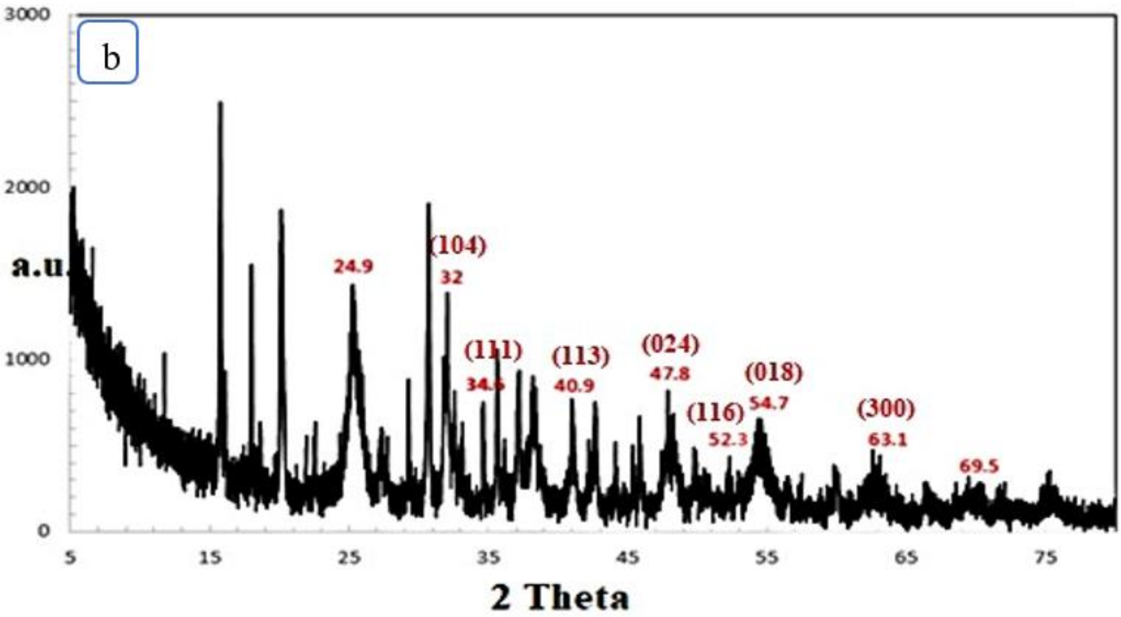

The crystallite size of perovskites has been determined using XRD measurements and calculated by Scherrer equation Equation (3.1) [94].

$$D = \frac{0.9\lambda}{b \cos\theta} \tag{3.1}$$

where D is the average crystallite diameter (nm), λ is the X-ray wavelength ~ (0.154 nm), b is the full width at half maximum (FWHM, radians) of the peak and θ is the peak position (radians). Calculations were made using 5 different planes in each case, using the equation. The average particle size for zinc titanate was ~17 nm while the average particle size for manganese titanate was ~15 nm. The perovskites structure were close-packed structure.

3.1.5 XPS analysis for Perovskites

X-ray photoelectron spectroscopy (XPS) analysis was performed for zinc titanate and manganese titanate as shown in Figure (3.5) to verify the elements already present in the perovskite. The spectrum of zinc titanate shows peaks corresponding to titanium Zn^{2+} (2p), Ti^{4+} (2p) and O^{2-} (1s) ions at 1022.09, 458.09 and 531 eV, respectively. The XPS spectrum of manganese titanate shows peaks corresponding to Mn^{2+} (2p), Ti^{4+} (2p) and O^{2-} (1s) ions at 644.05, 532.05 and 485.05 eV, respectively.

Figure 3.5

XPS of manganese titanate and zinc titanate

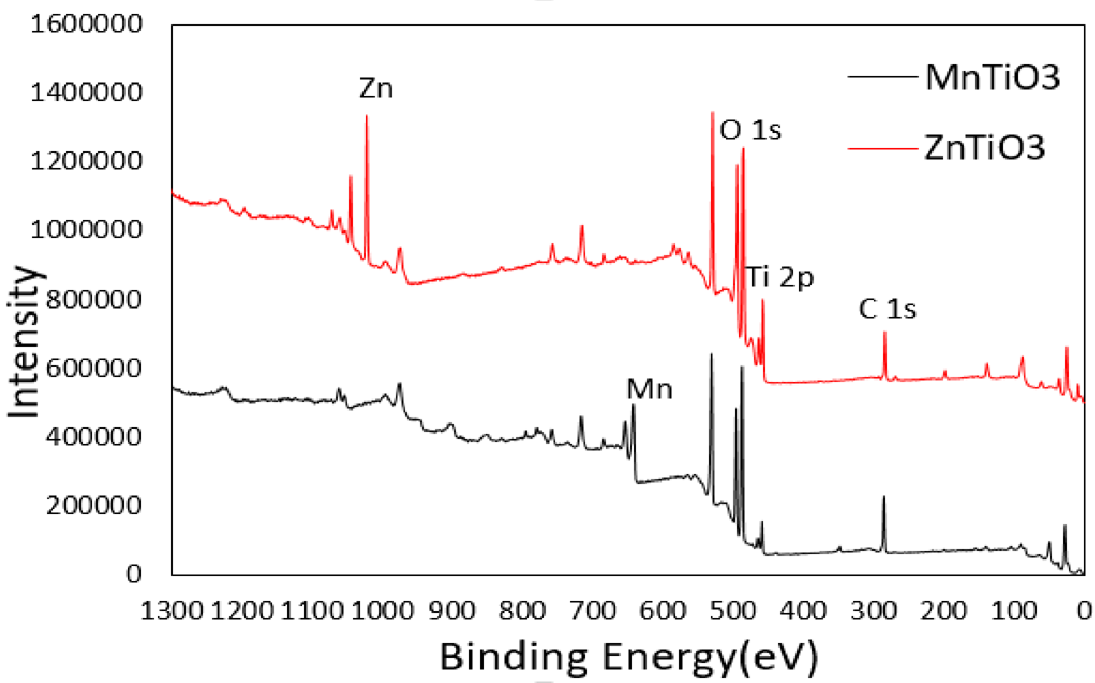

3.1.6 Surface Area Measurement

Surface areas were measured using the adsorbed acetic acid method. Plots of C/N versus C were constructed according to the equation of Langmuir adsorption isotherms as shown in Figure (3.6) and the surface area of the adsorbent was then calculated as explained in Chapter Two. The calculated surface areas for zinc titanate were 115 m^2/g and for manganese titanate 90 m^2/g.

Figure 3.6

Langmuir plots for acetic acid adsorption onto perovskites a) zinc titanate, b) manganese titanate . All experiments were conducted at room temperature

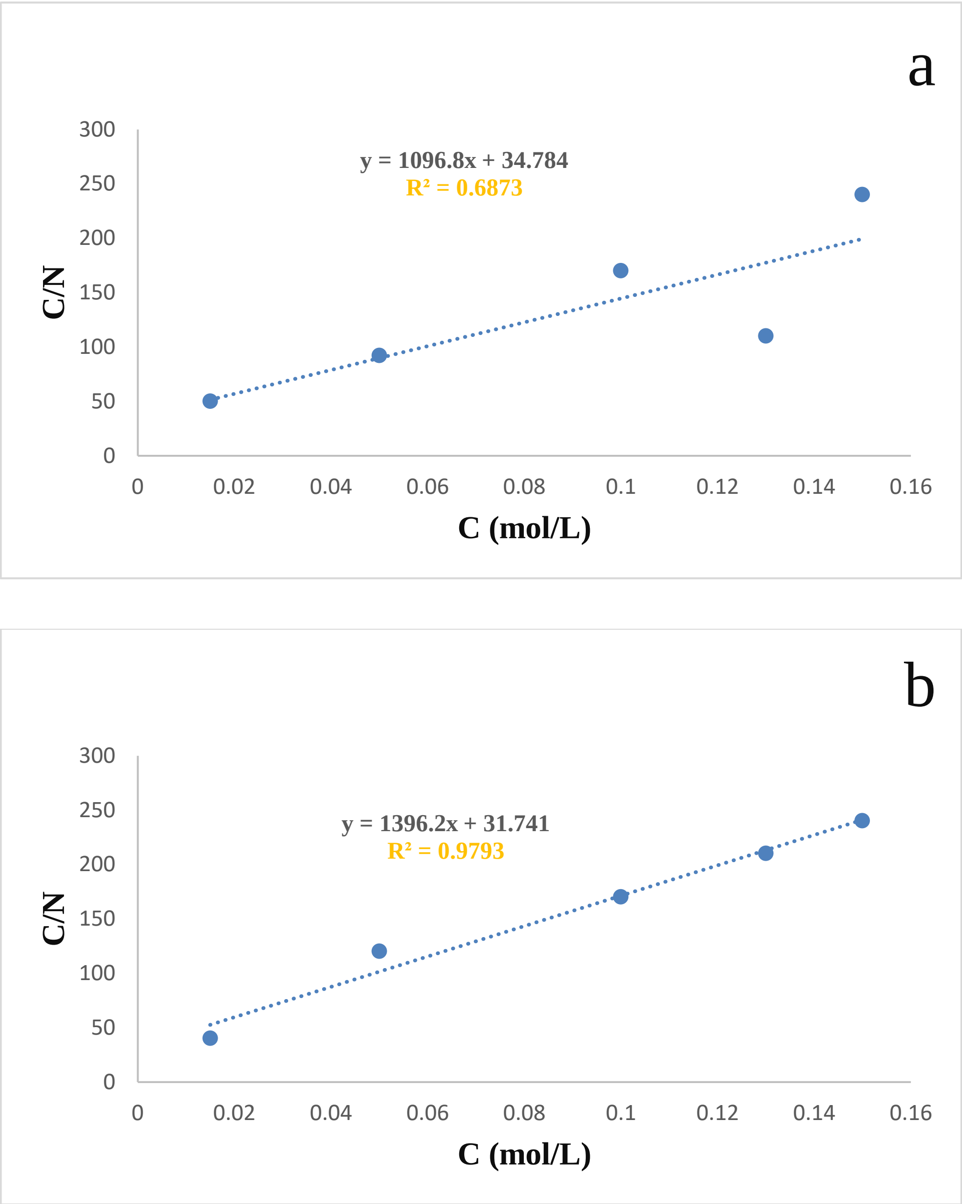

3.2 Photocatalytic result

As described in Chapter 2, methylene blue solutions were irradiated with solar-simulated radiations under various conditions. Both zinc titanate and manganese titanate were examined as photocatalysts. For each catalyst, three types of experiments were done, namely: powder suspension phase, film batch suspension phase and film continuous flow phase.

As described in Chapter 2, control experiments were made. The control experiments confirmed that the lowering in methylene blue was due to photodegradation.

3.2.1 Zinc titanate catalyst

3.2.1.1 Zinc titanate powder system

Zinc titanate powder was used to catalyze the photodegradation of methylene blue contaminant in water using direct light. As manganese titanate, the following reaction parameters were studied for this catalyst system.

- **Effect of contaminant concentration**

Using zinc titanate powder, the impact of contaminant concentration was studied under neutral conditions. 20, 40, 60 and 80 ppm of methylene blue were prepared, and 0.1 g of zinc titanate was added in 100 ml of solution. Zinc titanate powder catalyzed the photodegradation process, as shown in Figure (A.11, in Appendix A).

Figure (A.11, in Appendix A) demonstrates how raising the methylene blue concentration caused the photodegradation to increase. Additionally, the degradation was finished for 10 ppm after 44 min. and for 5 ppm after 41 min. But the amount of photodegradation in high concentrations was greater.

In Table (3.1) values of degradation percentage, amount consumed, turnover number (T.N.), turnover frequency (T.F.) and quantum yield (Q.Y.) were all calculated after 60 minutes for different concentrations of methylene blue (5, 10, 20, 40, 60 and 80 ppm) using 0.1 g of zinc titanate.

Table 3.1

Loss of methylene blue using various concentrations after 60 min radiation. Experiments were conducted with zinc titanate powder (0.10 g) at 25 ℃ and pH 7

Contaminant (ppm)	Degradation %	Amount consumed (ppm)	T.N $*10^6$	T.F $*10^8$	Q.Y $*10^{27}$
5	100	5	0.8	1.3	0.8
10	100	10	1.6	2.6	1.7
20	55	11	1.7	2.9	1.8
40	42.5	17	2.7	4.4	2.8
60	40	24	3.7	6.2	4.0
80	35.6	28.5	4.5	7.4	4.8

Depending on the contaminant degradation percentage, lower methylene blue contaminant concentration shows a higher degradation%. However, table (3.1) shows that the absolute amount of consumed contaminant is higher at higher methylene blue concentrations. Also, the catalyst efficiency calculated in terms of turnover number (T.N), turnover frequency (T.F) and quantum yield value (Q.Y) is higher for higher methylene blue concentration.

- **Photodegradation kinetics of zinc titanate powder**

The kinetics for zinc titanate using 0.1 g of powder at different concentrations of methylene blue was calculated. Figure (A.12, in Appendix A) represents the relationship between ln(initial rate) and ln(initial Conc.), the figure shows the rate order value is 0.7550 and ln k is -3.8592, Thus, the equilibrium constant k is equal to 0.0211 min^{-1}(0.1g $ZnTiO_3$).

- **Effect of zinc titanate loading**

At a constant concentration of methylene blue (40 ppm), under direct light and neutral conditions, the effect of zinc titanate amount (0.05, 0.1, 0.15, 0.2 g) on the photodegradation of methylene blue was studied in 100 ml solution. Look at Figure (A.13, in Appendix A).

For different amounts of zinc titanate powder (0.05, 0.10, 0.15 and 0.20 g), values of T.N., T.F., Q.Y., amount consumed and degradation percentage were calculated after 60 minutes as shown in Table (3.2).

Table 3.2

Effect of perovskite concentration on values of the amount consumed, % degradation, turnover number, turnover frequency and quantum yield for methylene blue degradation after 60 minutes, using zinc titanate powder under direct light

Catalyst weight (g)	Degradation %	Amount consumed (ppm)	T.N $*10^6$	T.F $*10^8$	Q.Y $*10^{27}$
0.05	25	10	3.1	5.2	3.3
0.1	42.5	17	2.7	4.4	2.8
0.15	57	23	2.4	3.9	2.5
0.2	70	28	2.2	3.6	2.3

The results show that the T.N. and T.F. and Q.Y. values decreased with increasing $ZnTiO_3$ amount, while the amount consumed of reaction, degradation percentage were higher with higher $ZnTiO_3$ amounts but higher catalyst amounts cause relative efficiency lowering.

- **Photodegradation kinetics of zinc titanate powder**

The kinetics for Zinc titanate using different amounts of powder at constant concentrations of methylene blue (40 ppm) was calculated. Figure (A.14, in Appendix A) shows that the rate order value is 0.9866 and ln k is -1.3266 and rate constant k = 0.2654 min^{-1}.

- **Effect of pH**

Using a fixed quantity of zinc titanate powder (0.10 g), the effect of pH on methylene blue photodegradation was investigated under simulated light at various pH values (3.5, 7.0, 8.5, and 11.0). Figure (A.15, in Appendix A) demonstrates that at pH = 8.5, photodegradation occurs more quickly.

Values of T.N., T.F., Q.Y., amount consumed of reaction and degradation percentage were calculated after 60 minutes as shown in Table (3.3). The results demonstrate that T.N., T.F., Q.Y., the amount consumed from the reaction, and degradation percentage at pH 8.5 > 11> 7> 3.5.

Table 3.3

Effect of pH on values of amount consumed, turnover number, turnover frequency, % degradation and quantum yield for zinc titanate degradation after 60 minutes under direct light using zinc titanate powder

pH	Degradation %	Amount consumed (ppm)	T.N $*10^6$	T.F $*10^8$	Q.Y $*10^{27}$
11	60	24	3.7	6.2	4.0
8.5	67.5	27	4.2	7.0	4.5
7	42.5	17	2.7	4.4	2.8
3.5	20	8	1.3	2.1	1.3

3.2.1.2 Zinc titanate films batch system

Under various circumstances, methylene blue contamination in water was photodegraded utilizing a zinc titanate film system that was manufactured in the lab.

- **Effect of contaminant concentration**

Zinc titanate film was used to study the impact of concentrations of contaminants under neutral conditions. The film, which contains one layer of zinc titanate on glass ($2.3x10^{-3}$ g), was centered in a 100 ml solution, of various concentrations of methylene blue (20, 40, 60, and 80) were prepared. The zinc titanate film promoted the photodegradation process, shown in Figure (A.16, in Appendix A).

Figure (A.16, in Appendix A) demonstrates how raising the concentration of contaminants caused the photodegradation to rise. Additionally, the degradation was finished for 10 ppm after 40 minutes and for 5 ppm after 35 minutes.

In Table (3.4) values of contaminant degradation percentage, amount consumed, turnover number (T.N.), turnover frequency (T.F.) and quantum yield (Q.Y.) were all calculated after 60 minutes for different concentrations of methylene blue (5, 10, 20, 40, 60 and 80 ppm).

Table 3.4

Effect of contaminant concentration on values of the amount consumed, turnover number, turnover frequency, %degradation and quantum yield for methylene blue degradation after 60 minutes, using one layer of zinc titanate film under direct light and neutral conditions

Contaminant (ppm)	Degradation %	Amount consumed (ppm)	T.N $*10^3$	T.F $*10^5$	Q.Y $*10^{25}$
5	100	5	0.3	0.6	3.6
10	100	10	0.7	1.1	7.3
20	62.5	12.5	0.9	1.4	9.1
40	50	20	1.4	2.3	14.6
60	46.7	28	1.9	3.2	20.3
80	39.4	31.5	2.2	3.6	28.9

The results show that the values of the amount consumed, T.N., T.F. and Q.Y. increased by increasing the concentration of methylene blue. As a result, larger initial contaminant concentrations result in better zinc titanate film catalytic efficiency.

- **Photodegradation kinetics of zinc titanate film**

One layer of zinc titanate film was used to calculate the kinetics at various methylene blue concentrations. The rate order value is 0.5799 and ln k is -2.9449, as shown in Figure (A.17, in Appendix A). Thus, the equilibrium constant k is equal to 0.0526 min^{-1} (monolayer $ZnTiO_3$).

- **Effect of zinc titanate layers**

With different amounts of zinc titanate (one layer equivalent to 0.1 g, two layers equivalent to 0.15 g, and three layers equivalent to 0.2 g) in a 100 ml solution and a constant concentration of methylene blue (40 ppm), the effect of zinc titanate film concentration on the photodegradation of methylene blue was also investigated. Figure (A.18, in Appendix A) demonstrates that using more zinc titanate layers speeds up the process.

Values of T.N., T.F., Q.Y., amount consumed and degradation percentage were calculated after 60 minutes for different layers of zinc titanate as shown in Table (3.5). The results show that the T.N. and T.F. and Q.Y. values increased with increasing layers of zinc titanate, while the amount consumed contaminant, degradation percentage were higher with higher zinc titanate layer.

Table 3.5

Effect of perovskite concentration on values of amount consumed, % degradation, turnover number, turnover frequency and quantum yield for methylene blue degradation after 60 minutes, using zinc titanate film under direct light

Catalyst weight	Degradation %	Amount consumed	T.N	T.F	Q.Y
(g)		(ppm)	$*10^3$	$*10^5$	$*10^{25}$
1 layer	50	20	1.4	2.3	14.5
2 layers	64	25.5	3.5	5.8	37.0
3 layers	74	29.5	6.0	10.0	64.2

- **Effect of pH**

The effect of pH on methylene blue photodegradation was investigated under direct light at different pH values (3.5, 7.0, 8.5, and 11.0) using a single layer of zinc titanate film in 50 ml solution of methylene blue (40 ppm). Figure (A.19, in Appendix A) demonstrates that at pH 8.5, photodegradation occurs more quickly.

Values of T.N., T.F., Q.Y., amount consumed of reaction and degradation percentage were calculated after 60 minutes as shown in Table (3.6). The results show that the values of T.N., T.F., Q.Y., amount consumed and degradation percentage are higher at pH 8.5.

Table 3.6

Effect of pH on values of amount consumed, turnover number, turnover frequency, %degradation and quantum yield for zinc titanate degradation after 60 minutes under direct light using one layer of zinc titanate film

pH	Degradation %	Amount consumed	T.N	T.F	Q.Y
		(ppm)	$*10^3$	$*10^5$	$*10^{25}$
11	62.5	25	1.7	2.8	18.2
8.5	71.2	28.5	1.9	3.2	20.7
7	50	20	1.4	2.3	14.6
3.5	27.5	11	0.75	1.2	8.0

3.2.1.3 Zinc titanate powder vs. zinc titanate film

Zinc titanate powder and film were compared as catalysts for the photodegradation of methylene blue at 40 ppm under direct light. In Figure (A.20, in Appendix A). When both zinc titanate powder and zinc titanate films were used, the photodegradation process progressed with both catalysts. However, Figure (A.20, in Appendix A) demonstrates that zinc titanate film is slightly more efficient than zinc titanate powder in photodegrading methylene blue.

3.2.2 Manganese titanate catalyst

3.2.2.1 Manganese titanate powder system

Manganese titanate powder was used to catalyze the photodegradation of methylene blue contaminant in water using solar simulated light. As zinc titanate, the following reaction parameters were studied for this catalyst system.

- **Effect of contaminant concentration**

Using manganese titanate powder, the effect of contaminant concentration was studied under neutral conditions. Manganese titanate was combined with various concentrations of methylene blue (20, 40, 60, and 80 ppm) in 100 ml solutions. Figure (A.21, in Appendix A) shows how the photodegradation process was accelerated by manganese titanate powder.

Figure (A.21, in Appendix A) shows that the photodegradation amount increased by increasing methylene blue concentration. Additionally, the degradation was finished for 10 ppm after 37 min. and for 5 ppm after 34 min. only.

Table (3.7) shows values of degradation percentage, amount consumed, turnover number (T.N.), turnover frequency (T.F.) and quantum yield (Q.Y.) after 60 minutes for different concentrations of methylene blue (5, 10, 20, 40, 60 and 80 ppm) using 0.1 g of manganese titanate.

Table 3.7

Loss of methylene blue using various concentrations after 60 min radiation. Experiments were conducted with manganese titanate powder (0.1 g) at 25 ℃ and pH 7

Contaminant (ppm)	Degradation %	Amount consumed (ppm)	T.N $*10^6$	T.F $*10^8$	Q.Y $*10^{27}$
5	100	5	0.8	1.3	0.8
10	100	10	1.6	2.6	1.7
20	75	15	2.3	3.9	2.5
40	66.3	26.5	4.1	6.9	4.4
60	56.7	34	5.3	8.8	5.7
80	48.8	39	6.0	10.1	6.5

Lower methylene blue contaminant concentrations exhibit greater degradation% values. Table (3.7) demonstrates that, at increasing methylene blue concentration, the absolute amount of consumed contaminant is larger. Additionally, increased methylene blue concentrations result in higher relative catalytic efficiency as measured by turnover number (T.N), turnover frequency (T.F), and quantum yield value (Q.Y).

- **Photodegradation Kinetics of manganese titanate powder**

The plot of ln(initial rate) vs. ln(conc.) was made to compute the kinetics of manganese titanate using 0.10 g of powder, Figure (A.22, in Appendix A). The rate order value is 0.7083, and the ln k is -3.1384, hence the equilibrium constant k equals 0.0433 min^{-1} (0.1g $MnTiO_3$)

- **Effect of manganese titanate loading**

The effect of manganese titanate powder amount (0.05, 0.1, 0.15, 0.2 g) on photodegradation of methylene blue in 100 ml solution was studied at a constant concentration of methylene blue (40 ppm), under solar simulated light and neutral conditions. Figure (A.23, in Appendix A) shows that increasing the manganese titanate concentration increased the percentage of degradation at the default temperature.

T.N., T.F., Q.Y., amount consumed, and degradation% were calculated after 60 minutes for various amounts of manganese titanate powder (0.05, 0.10, 0.15, and 0.20 g). Table (3.5) summarized these results. The results show that as the $MnTiO_3$ amount increased, the T.N., T.F., and Q.Y. values decreased but the amount consumed of reaction and the degradation% increased. However, an increased catalyst amount results in lower relative catalyst efficiency.

Table 3.8

Effect of perovskite concentration on values of the amount consumed, degradation%, turnover number, turnover frequency and quantum yield for methylene blue degradation after 60 minutes, using manganese titanate powder under solar simulated light

Catalyst weight (g)	Degradation%	Amount consumed (ppm)	T.N $*10^6$	T.F $*10^8$	Q.Y $*10^{27}$
0.05	46.3	18.5	5.8	9.6	6.2
0.1	61.3	24.5	3.8	6.4	4.1
0.15	75	30	3.1	5.2	3.3
0.2	86.3	34.5	2.7	4.5	2.9

- **Photodegradation kinetics of manganese titanate powder**

Figure (A.24, in Appendix A) was used to calculate the kinetics of manganese titanate using varied amounts of powder at constant concentrations of methylene blue (40 ppm). The rate order value is 0.4413 and the ln k is -0.4762, implying that the rate constant k = 0.6211.

- **Effect of pH**

The effect of pH on methylene blue photodegradation was investigated using an equal amount of manganese titanate powder (0.10 g) under direct light and different pH values (3.5, 7.0, 8.5 and 11). Figure (A.25, in Appendix A) indicates that photodegradation was highest at pH 8.5.

After 60 minutes, the values of T.N., T.F., Q.Y., the amount consumed by the reaction, and degradation % were calculated as shown in Table (3.9). The results show that the values of T.N., T.F., Q.Y., amount consumed from reaction and degradation percentage at pH 8.5 is higher than 11 higher than 7 and 3.5.

Table 3.9

Effect of pH on values of the amount consumed, turnover number, turnover frequency, % degradation and quantum yield for manganese titanate degradation after 60 minutes under solar simulated light using 0.1g of manganese titanate

pH	Degradation %	Amount consumed (ppm)	T.N $*10^6$	T.F $*10^8$	Q.Y $*10^{27}$
11	73.8	29.5	4.6	7.7	4.9
8.5	82.5	33.0	5.2	8.6	5.5
7	61.3	24.5	3.8	6.4	4.0
3.5	33.8	13.5	2.1	3.5	2.3

3.2.2.2 Manganese titanate films system

A manganese titanate films system was prepared in the lab and used to catalyze photodegradation of methylene blue contaminant in water using direct light under different conditions.

- **Effect of methylene blue concentration**

Manganese titanate films were utilized to investigate the effect of contaminant concentration on methylene blue degradation under neutral conditions. Methylene blue concentrations of 5, 10, 20, 40, 60, and 80 ppm were employed in 100 mL distilled water with one layer of manganese titanate on glass ($1.8x10^{-3}$ g). Figure (A.26, in Appendix A) depicts how manganese titanate film promotes photodegradation.

Figure (A.26, in Appendix A) shows that as the concentration of contaminant increased so did the rate of photodegradation. The contaminant was completely degraded for 10 ppm after 32 minutes and for 5 ppm after 26 minutes.

The degradation percentage, amount consumed, turnover number (T.N.), turnover frequency (T.F.), and quantum yield (Q.Y.) were all calculated after 60 minutes in Table (B.1, in Appendix B) for varied methylene blue concentrations (5, 10, 20, 40, 60, and 80 ppm). The results show that the values of the amount consumed, T.N., T.F. and Q.Y. increased by increasing the concentration of contaminant. Therefore the efficiency of manganese titanate film catalyst is higher with a higher initial contaminant concentration.

- **Photodegradation kinetics of manganese titanate film**

Using different concentrations of methylene blue, the kinetics of the manganese titanate film were calculated using Figure (A.27, in Appendix A). The rate order value is 0.6536 and ln k -2.5987. The rate constant k = 0.074.

- **Effect of Manganese titanate layers**

The effect of manganese titanate film layers on methylene blue photodegradation was also investigated under direct light and neutral conditions using different layers of manganese titanate (in 100 ml solution and constant concentration of methylene blue (40 ppm). Figure (A.28, in Appendix A) illustrates that adding more layers of manganese titanate slightly speeds up the process.

Values of T.N., T.F., Q.Y., amount consumed and degradation percentage were calculated after 60 minutes for different layers of manganese titanate as shown in Table (B.2, in Appendix B). The results show that the T.N. and T.F. and Q.Y. values increased with increasing layers of manganese titanate. The amount consumed of reaction, and degradation percentage were higher with a higher $MnTiO_3$ layer.

- **Effect of pH**

The effect of pH on methylene blue photodegradation was studied under solar simulated light at various pH values (3.5, 7.0, 8.5, and 11) using one layer of Manganese titanate film in 50 ml solution of methylene blue (40 ppm). Figure (A.29, in Appendix A) indicates that photodegradation is fastest at pH 8.5.

Values of T.N., T.F., Q.Y., amount consumed of reaction and degradation percentage were calculated after 60 minutes as shown in Table (B.13, in Appendix B). The results indicate that at pH 8.5, the values of T.N., T.F., Q.Y., amount consumed during the reaction, and degradation percentage are higher than those at pH 11 and pH 7 and 3.5.

3.2.2.3 Manganese titanate powder vs. manganese titanate film

Manganese titanate powder and film were compared as catalysts for the photodegradation of methylene blue at 40 ppm under solar simulated light.

Both manganese titanate powder and films catalyze the photodegradation reaction. However, Figure (A.30, in Appendix A) demonstrates that in the photodegradation of methylene blue, manganese titanate film is more efficient than manganese titanate powder.

3.3 Zinc titanate vs. manganese titanate catalysts

Zinc titanate and manganese titanate were compared for photodegradation of methylene blue (40 ppm) under neutral conditions. Figure (3.7) shows that manganese titanate is more effective than zinc titanate in methylene blue photodegradation in both cases, powder and film.

Figure 3.7

Zinc titanate and manganese titanate, powders and films, in photodegradation of methylene blue at 40 ppm under neutral conditions

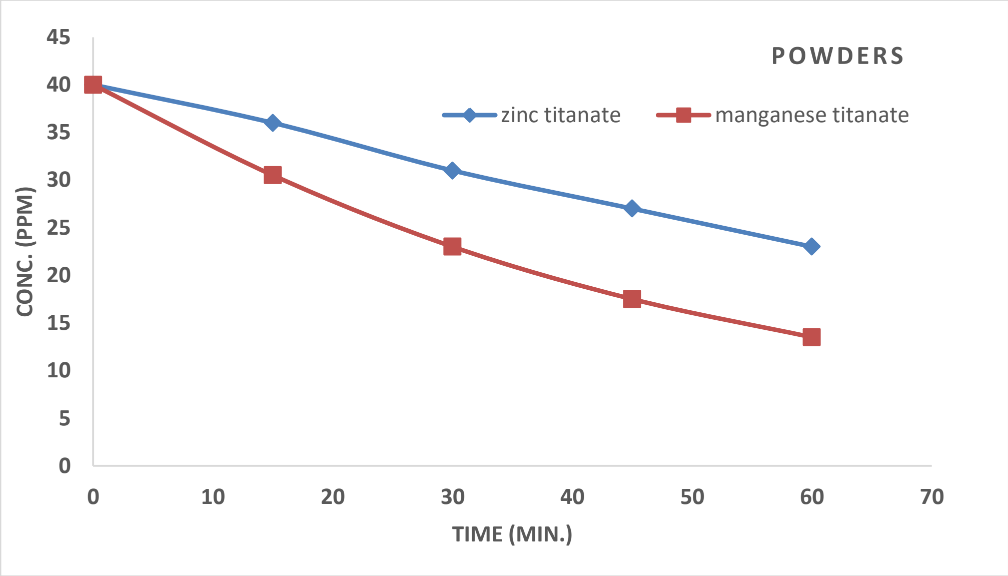

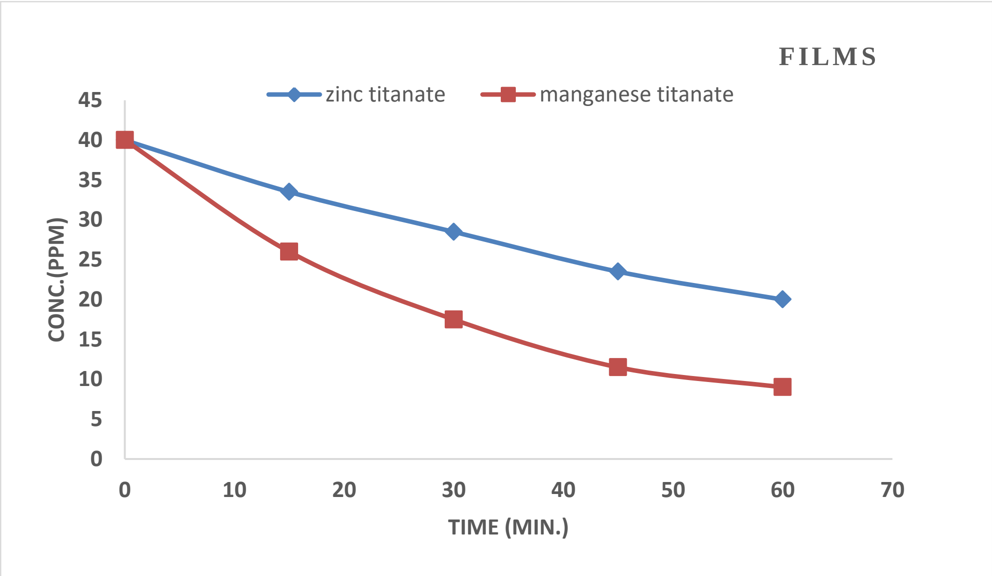

3.4 Continuous flow rate studies

The photodegradation of methylene blue was studied under solar simulated light and neutral conditions using a continuous flow rate technique. In an 80 ppm methylene blue solution, one layer of perovskite film was used. The results of photodegradation of a continuous flow rate and batch systems are not different, as shown in Figure (3.8) in both cases of zinc titanate and manganese titanate. Moreover, manganese titanate is more effective than zinc titanate in both batch and continuous flow rate.

Figure 3.8

Manganese titanate film and zinc titanate film using continuous flow rate technique and steady solution were compared as catalysts for photodegradation of methylene blue at 80 ppm under solar simulated light and neutral conditions

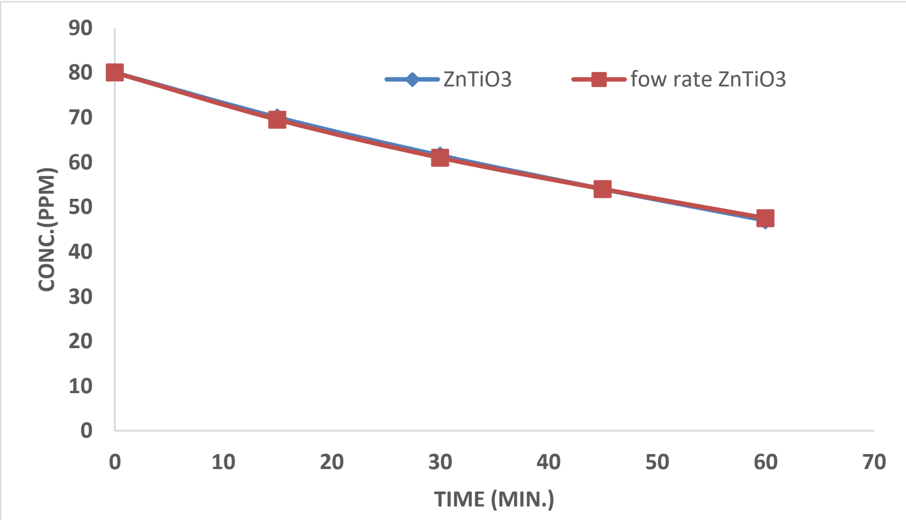

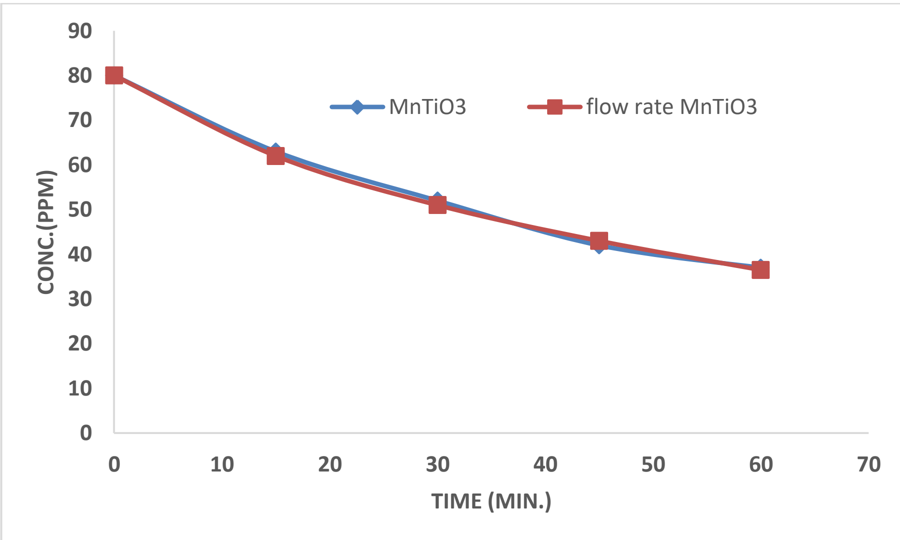

3.5 Recovery and reuse of catalyst powder and Films

Perovskite powder and film recovery were studied twice at room temperature. Figure (3.9) shows that the powder of manganese titanate is a little decreased and 85% of the powder is recovered but the film remained the same. In the case of zinc titanate, the powder decreased and ~80% of the powder is recovered but the film remained the same. For zinc titanate, only ~80% of catalyst powder is recovered and the efficiency has been lowered by ~12% on reuse. Similarly, only about 85% of manganese titanate powder is recovered with efficiency lowering ~20% on reuse.

Additionally, Perovskite powder and film reuse were studied at room temperature. Figure (3.30) shows that the photodegradation for manganese titanate powder decreased by ~12% on reuse while and the photodegradation for zinc titanate powder decreased by ~20% on reuse. In the case of the film, the photodegradation was not affected much.

Figure 3.9

Recovery of perovskite powder and Film (1) fresh, (2) first recovery and (3) second recovery

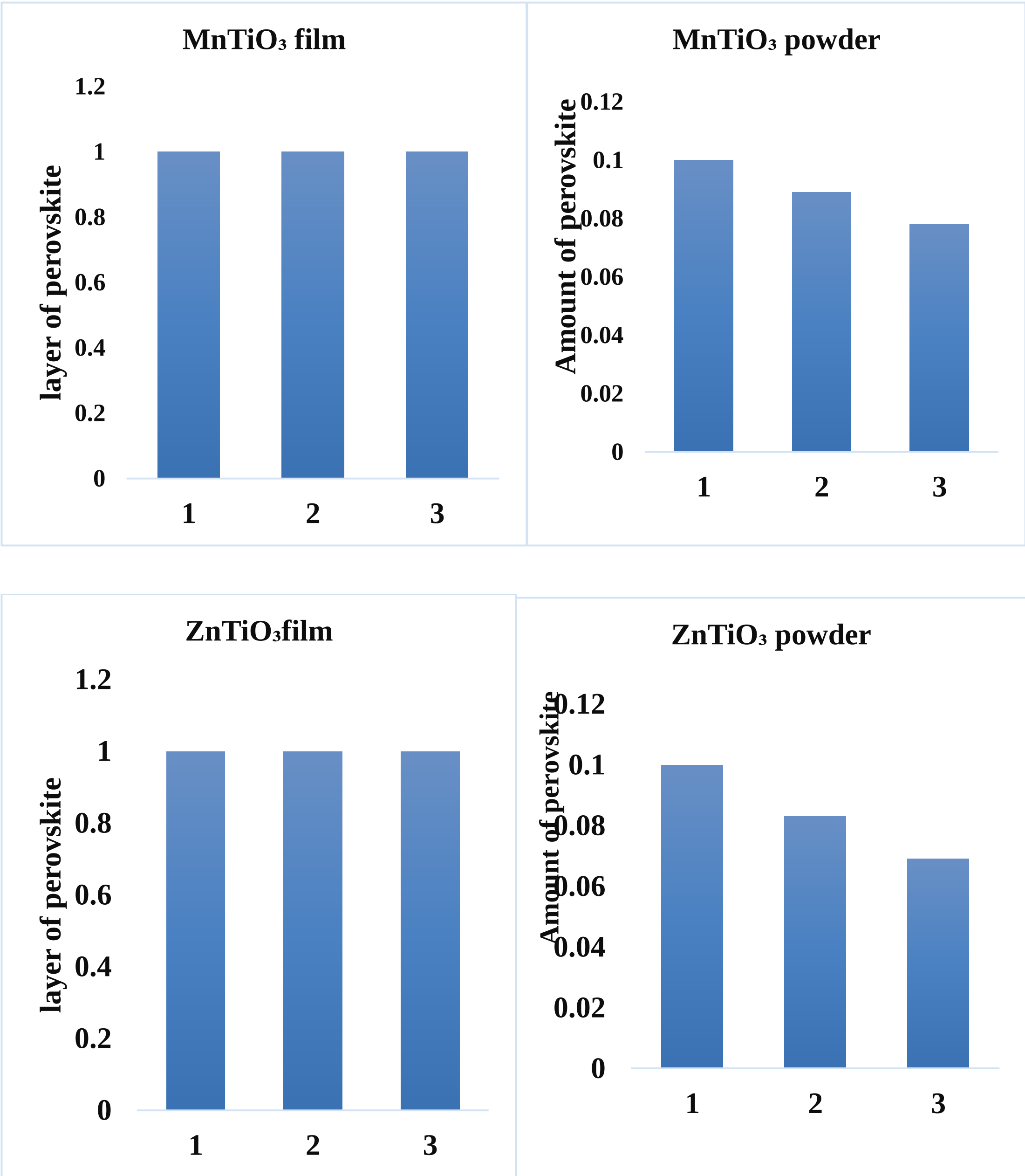

Figure 3.10

Reuse of perovskite powder and Film (a) photodegradation first time, (b) after reuse

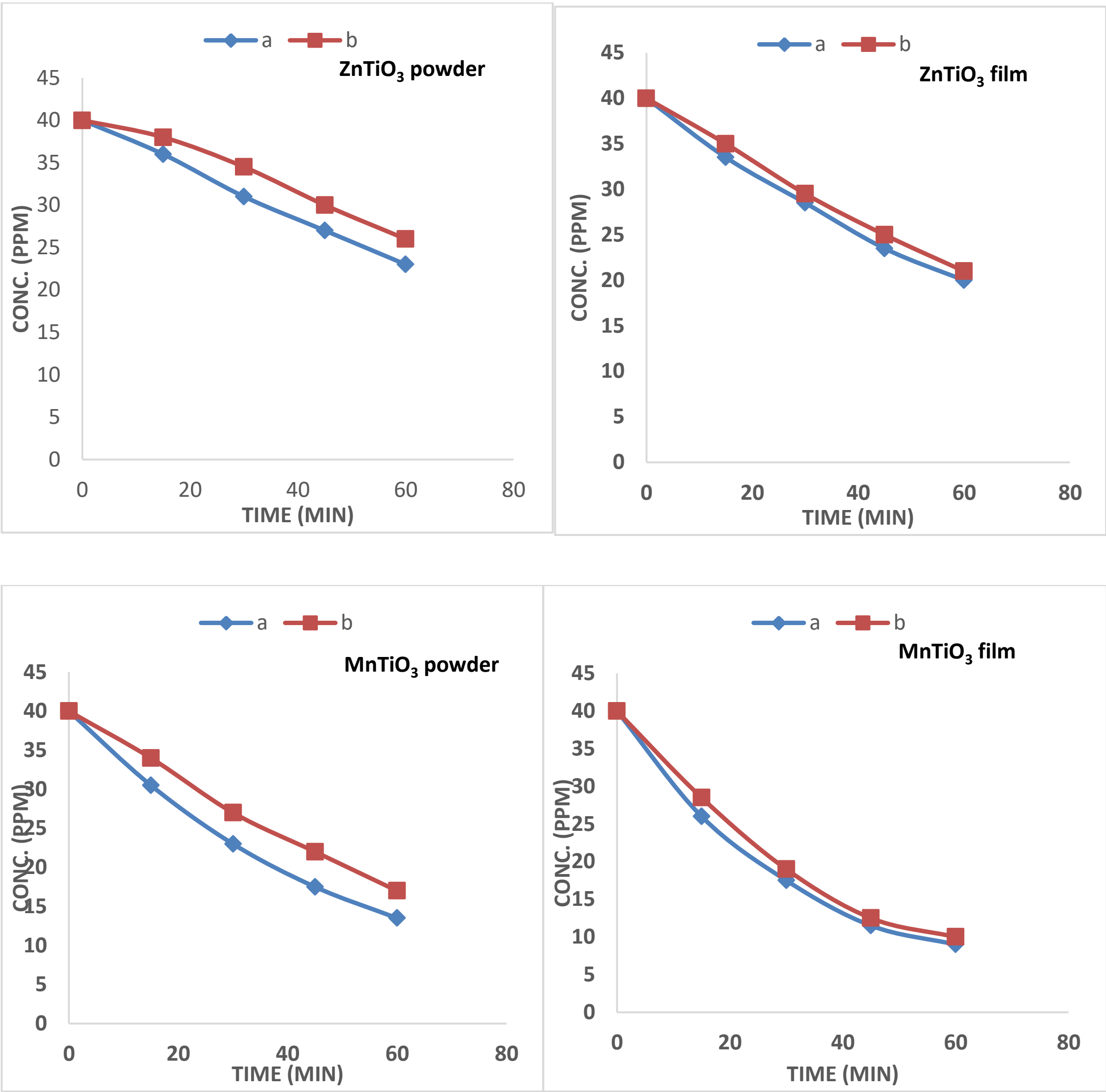

3.6 Photodegradation of perovskite powders and film for longer hours at pH 8.5

The photodegradation of powders and film was studied for long times at 40 ppm of methylene blue at pH 8.5. This was to know the duration of the photodegradation, and it was confirmed by studying the analysis of produced nitrate ions after the photodegradation end as explained in Chapter 2 as shown in Table (B.4, in Appendix B). The photodegradation of perovskite powders and film vs. time are shown in Figure (A.31, in Appendix A).

Chapter Four

Discussion

The results shown in Chapter 3 indicated that two types of perovskites were prepared in their powder and film forms. The materials were then characterized to confirm their preparation, and then employed as photocatalysts to degrade methylene blue contaminant in water under solar simulated radiations. The characterization and photocatalytic results are discussed in this Chapter.

4.1 Catalyst characterization

Characterizations of the zinc titanate and manganese titanate powders used in the photodegradation experiments and used to prepare the films are discussed here.

4.1.1 Photoluminescence (PL) spectra

In the photoluminescence spectra, Figure (3.1, in Chapter 3), the zinc titanate emission peak (352) occurred at a shorter wavelength than that for manganese titanate (403). The value for zinc titanate matches an earlier literature which displays that emission is at wavelength 360 nm [95], while the value for manganese titanate is similar to value the literature value of 410 nm [96]. The emission appears at a shorter wavelength in both synthesized perovskites than was previously reported. This is a result of the prepared materials being more disorderly than usual. Bigger levels of disorder result in bigger band gap values and shorter emission wavelengths.

The emission spectra indicated that the band gap value for zinc titanate is 3.52 eV, which is close to literature values reported earlier that is 3.1-3.65 eV [97, 98]. For manganese titanate, the band gap was 3.08 eV, which resembles the literature value of 3.18 eV [99]. These findings are useful in explaining the photocatalytic differences between the two perovskite materials.

4.1.2 Electronic absorption (UV-visible) spectra

In the spectrum of the zinc titanate suspension, a band of maximum wavelengths appears at 338 nm, and an edge can be seen at ~350 nm as shown in Figure (3.2, a in Chapter 3) whereas maximum wavelengths absorption of manganese titanate suspension appears at 390 nm and an edge can be seen at ~400 nm as shown in Figure (3.2, b in Chapter 3) this mean manganese titanate showed a spectrum with a maximum absorbance at a longer wavelength than that for zinc titanate suspension. The results here are consistent with the PL spectra results, and confirm the fact that manganese titanate has a narrower band gap value than zinc titanate.

4.1.3 Surface Morphology (SEM Analysis)

The results showed that both perovskites had agglomerates, but zinc titanate powder exists in smaller agglomerates than the manganese titanate powder as shown in Figures (3.3, a in Chapter 3) and (3.3, b in Chapter 3) with sizes of ~300 and ~250 for manganese titanate and zinc titanate, respectively. The SEM micrographs also showed that the large agglomerates themselves involve smaller agglomerates as well. The SEM for zinc titanate showed agglomerates of roughly spherical shapes, which live more independently. For manganese titanate, the SEM micrograph shows agglomerates with more flat surfaces.

In perovskite film form zinc titanate film also shows agglomerates of more spherical shapes packaged sparingly as shown in Figure (3.3,c in Chapter 3) whereas in manganese titanate film, the agglomerates are more uniformly distributed, flattened in shape, and more compact as shown in Figure (3.3, d in Chapter 3).

Figures (3.3, e in Chapter 3) and (3.3, f in Chapter 3) display the film cross-sectional micrographs for the zinc titanate film and manganese titanate film, respectively. The average thickness of both films is nonuniform. The Figures also show that the film of manganese titanate contains more compact and larger agglomerates than zinc titanate film

Values obtained from cross-sectional micrographs directly depict the film thicknesses, making them more trustworthy than those obtained from gravimetric calculations. The total quantities of perovskites in the monolayer films (1x4 cm^2) for zinc titanate and manganese titanate are $2.3x10^{-3}$ and $1.8x10^{-3}$ g, respectively, based on SEM film thickness data. In this calculation of film efficiency, these factors will be taken into consideration.

4.1.4 XRD structural Analysis

XRD patterns were measured for both zinc titanate powder and manganese titanate powder at room temperature as shown in Figure (3.4, in Chapter 3). The results showed that the average crystallite size for zinc titanate (~17 nm) is larger than that for manganese titanate (~15 nm) based on the Scherrer equation.

It is well known that for the same material, larger particle size is associated with smaller band gap values [100]. These results indicate that the difference in band gap values for the two perovskites is not due to crystallite size itself. The difference between the two material band gap values is thus due to the intrinsic properties of the two perovskites. Two different materials tend to have two different band gap values.

By comparing the observed reflections to prior publications [101] it has been shown that zinc titanate has a cubic structure. This is proof that the perovskite substance is present. Additional signals can be due to the formation of TiO_2 and $Zn_2Ti_3O_8$ [99]. Also for manganese titanate structure, the reflections are consistent with earlier reports [64]. Additional signals can be due to other phases such as TiO_2 [102].

4.1.5 XPS analysis

In order to characterize the prepared materials, additional analysis for existing elements was performed. X-ray photoelectronic spectroscopy (XPS) was used as shown in Figure (3.5, in Chapter 3). The method is useful to show existing elements in each material, together with their oxidation states. For zinc titanate, it is possible to clearly see all peaks associated with Zn^{2+} (2p) at 1022.09 eV, Ti^{4+} (2p) at 458.09 eV, and O^{2-} (1s) ions at 531 eV. Similar peaks for $ZnTiO_3$ were previously reported at 1021, 458.5, and 530.2 eV [94]. the carbon 1s peak, which appears in XPS spectra around 284.09 eV, is attributed to the presence of impurities.

The XPS spectrum for manganese titanates presents Mn^{2+} 2p, Ti^{4+} (2p) and and O^{2-} (1s) at 644.05 eV, 532.05 at eV and 485.05 eV, respectively are similar to the published values for $MnTiO_3$ perovskite at 645.6, 485.3, and 531.1 eV [70]. The carbon 1s peak that was found at 285.05 eV, is due to impurities.

The results of XPS confirmed the nature of materials observed by the XRD patterns for both zinc titanate and manganese titanate and confirmed the preparation of both perovskites in this work. The results are consistent with PL spectra, electronic absorption spectra and XRD pattern analysis, as previously described

4.1.6 Surface Area Measurement

Figure (3.6, in Chapter 3) shows the specific surface area (SSA) for zinc titanate and manganese titanate powers, measured at room temperature by Langmuir plots for acetic acid adsorption. And the powder surface areas for monolayer coverage have been calculated. The results showed that the specific surface area is 115 m^2/g and 90 m^2/g for zinc titanate and manganese titanate, respectively. That means zinc titanate is a larger SSA than manganese titanate. This is caused by the randomness of zinc titanate more than manganese titanate, where manganese titanate is more uniform. This has been confirmed by SEM, zinc titanate is more spherical in shape whereas manganese titanate has flat surfaces. In both instances, the current perovskite materials exhibit greater SSA values than their equivalents from prior literature [70, 75].

4.2 Methylene blue photocatalytic degradation

Both perovskites were examined as photocatalysts for photodegradation of methylene blue contaminate in water. Powder and film forms of each perovskite were examined, in batch experiments, and showed efficiency in removing methylene blue by photodegradation. Moreover, film forms of both perovskites were examined in continuous flow rate experiments. The results described in Chapter 3 are discussed here.

4.2.1 Effect of pH

The results demonstrate that T.N., T.F., Q.Y., the amount consumed from the reaction, and degradation percentage at pH 8.5. For the two perovskites, values of T.N., T.F., and Q.Y., the amount consumed and degradation percentage are highest at pH 8.5. The degradation percent varied with pH value in the order 8.5>11.0>7.0>3.5. The trend shows that catalytic activity increases under basic conditions. However, pH 8.5, which is slightly basic, shows the highest catalyst activity among the series. This applies to manganese titanate and zinc titanate catalysts in their various forms, powder, batch films and continuous flow films. As shown in Figures (A.15, A.19, A.25 and A.29 in

Appendix A). The effect of pH on catalyst activity can be justified by values of point of zero charge (P_{ZC}) for the catalyst surfaces and the states of the contaminant molecules. Figure (A.32 in Appendix A) shows the structural change of methylene blue with solution pH value.

In literature, the methylene blue structure varies with the solution pH value, as described in Figure (4.1, in Appendix A). At pH values lower than 5.6, the material exists in the cationic acidic form with a positive charge at one N atom. At a higher pH value, the molecule exists in the neutral form with no positive charges [103].

The values of P_{ZC} for zinc titanate and manganese titanate are 7.83 and 7.80, respectively [104, 105]. Therefore, both solid material surfaces are positively at a pH lower than 7.8 and are negatively charged when the pH value is above 7.8. At a pH of approximately 7.8, the solid surfaces should have nearly zero net charges.

In photocatalytic degradation processes, the semiconductor surface is excited by radiation to yield oxidizing active species such as ($OH^{\cdot}$), as described in the mechanism section. For the contaminant molecule to react, it must be close to the semiconductor surface, preferably being adsorbed there onto. Therefore, the semiconductor surface charge and the methylene blue charge affect the degradation, as follows:

- At low pH values: Methylene blue exists in cationic form (MB^+) in an acidic medium and a neutral in highly basic medium [106]. The semiconductor surface is also positively charged. Therefore, the methylene blue molecules are repelled away from the surface. In this case, the methylene blue is kept away from the resulting oxidizing species (which occur nearby the surface). The degradation reaction is therefore slowed down.
- At high pH (11) values, the semiconductor surface carries a negative charge, while the methylene blue carries a neutral charge. In this case, there are some electrostatic attractions between the positively charged H atom of methylene blue and the surface negative charges. Such attractions encourage the methylene blue to come close to the surface and interact with the oxidizing species near the surface. This explains why at higher pH the reaction is faster than at lower pH. However, the negatively charged N atoms in the methylene blue are repelled by the negatively charged

surface. Therefore, the reaction is still slowed down at high pH.

- At pH value 8.5 (which is close to 7.8) the semiconductor surface is approximately neutral, and the methylene blue is also neutral. This allows better adsorption of the methylene blue to the semiconductor surface. In this case, the methylene blue H atoms (positively charged) can be attracted to the semiconductor surface O atoms (negatively charged). Moreover, the methylene blue N atoms (negatively charged) can also be attracted to the semiconductor surface H atoms (positively charged). Therefore, the pH 8.5 value encourages more and more adsorption of methylene blue molecules onto the semiconductor surface. This adsorption keeps the contaminant molecules close to te surface and close to the oxidizing $OH^{\cdot}$ species that result after semiconductor excitation with incident radiations. This justifies the relatively fast photodegradation reaction at pH 8.5.

Typically speaking, surface waters have pH values in range 6.5 – 8.5, while ground waters have pH values of 6-8.5 [107]. The results show the value of using both semiconductor materials as photocatalysts for water treatment under natural conditions of pH ~8.5. These results are partially consistent with previous results for perovskite powder, where degradation of methylene blue increased with higher pH [67, 108]. The results here are more accurately specified at moderate pH and more practical for future application.

4.2.2 Effect of contaminant concentration

For both perovskite (zinc titanate and manganese titanate), with increasing initial concentration of the methylene blue contaminant, the photodegradation reaction is faster whether it's powder or film as shown in Figure (A.11, A.16, A.21and A.26 in Appendix A). This is due to the arrival of contaminant molecules to the active sites of the photocatalyst surface, where at high concentrations the probability of the reaction of reactive species (•OH and $•O^{2-}$) with methylene blue is higher. Details of proposed mechanisms, based on earlier mechanisms proposed for other photocatalytic processes, described in literature, will be discussed later in this Chapter.

Therefore, the higher the concentration of the contaminant, the faster the reaction must proceed. This is due to exposure of more contaminant molecules to the catalytically active sites and the active species that result nearby, as will be discussed later. These results are consistent with the results of other previously reported research showing that the concentration of contaminant increases the rate of photodegradation reactions of methylene blue in the presence of these perovskites powder [67, 75].

Although lower contaminant concentrations showed higher percent of degradation, the real amounts of degraded molecules were higher in the case of higher contaminant concentrations. This was confirmed by comparing the values of T.N., T.F. and Q.Y. for experiments performed using various contaminant concentrations, as shown in Tables (3.1, 3.4, 3.7 and 3.10 in Chapter 3). These results indicate that the efficiency of perovskite powder is higher with a higher initial concentration of methylene blue. These results were observed for both perovskites in their powder and film forms in batch and in continuous flow experiments.

4.2.3 Effect of perovskite loading

Photodegradation of methylene blue was faster with higher perovskite loading for both catalysts in their powder and film as shown in Figures (A.13, A.18, A.23 and A.28 in Appendix A). With more perovskite particles, there will be higher numbers of active catalyst sites. Therefore, the reactant molecules will have higher chance to interact with the catalyst sites in case of higher catalyst loading. These results are consistent with earlier studies [109].

For the two perovskites, values of T.N., T.F. and Q.Y. decreased with increasing perovskite amount. That means that the relative catalyst perovskite is lowered in case of higher perovskite amounts. This is because the presence of large amounts of perovskite particles blocks the entry of more light into the reaction mixture. Therefore, less perovskite particles are excited by the incident photons, and consequently, less oxidizing species of free radicals can be formed.

4.3 Powders vs. Films

Zinc titanate film is more efficient than zinc titanate powder in photodegrading methylene blue. Also, manganese titanate film is slightly more effective than manganese titanate powder in methylene blue photodegradation as shown in Figure (A.20 and A.30 in Appendix A).

This is because powder particles at the reaction mixture surface obstruct the photons from reaching other particles in the solution. In this case, the catalyst particles inside the reaction mixture bulk may not be oxidized. This lowers the catalyst efficiency in case of particle systems. On the other hand, the film electrode surfaces are fully exposed to reaching photons. Therefore, the catalyst active sites will be exposed to the photons.

The perovskite higher efficiency in their film form compared to their powder form counterparts is important for application purposes. It is known that nanopowder photocatalysts are suspended in the water during treatment. Due to their small sizes, they cannot be easily removed from the treated water. This creates technical difficulties for water treatment processes at large commercial scales. Using the film catalysts is therefore advantageous. In case of film catalyst experiments, the films can be removed and recovered from the reaction mixtures with simple methods. This is a great advantage for using the film catalyst systems here. With their higher catalyst efficiency, the film catalyst systems can provide solutions for the technical difficulty shown above.

4.4 Zinc titanate vs. manganese titanate

Manganese titanate is more efficient than zinc titanate at photodegrading methylene blue in both powder and film forms as shown in Figure (3.7 in Chapter 3), this is because the energy gap of the zinc titanate (3.52 eV) is larger than that of manganese titanate (3.08 eV). Additionally, manganese titanate has a lower surface area than zinc titanate. The photodegradation process is accelerated by this factor, which increases absorption capabilities.

Manganese titanate requires longer wavelength radiations since its band gap is smaller than zinc titanate. More radiation is emitted at wavelengths greater than 400 nm by the solar simulation lamp. Manganese titanate is hence more susceptible to solar-simulated radiations. Because of this, manganese titanate is a more effective catalyst than zinc titanate.

4.5 Continuous flow rate studies

Using a continuous flow rate technique, the photodegradation of methylene blue was investigated under neutral conditions and solar simulated light by using films for both perovskites because the film is more active than powder and better at the photodegradation of methylene blue. The results are summarized in Figure (3.8 in Chapter 3). the result shows that the continuous flow rate for both perovskite films does not slow down the reaction and the reaction is the same speed as batch systems at the same time, also manganese titanate film is still more active than zinc titanate film, where the degradation% at 80 ppm for manganese titanate film in continuous flow rate is 53.8% while in zinc titanate is 39.4 %. This is a benefit and feature for film catalyst systems since the continuous flow reaction shows very high catalytic efficiency in the photodegradation of methylene blue. Future large-scale purifying procedures may benefit from the current procedure.

4.6 Photodegradation kinetics discussion

The photodegradation kinetics reaction of methylene blue contaminant in water was calculated in terms of contaminant concentration effect, using powder and film forms of each perovskite. The well-known initial rate method was followed by plots of ln(initial rate) against ln(initial conc) to find the reaction rate order and rate constant. Figures (A.12, A.17, A.22 and A.27 in Appendix A) summarize the findings.

In case of zinc titanate powder catalyst, the rate order with respect to contaminant was ~0.76, and the rate constant value was 0.021 min-1. In case of zinc titanate film, the rate constant value was 0.0526 min^{-1}. Depending on the rate constant value, zinc titanate film shows slightly higher efficiency than the powder form.

For the manganese titanate powder catalyst, the reaction rate order with respect to the contaminant was 0.7083 min-1 and for manganese titanate film was 06536. This means that the reaction rate increases with higher contaminant concentration, like the case with zinc titanate. Additionally, the reaction rate constant of manganese titanate powder was 0.6211 min-1 while the rate constant of manganese titanate film was 0.0740 min-1, this means also manganese titanate film shows slightly higher efficiency than the powder form.

According to the rate constant values in both powder and film forms, zinc titanate is less effective than manganese titanate as a catalyst. As described earlier, the explanation is attributed to that zinc titanate has a bigger band gap, corresponding to ~352 nm, than manganese titanate with ~403 nm.

Additionally, both perovskites film catalysts have larger rate constant (k) values than their powder counterparts. The differences between films and powders here may not be evident from the rate constant values of 0.0211, 0.0433, 0.0526, and 0.0740 min-1 for zinc titanate powder, manganese titanate powder, zinc titanate film, and manganese titanate film, respectively. However, because there are significantly fewer amount of catalysts in the film form than in the powder form, the rate constant values (min^{-1}/g catalyst) would be substantially larger for the film counterparts than for the powder counterparts.

To confirm these results, the rate constant with respect to the powders catalyst loading on photodegradation of methylene blue was studied using the initial rate method as shown in Figures (A.14 and A.24 in Appendix A) which indicates the higher loading of the catalyst, the faster the reaction and causes a greater degradation of methylene blue molecules through 60 min.

The catalyst sites in the reaction bulk may be obscured from incident photons by moving catalyst particles in the powder form. As a result, under the experimental circumstances, a quicker reaction is induced by increased catalyst loading.

At different loading of catalysts, reaction order values are 0.9866 and 0.4413 for zinc titanate powder and manganese titanate powder respectively. While the rate constant k with respect to the catalyst is 0.2654 min^{-1} and 0.6211 min^{-1} for zinc titanate powder and manganese titanate powder respectively. This means manganese titanate powder shows higher efficiency than zinc titanate. Increasing catalyst loading accelerates the reaction in both perovskite powders, but not necessarily linearly.

4.7 Recovery and reuse of catalyst powder and Films

Perovskite powder and film recovery and reuse were investigated as shown in Figure (3.9) and (3.0) which summarizes each system's efficiency for reusing catalyst. The recovered mass is lower than the fresh catalyst mass in each recovered powder. When zinc titanate is reused, only 80% of the catalyst powder is recovered, and the efficiency decreases by 12%. Similar to manganese titanate, only around 85% of the powder is recovered, and efficiency decreases by about 20% when it is reused. The findings demonstrate that both powders may maintain their efficiency during recovery and reuse, and the effectiveness reduction is caused by catalyst loss during handling.

Simple recovery techniques were used to recover the film catalysts with no mass loss with retaining the efficiency of perovskite films upon recovery. In terms of simple recovery and efficiency retention, while reusing, the results support the appropriateness of film catalyst systems when doing large-scale photodegradation procedures, this should be helpful.

4.8 Perovskite powders and film for longer hours at pH 8.5

The photodegradation of perovskite powders and film vs. time for a long time at 8.5 pH is shown in Figure (A.31 in Appendix A). The time needed for complete photodegradation was 5, 4.5, 3.5 and 3 h for zinc titanate powder, zinc titanate film, manganese titanate powder and manganese titanate film, respectively as shown in Table (B.4 in Appendix B).

To verify that the methylene blue contamination was indeed photodegraded, the concentration of nitrate ions was measured. The amount of nitrate ion is 3.32, 3.4, 4.34 and 4.5 for zinc titanate powder, zinc titanate film, manganese titanate powder and manganese titanate film, respectively as shown in Table (B.4 in Appendix B).

Knowing that one methylene blue contaminant includes 42 g of nitrogen and that methylene blue has a molar mass of 319.85 g/mole, the maximum predicted NO^{3-} ion concentration in the resultant solution would have to be 5.2 ppm. Table 1 displays the nitrate ion production at quantifiable quantities that are close to the predicted value. This demonstrates that the contaminating molecules achieved full mineralization during photodegradation. Other nitrogen species, such as nitrite ions, nitrogen gas, ammonia gas, nitrogen oxide gases, or other species may also produce.

As described above in the introduction, 25 ppm is the maximum amount of methylene blue that can be present in drinking water. Also, the maximum allowable nitrate value is between 10 and 50 ppm According to earlier research [92]. Therefore, complete mineralization of 40 ppm methylene blue is useful and results in water with permissible limits.

Manganese titanate is more active than zinc titanate, this is because the energy band gap of manganese titanate is shorter than zinc titanate which increases the photodegradation reaction for manganese titanate, also the film is more active than powder, this is due to the reason that powder particles in the reaction mixture's surface prevent photons from reaching other particles in the solution.

According to the experiments, both of the perovskites need UV light. The reaction can't go forward efficiently with just visible light. This is because the two systems' wide bandgap nature necessitates short wavelengths. Thankfully, both catalysts successfully operate under solar simulated radiations utilizing the UV tail of 5% of the arriving solar radiations.

4.9 Conclusions

Two types of perovskite powders, $ZnTiO_3$ and $MnTiO_3$, involving mixed phases, were prepared, characterized and examined as photocatalysts for methylene blue removal from water using solar simulated radiation. Complete mineralization of the contaminant was confirmed by the loss of the stable phenyl group and the production of nitrate ions in the treated water. Both catalysts showed high efficiency, with MnTiO3 having the upper edge due to its narrower band gap. The values of turnover frequency and quantum yield for both catalysts were studied. The catalysts functioned under various pH values, but more profoundly at 8.5 based on the point of zero charge. Films prepared from the perovskite powders exhibited much higher photocatalytic efficiency in batch reaction systems than their powder counterparts, as evidenced from values of turnover frequency and quantum yield values. Continuous flow experiments also showed the feasibility of both perovskite films for water purification through photodegradation of organic contaminants in future commercial processes. Both catalysts readily functioned under various contaminant concentrations, which showed their abilities to yield contaminant-free water. Compared to earlier studies, the results show the value of replacing powder from catalyst systems with film catalysts to facilitate catalyst recovery and reuse with no efficiency loss. The results also confirm the usefulness of film catalysts for using non-costly solar-driven processes in water purification from organic contaminants, with methylene blue being a model contaminant.

References

[1] Hassaan, M.A., A. El Nemr, and A. Hassaan, *Health and environmental impacts of dyes: mini review.* American Journal of Environmental Science and Engineering, 2017. 1(3): p. 64-67.

[2] Inamuddin, *Xanthan gum/titanium dioxide nanocomposite for photocatalytic degradation of methyl orange dye.* International Journal of Biological Macromolecules, 2019. 121: p. 1046-1053.

[3] Santika, N. *Water Pollution Analysis in Yogyakarta Special Region In 2019*. in *Journal of International Conference Proceedings*. 2021.

[4] Benkhaya, S., S. M'rabet, and A. El Harfi, *A review on classifications, recent synthesis and applications of textile dyes.* Inorganic Chemistry Communications, 2020. 115: p. 107891.

[5] Abd-Elhamid, A., et al., *Enhanced removal of cationic dye by eco-friendly activated biochar derived from rice straw.* Applied Water Science, 2020. 10: p. 1-11.

[6] Bouras, H.D., et al., *Biosorption characteristics of methylene blue dye by two fungal biomasses.* International Journal of Environmental Studies, 2021. 78(3): p. 365-381.

[7] Yahyaa, F., et al., *Photodegradation of methylene blue catalyzed by tungstophosphate/aerogel hybrid materials under ultraviolet irradiation.* DESALINATION AND WATER TREATMENT, 2020. 195: p. 321-333.

[8] Lachheb, H., et al., *Photocatalytic degradation of various types of dyes (Alizarin S, Crocein Orange G, Methyl Red, Congo Red, Methylene Blue) in water by UV-irradiated titania.* Applied Catalysis B: Environmental, 2002. 39(1): p. 75-90.

[9] Pandey, S., et al., *Fast and highly efficient removal of dye from aqueous solution using natural locust bean gum based hydrogels as adsorbent.* International Journal of Biological Macromolecules, 2020. 143: p. 60-75.

[10] Forgacs, E., T. Cserháti, and G. Oros, *Removal of synthetic dyes from wastewaters: a review.* Environment international, 2004. 30(7): p. 953-971.

[11] Jabbari, V., et al., *Green synthesis of magnetic MOF@ GO and MOF@ CNT hybrid nanocomposites with high adsorption capacity towards organic pollutants.* Chemical Engineering Journal, 2016. 304: p. 774-783.

[12] Sahu, S., et al., *Kendu (Diospyros melanoxylon Roxb) fruit peel activated carbon—an efficient bioadsorbent for methylene blue dye: equilibrium, kinetic, and thermodynamic study.* Environmental Science and Pollution Research, 2020. 27: p. 22579-22592.

[13] Khan, I., et al., *Review on methylene blue: Its properties, uses, toxicity and photodegradation.* Water, 2022. 14(2): p. 242.

[14] Zhang, J., et al., *Photocatalytic and degradation mechanisms of anatase TiO 2: a HRTEM study.* Catalysis Science & Technology, 2011. 1(2): p. 273-278.

[15] Saad, M.E.K., et al., *Removal of methylene blue onto mineral matrices.* Desalination and Water Treatment, 2015. 56(10): p. 2773-2780.

[16] Wijaya, R., et al., *Green reduction of graphene oxide using kaffir lime peel extract (Citrus hystrix) and its application as adsorbent for methylene blue.* Scientific reports, 2020. 10(1): p. 667.

[17] Kulis-Kapuscinska, A., et al., *Photocatalytic degradation of methylene blue at nanostructured ZnO thin films.* Nanotechnology, 2023. 34(15): p. 155702.

[18] Tkach, V.V., et al., *The theoretical description for methylene blue electrochemical determination and decolorization, assisted by polynaphthoquinones/Ti/TiO2/VO (OH) composite.* Applied Journal of Environmental Engineering Science, 2020. 6(1): p. 6-1 (2020) 14-21.

[19] Kellermann, A.L. and S.S. Jones, *What it will take to achieve the as-yet-unfulfilled promises of health information technology.* Health affairs, 2013. 32(1): p. 63-68.

[20] Yagub, M.T., T.K. Sen, and M. Ang, *Removal of cationic dye methylene blue (MB) from aqueous solution by ground raw and base modified pine cone powder.* Environmental earth sciences, 2014. 71: p. 1507-1519.

[21] Bharti, V., et al., *Biodegradation of methylene blue dye in a batch and continuous mode using biochar as packing media.* Environmental research, 2019. 171: p. 356-364.

[22] Al-Tohamy, R., et al., *A critical review on the treatment of dye-containing wastewater: Ecotoxicological and health concerns of textile dyes and possible remediation approaches for environmental safety.* Ecotoxicology and Environmental Safety, 2022. 231: p. 113160.

[23] Bal, G. and A. Thakur, *Distinct approaches of removal of dyes from wastewater: A review.* Materials Today: Proceedings, 2022. 50: p. 1575-1579.

[24] Moosavi, S., et al., *Application of efficient magnetic particles and activated carbon for dye removal from wastewater.* ACS omega, 2020. 5(33): p. 20684-20697.

[25] Miyah, Y., et al., *Adsorption of methylene blue dye from aqueous solutions onto walnut shells powder: equilibrium and kinetic studies.* Surfaces and Interfaces, 2018. 11: p. 74-81.

[26] Mohammed, M., Shitu, A. and Ibrahim, A. *Removal of methylene blue using low cost adsorbent*: a review. Res. J. Chem. Sci. ISSN, 2014, 2231: p.606X.

[27] Bhatia, D., et al., *Biological methods for textile dye removal from wastewater: A review.* Critical Reviews in Environmental Science and Technology, 2017. 47(19): p. 1836-1876.

[28] Zhang, Q., Fan, L., Wang, H., Han, H., Zhu, Z., Zhao, X. and Wang, Y. *A review of physical and chemical methods to improve the performance of water for dust reduction*. Process Safety and Environmental Protection. 2022. 166: p. 86-98.

[29] Mounes, H.A.M. and R.A. Abdelhay, *Comparison between traditional and low cost material to remove residues of Methylene Blue dye from aqueous solutions.* Egyptian Journal for Aquaculture, 2020. 10(4): p. 39-56.

[30] Badwal, S.P., Giddey, S.S., Munnings, C., Bhatt, A.I. and Hollenkamp, A.F. *Emerging electrochemical energy conversion and storage technologies*. Frontiers in chemistry, 2014. 2: p.79.

[31] Oturan, M.A., I. Sirés, and M. Zhou, *Electro-Fenton Process: new trends and scale-up*. 2018: Springer Singapore.

[32] Basak, S., et al., *The inhibition effect of ozonation in textile wastewater.* World Journal of Environmental Research, 2015. 5(1): p. 129-36.

[33] Jabbar, Z.H. and B.H. Graimed, *Recent developments in industrial organic degradation via semiconductor heterojunctions and the parameters affecting the photocatalytic process: A review study.* Journal of Water Process Engineering, 2022. 47: p. 102671.

[34] Al-Nuaim, M.A., A.A. Alwasiti, and Z.Y. Shnain, *The photocatalytic process in the treatment of polluted water.* Chemical Papers, 2023. 77(2): p. 677-701.

[35] Constantino, D.S., et al., *Intensification strategies for improving the performance of photocatalytic processes: A review.* Journal of Cleaner Production, 2022. 340: p. 130800.

[36] Jabbar, Z.H. and S.E. Ebrahim, *Recent advances in nano-semiconductors photocatalysis for degrading organic contaminants and microbial disinfection in wastewater: A comprehensive review.* Environmental Nanotechnology, Monitoring & Management, 2022. 17: p. 100666.

[37] Yuan, H., et al., *Dual-channels separated mechanism of photo-generated charges over semiconductor photocatalyst for hydrogen evolution: Interfacial charge transfer and transport dynamics insight.* Chemical Engineering Journal, 2023. 454: p. 140442.

[38] Wang, Y., Y. Ding, and Y. Yin, *Reliability of Wide Band Gap Power Electronic Semiconductor and Packaging: A Review.* Energies, 2022. 15(18): p. 6670.

[39] Poliakov, P., O. Tisov, and A. Kornienko, *Polymeres with enhanced energy capacity modified by semiconductor materials.* Funct. Mater, 2019. 26: p. 629-634.

[40] Balkan, N., et al., *Intrinsic and Extrinsic Semiconductors.* Semiconductors for Optoelectronics: Basics and Applications, 2021: p. 37-78.

[41] Elgohary, E.A., et al., *A review of the use of semiconductors as catalysts in the photocatalytic inactivation of microorganisms.* Catalysts, 2021. 11(12): p. 1498.

[42] Xin, Y., et al., *Continuous flow synthesis of porous materials.* Chinese Chemical Letters, 2020. 31(6): p. 1448-1461.

[43] Cambie, D., et al., *Applications of continuous-flow photochemistry in organic synthesis, material science, and water treatment.* Chemical reviews, 2016. 116(17): p. 10276-10341.

[44] Anindika, G.R., et al. *Alkali metal doped ZnO nanoclusters for methylene blue photodegradation: Computational studies*. in *AIP Conference Proceedings*. 2021. AIP Publishing.

[45] Hong, J., et al., *Recent advances in wastewater treatment using semiconductor photocatalysts.* Current Opinion in Green and Sustainable Chemistry, 2022. 36: p. 100644.

[46] Chanu, L.A., et al., *Effect of operational parameters on the photocatalytic degradation of Methylene blue dye solution using manganese doped ZnO nanoparticles.* Results in Physics, 2019. 12: p. 1230-1237.

[47] Sarkar, M., et al., *Zinc titanate nanomaterials—Photocatalytic studies and sensitization of hydantoin derivatized porphyrin dye.* Nano-Structures & Nano-Objects, 2020. 21: p. 100412.

[48] Akbari, A., et al., *Effect of nickel oxide nanoparticles as a photocatalyst in dyes degradation and evaluation of effective parameters in their removal from aqueous environments.* Inorganic Chemistry Communications, 2020. 115: p. 107867.

[49] Chen, T., J. Xie, and P. Gao, *Ultraviolet photocatalytic degradation of perovskite solar cells: Progress, challenges, and strategies.* Advanced Energy and Sustainability Research, 2022. 3(6): p. 2100218.

[50] Meisheng, H., H.-R. Wenk, and D. Sinitsyna, *Microstructures in natural perovskites.* American Mineralogist, 1992. 77(3-4): p. 359-373.

[51] Attfield, J.P., P. Lightfoot, and R.E. Morris, *Perovskites.* Dalton Transactions, 2015. 44 (23): p. 10541-10542.

[52] Petrović, M., Chellappan, V. and Ramakrishna, S. Perovskites: *solar cells & engineering applications–materials and device developments*. Solar Energy, 2015. 122: p. 678-699.

[53] Clabel H, J., J. Chacaliaza-Ricaldi, and E. Marega Jr, *Potential application of perovskite structure for water treatment: effects of band gap, band edges, and lifetime of charge carrier for photocatalysis.* Frontiers in Nanotechnology, 2022. 4: p. 827925.

[54] Tress, W., et al., *Understanding the rate-dependent J–V hysteresis, slow time component, and aging in CH 3 NH 3 PbI 3 perovskite solar cells: the role of a compensated electric field.* Energy & Environmental Science, 2015. 8(3): p. 995-1004.

[55] Kumar, A., A. Kumar, and V. Krishnan, *Perovskite oxide based materials for energy and environment-oriented photocatalysis.* Acs catalysis, 2020. 10(17): p. 10253-10315.

[56] Ernawati, L., et al., *Experimental data of CaTiO3 photocatalyst for degradation of organic pollutants (Brilliant green dye)–Green synthesis, characterization and kinetic study*. Data in brief, 2020. 32: p. 106099.

[57] Anitha, B. and L.G. Devi, *Study of reaction dynamics of photocatalytic degradation of 4-chlorophenol using SrTiO3, sulfur doped SrTiO3, silver metallized SrTiO3 and silver metallized sulfur doped SrTiO3 catalysts: Detailed analysis of kinetic results.* Surfaces and Interfaces, 2019. 16: p. 50-58.

[58] Khan, S.R., et al., *A versatile material: perovskite bismuth ferrite microparticles as a potential catalyst for enhancing fuel efficiency and degradation of various organic dyes.* Journal of Inorganic and Organometallic Polymers and Materials, 2020. 30: p. 3761-3770.

[59] Chang, S., Y. Sang, and H. Liu, *Efficient Photocatalytic Degradation of RhB by Constructing Sn3O4 Nanoflakes on Sulfur-Doped NaTaO3 Nanocubes.* Crystals, 2021. 11(1): p. 59.

[60] Nkwachukwu, O.V. and O.A. Arotiba, *Perovskite oxide–based materials for photocatalytic and photoelectrocatalytic treatment of water.* Frontiers in Chemistry, 2021. 9: p. 634630.

[61] Vickers, N.J., *Animal communication: when i'm calling you, will you answer too?* Current biology, 2017. 27(14): p. R713-R715.

[62] Taguchi, H., et al., *CO oxidation on perovskite-type LaCoO3 synthesized using ethylene glycol and citric acid.* Catalysis Communications, 2008. 9(9): p. 1913-1915.

[63] Navas, D., et al., *Review on Sol-Gel Synthesis of Perovskite and Oxide Nanomaterials. Gels 2021, 7, 275*. 2021, s Note: MDPI stays neu-tral with regard to jurisdictional claims in ….

[64] Acharya, T. and R. Choudhary, *Studies of structural, dielectric, and electrical characteristics of 0.5 (BiMn1/2Ti1/2O3)–0.5 PbTiO3 electronic system.* Journal of Materials Science: Materials in Electronics, 2020. 31(13): p. 9997-10005.

[65] Nakhowong, R., *Fabrication and characterization of MnTiO3 nanofibers by sol–gel assisted electrospinning.* Materials Letters, 2015. 161: p. 468-470.

[66] Sharma, A., et al., *Study of electrochemical sensor and energy storage properties of MnTiO3 nano-perovskite.* Energy Storage, 2023. 5(1): p. e385.

[67] Alkaykh, S., A. Mbarek, and E.E. Ali-Shattle, *Photocatalytic degradation of methylene blue dye in aqueous solution by MnTiO3 nanoparticles under sunlight irradiation.* Heliyon, 2020. 6(4).

[68] Zhang, H., et al., *Design and Modification of Perovskite Materials for Photocatalysis Performance Improvement.* Journal of Environmental Chemical Engineering, 2022: p. 109056.

[69] Lee, J.-C., et al., *Manganese and graphene included titanium dioxide composite nanowires: Fabrication, characterization and enhanced photocatalytic activities.* Nanomaterials, 2020. 10(3): p. 456.

[70] Kitchamsetti, N., et al., *Photocatalytic activity of MnTiO3 perovskite nanodiscs for the removal of organic pollutants.* Heliyon, 2021. 7(6).

[71] Gabal, M. and Y. Al Angari, *Zinc titanates nanopowders: Synthesis and characterization.* Materials Research Express, 2022. 9(2): p. 025010.

[72] Abdul Haroon Rashid, S.S.A., et al., *Zinc titanate nanoarrays with superior optoelectrochemical properties for chemical sensing.* ACS Applied Materials & Interfaces, 2019. 11(32): p. 29255-29267.

[73] Naidu, K., et al., *Phase formation and electrical properties of zinc titanate ceramics.* Adv Mater, 2018. 2: p. 37-48.

[74] Chen, W., et al., *High performance Na-doped lithium zinc titanate as anode material for Li-ion batteries.* RSC Advances, 2015. 5(62): p. 49890-49898.

[75] Chen, W.-Y., et al., *Perovskite zinc titanate photocatalysts synthesized by the sol–gel method and their application in the photocatalytic degradation of emerging contaminants.* Catalysts, 2021. 11(7): p. 854.

[76] Salavati-Niasari, M., et al., *Synthesis, characterization, and morphological control of ZnTiO3 nanoparticles through sol-gel processes and its photocatalyst application.* Advanced Powder Technology, 2016. 27(5): p. 2066-2075.

[77] Xin, Y., et al., *Synthesis and characterization of ZnTiO3 with high photocatalytic activity.* Transactions of Nonferrous Metals Society of China, 2015. 25(7): p. 2272-2278.

[78] Olaleru, A., et al., *Hybrid Perovskite Thin Film.* Thin Films Photovoltaics, 2022: p. 85.

[79] Park, N.-G., *Perovskite solar cells: an emerging photovoltaic technology.* Materials today, 2015. 18(2): p. 65-72.

[80] Lin, K., et al., *Perovskite light-emitting diodes with external quantum efficiency exceeding 20 per cent.* Nature, 2018. 562(7726): p. 245-248.

[81] Liang, C., et al., *High-performance flexible perovskite photodetectors based on single-crystal-like two-dimensional Ruddlesden–Popper thin films.* Carbon Energy, 2023. 5(2): p. e251.

[82] Wu, Y., et al., *Halide Perovskite: A Promising Candidate for Next-Generation X-Ray Detectors.* Advanced Science, 2023. 10(1): p. 2205536.

[83] Schanze, K.S., et al., *Progress in perovskite photocatalysis*. 2020, ACS Publications.

[84] Wang, M. and C.J. Carmalt, *Film Fabrication of Perovskites and Their Derivatives for Photovoltaic Applications via Chemical Vapor Deposition.* ACS Applied Energy Materials, 2021. 5(5): p. 5434-5448.

[85] Berni, A., M. Mennig, and H. Schmidt, *Doctor blade*. 2004: Springer.

[86] Frederichi, D., M.H.N.O. Scaliante, and R. Bergamasco, *Structured photocatalytic systems: photocatalytic coatings on low-cost structures for treatment of water contaminated with micropollutants—a short review.* Environmental Science and Pollution Research, 2021. 28: p. 23610-23633.

[87] Vishwas, M., et al., *Sol–gel synthesis and optical characterization of nano-crystalline ZnTiO 3 thin films.* Journal of Optics, 2012. 41: p. 60-64.

[88] Martin, E. and M.-A. Sahiner. *Synthesis and Analysis of MnTiO 3 Thin Films on ITO Coated Glass Substrates*. in *APS March Meeting Abstracts*. 2016.

[89] Rheima, A.M., et al., *Synthesis and structural characterization of ZnTiO3 nanoparticles via modification sol-gel prosses for assessment of their antimicrobial activity.* International journal of pharmaceutical research, 2021. 13(1): p. 342-347.

[90] Zyoud, A., et al., *Solid olive waste in environmental cleanup: enhanced nitrite ion removal by ZnCl2-activated carbon.* Journal of environmental management, 2015. 152: p. 27-35.

[91] Nassar, H.N.I., *Nitrate and nitrite ion removal from aqueous solutions by activated carbon prepared from olive stones*. 2012.

[92] Khudhair, A.R., S.T.H. Sherazi, and M.N. Al-Baiati. *Adsorption of methylene blue from aqueous solutions by using a novel nano co-polymer*. in *AIP Conference Proceedings*. 2020. AIP Publishing.

[93] Kadam, A., et al., *Morphological evolution of Cu doped ZnO for enhancement of photocatalytic activity.* Journal of Alloys and Compounds, 2017. 710: p. 102-113.

[94] Tang, M., et al., *Preparation, Characterization of ZnTiO3/ZnO Composite Materials and Their Photocatalytic Performance.* Nanomaterials, 2022. 12(8): p. 1345.

[95] Arin, J., et al., *Characterization of ZnO–TiO 2 and zinc titanate nanoparticles synthesized by hydrothermal process.* Research on Chemical Intermediates, 2017. 43: p. 3183-3195.

[96] Enhessari, M., et al., *Synthesis, characterisation and optical properties of MnTiO3 nanopowders.* Journal of Experimental Nanoscience, 2012. 7(3): p. 327-335.

[97] Gao, Z. and X. Qu, *Construction of ZnTiO 3/Bi 4 NbO 8 Cl heterojunction with enhanced photocatalytic performance.* Nanoscale Research Letters, 2020. 15: p. 1-9.

[98] Acosta-Silva, Y., et al., *Analysis of the photocatalytic activity of CdS+ ZnTiO3 nanocomposite films prepared by sputtering process.* Superlattices and Microstructures, 2016. 100: p. 148-157.

[99] Koop-Santa, C., et al., *Physicochemical properties of MnTiO3 powders obtained by molten salt method.* Ceramics International, 2021. 47(23): p. 33315-33321.

[100] Alwany, A.B., et al., *Annealing temperature effects on the size and band gap of ZnS quantum dots fabricated by co-precipitation technique without capping agent.* Scientific Reports, 2023. 13(1): p. 10314.

[101] Wang, C.-L., et al., *Formation and morphology of Zn2Ti3O8 powders using hydrothermal process without dispersant agent or mineralizer.* International journal of molecular sciences, 2011. 12(2): p. 935-945.

[102] John, A.K., S. Palaty, and S.S. Sharma, *Greener approach towards the synthesis of titanium dioxide nanostructures with exposed {001} facets for enhanced visible light photodegradation of organic pollutants.* Journal of Materials Science: Materials in Electronics, 2020. 31: p. 20868-20882.

[103] Uddin, M.T., Rahman, M.A., Rukanuzzaman, M. and Islam, M.A. *A potential low cost adsorbent for the removal of cationic dyes from aqueous solutions*. Applied Water Science, 2017. *7*: p.2831-2842.

[104] Bae, K.-N., et al., *Effect of MnTiO3 surface treatment on the performance of dye-sensitized solar cells.* Materials Letters, 2013. 96: p. 67-70.

[105] Jaramillo-Fierro, X., et al., *Faujasite-Type Zeolite Obtained from Ecuadorian Clay as a Support of ZnTiO3/TiO2 NPs for Cyanide Removal in Aqueous Solutions.* International Journal of Molecular Sciences, 2023. 24(11): p. 9281.

[106] Zyoud, A., et al., *Photocatalytic degradation of aqueous methylene blue using ca-alginate supported ZnO nanoparticles: point of zero charge role in adsorption and photodegradation.* Environmental Science and Pollution Research, 2023: p. 1-15.

[107] Musiba, M.M. and M.J. Rwiza, *Isotopic and hydrogeochemical characterization of groundwater and surface water from a mine site in Tanzania.* H2Open Journal, 2021. 4(1): p. 366-380.

[108] Jaramillo Fierro, X.V., *Synthesis, characterization and theoretical calculations of ZnTiO3 for the adsorption and photocatalytic removal of Methylene Blue dye.*

[109] Mardiroosi, A., et al., *Effects of functionalized magnetic graphene oxide on the visible-light-induced photocatalytic activity of perovskite-type MTiO3 (M= Zn and Mn) for the degradation of Rhodamine B.* Journal of Molecular Structure, 2023. 1284: p. 135298.

Appendices

Appendix A

Figures of Study

Figure A.1

(a): the structure of methylene blue, (b): model of methylene blue, (c): Different resonance structures of MB

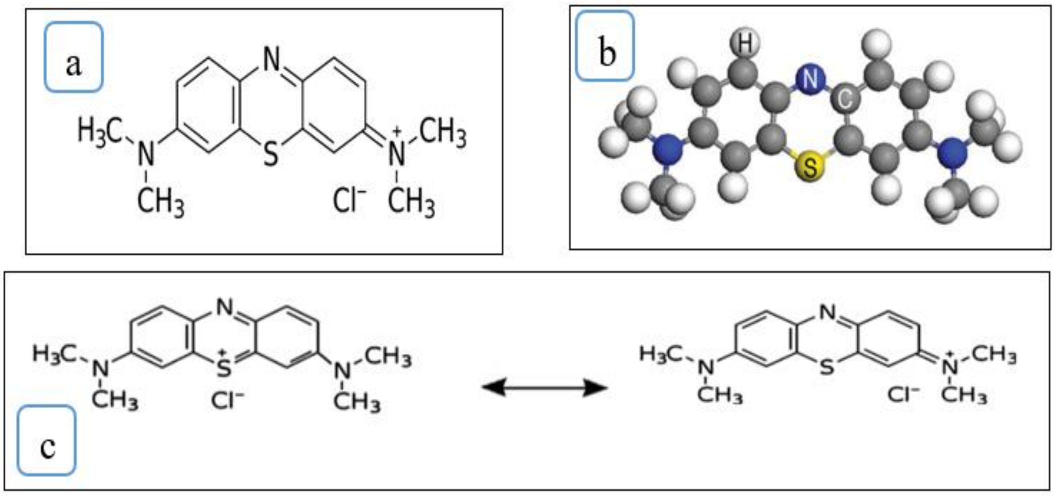

Figure A.2

Mechanisms for producing charged carriers in semiconductors

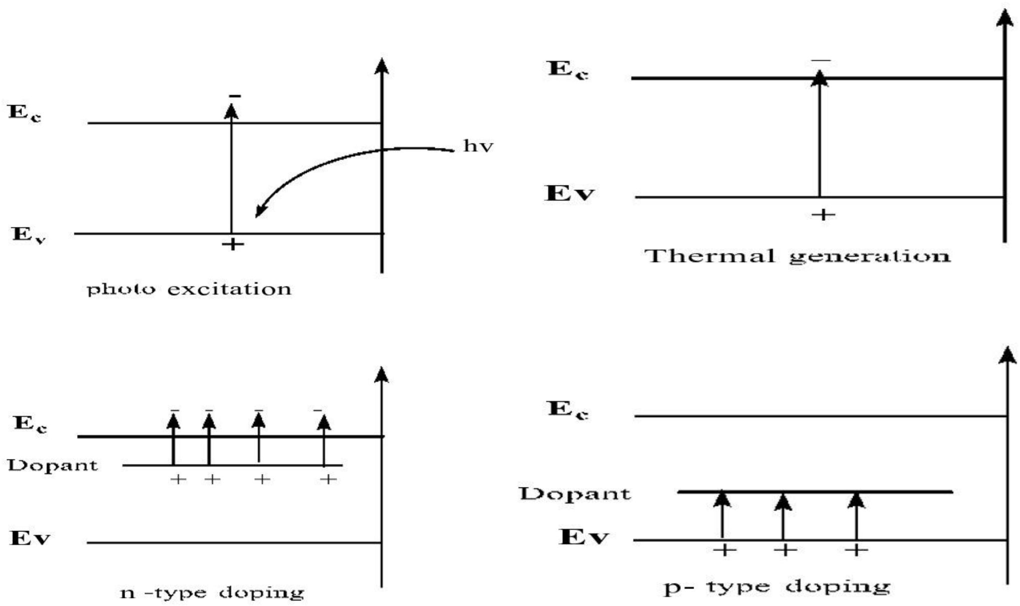

Figure A.3

Mechanism of photocatalysis

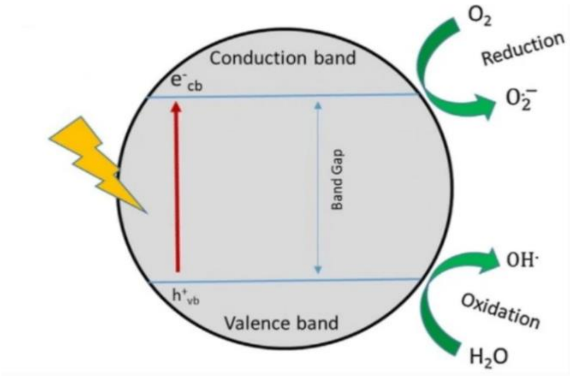

Figure A.4

ABO_3 type perovskite crystal structure

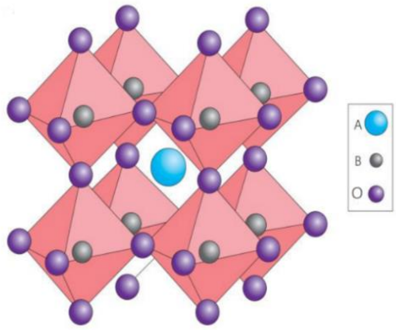

Figure A.5

Mechanism of Doctor Blade method

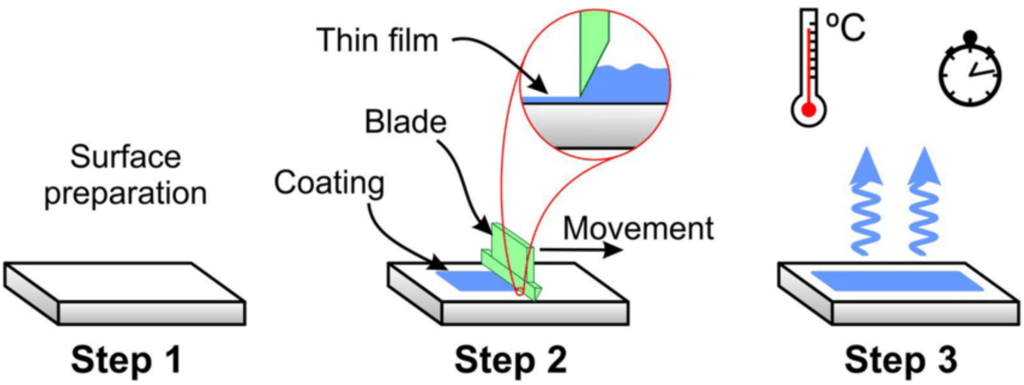

Figure A.6

Emission spectra for a) halogen lamp, b) solar radiation

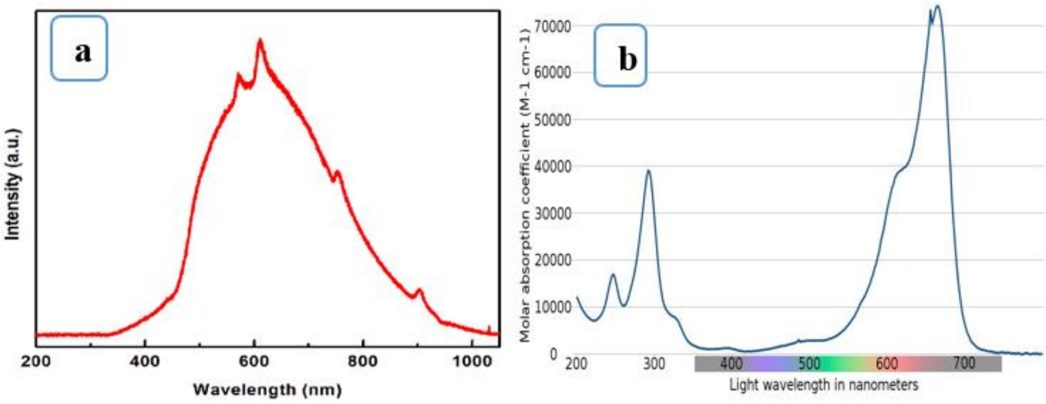

Figure A.7

Photo-catalytic experiments system apparatus arrangement using catalyst film

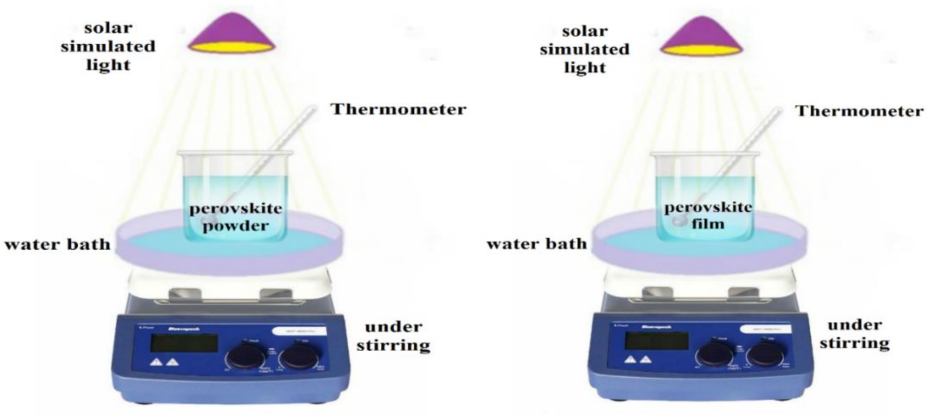

Figure A.8

Continuous flow system apparatus arrangement

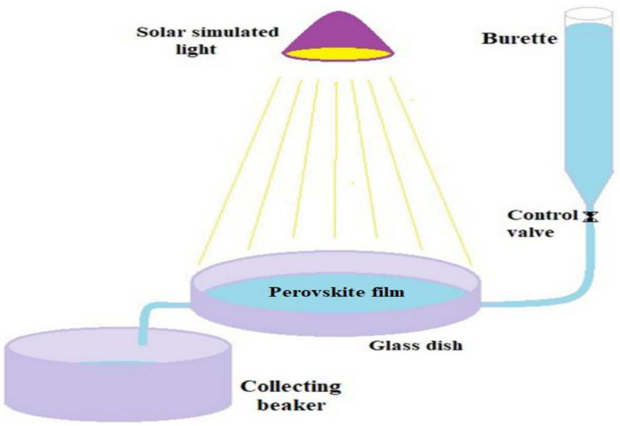

Figure A.9

UV-visible spectrum for methylene blue in water, at 25 ℃ and pH 7

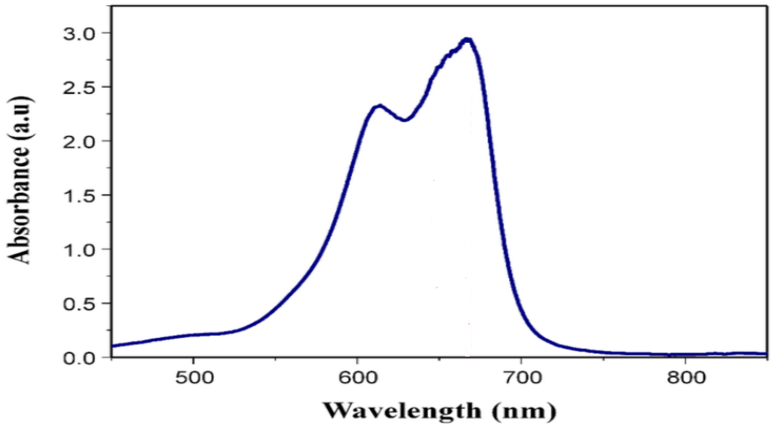

Figure A.10

A calibration curve showing a plot of electronic absorbance vs. Methylene blue concentration (ppm) in water, at room temperature. The maximum wavelength was 664 nm

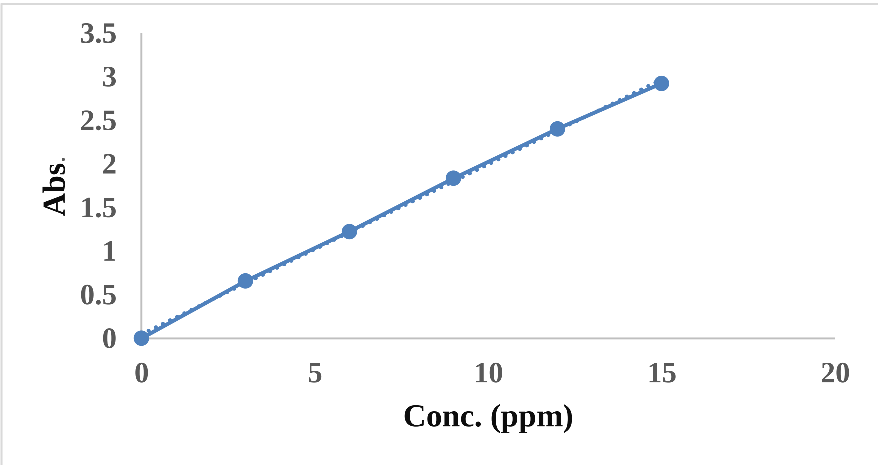

Figure A.11

Effect of contaminant concentration on photodegradation of methylene blue using zinc titanate powder under direct light at 25 ℃ and pH 7

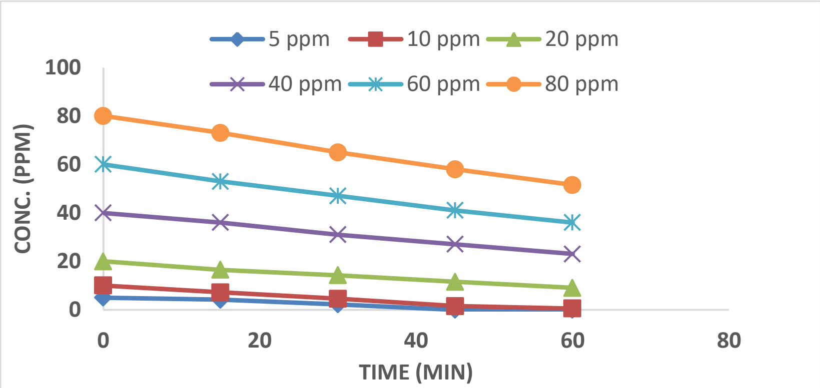

Figure A.12

Photodegradation kinetics of zinc titanate powder at different concentration of methylene blue

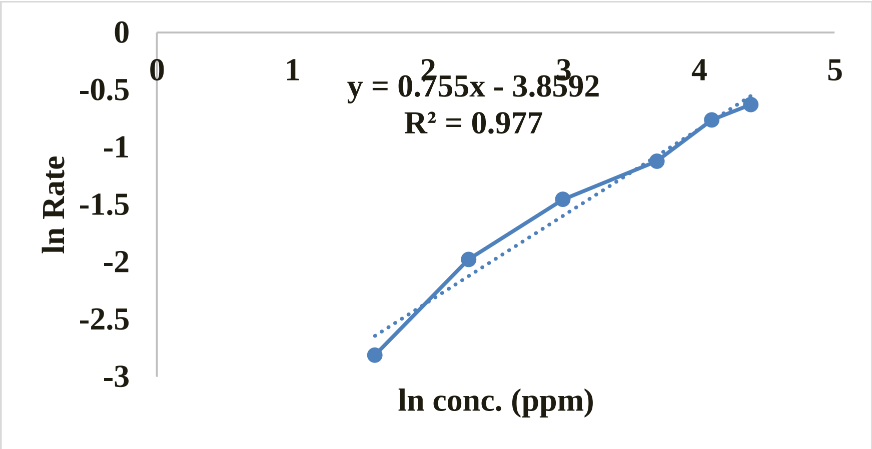

Figure A.13

Effect of concentration of zinc titanate on photodegradation of methylene blue under direct light at 25 ℃ and pH 7

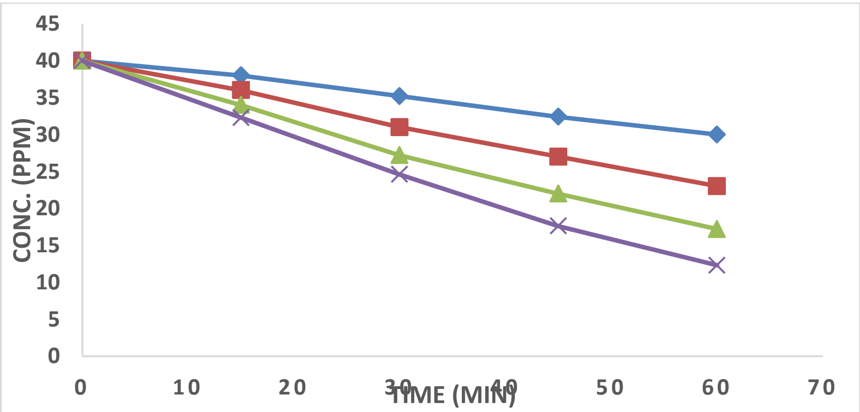

Figure A.14

Photodegradation kinetics at different amounts of zinc titanate powder

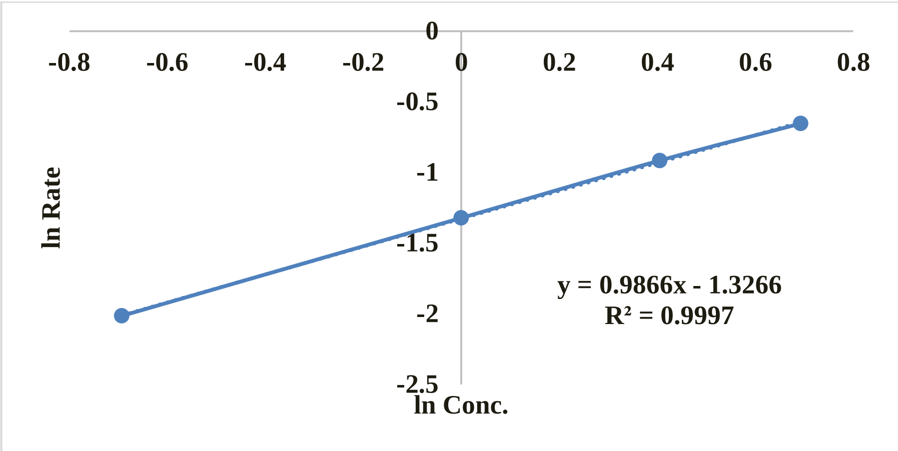

Figure A.15

Effect of pH of methylene blue degradation under direct light using zinc titanate powder

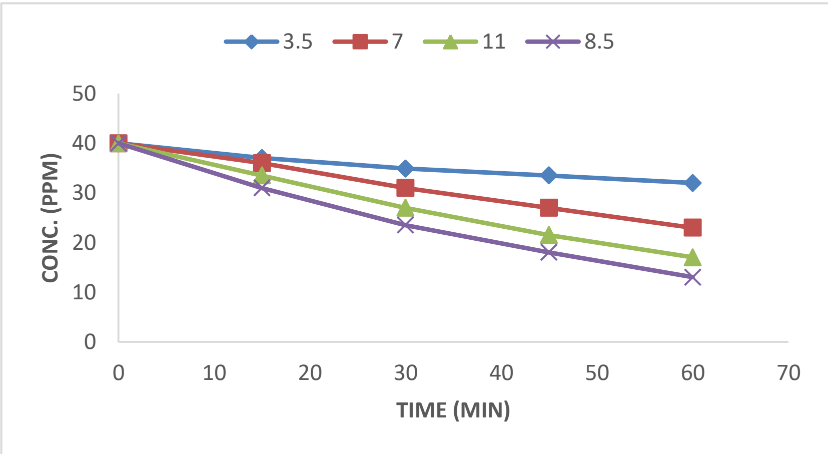

Figure A.16

Effect of contaminant concentration on photodegradation of methylene blue using zinc titanate films under direct light at 25 °C and pH 7

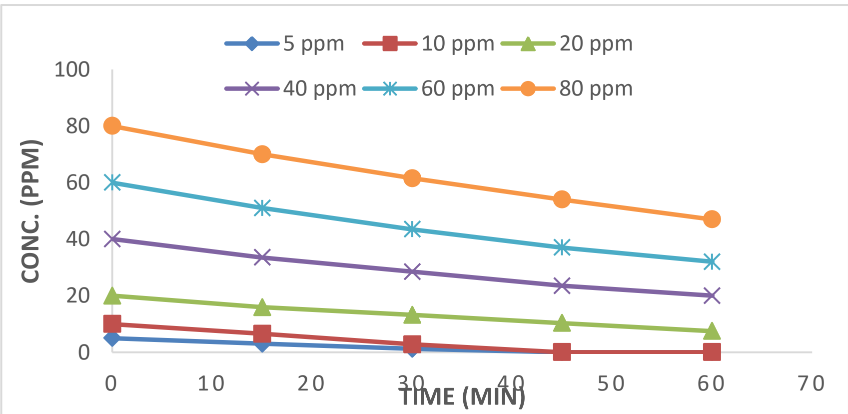

Figure A.17

Photodegradation kinetics of zinc titanate film at different concentration of methylene blue

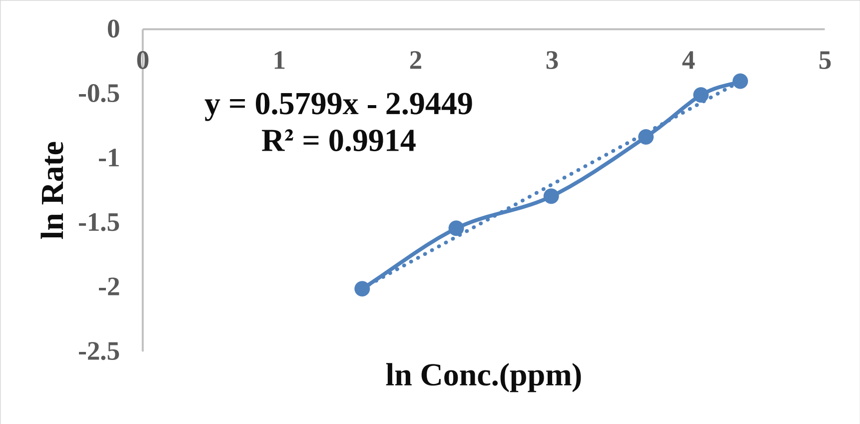

Figure A.18

Effect of concentration of zinc titanate film on photodegradation of methylene blue under direct light at 25 °C and pH 7

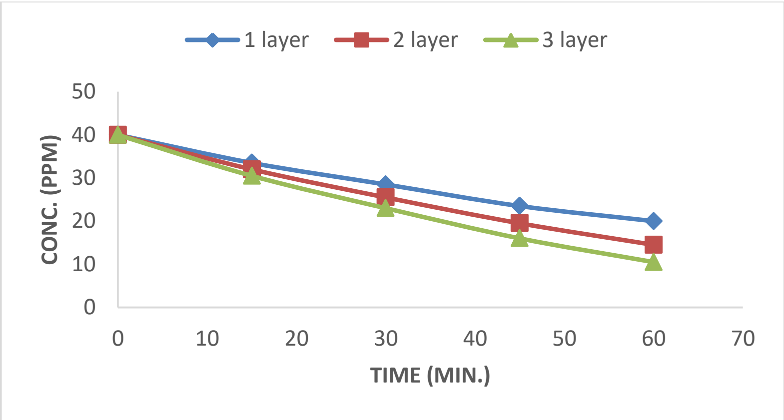

Figure A.19

Effect of pH on methylene blue degradation using zinc titanate film under solar simulated light

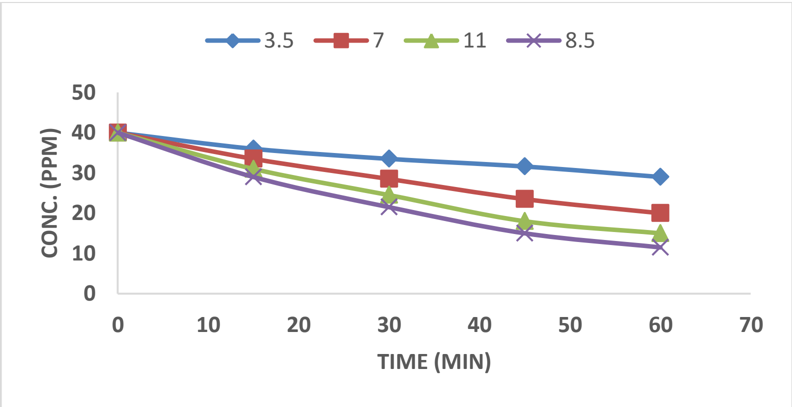

Figure A.20

Comparison between zinc titanate powder and film were compared as catalysts for photodegradation of methylene blue at 40 ppm under solar simulated light at 25 ℃ and pH 7

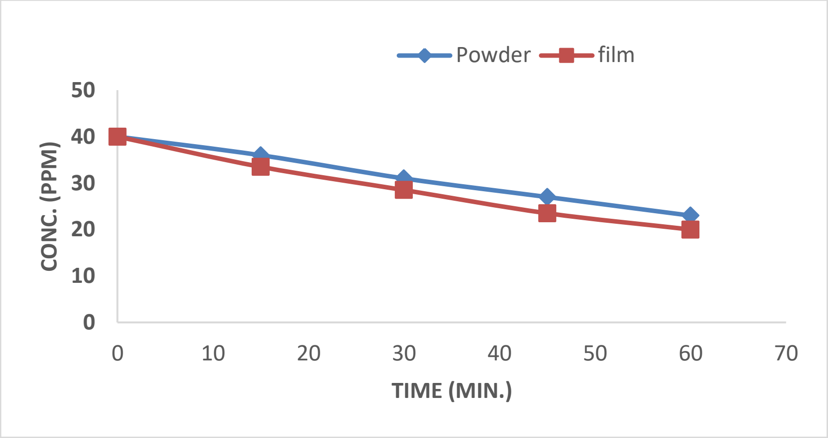

Figure A.21

Effect of contaminant concentration on photodegradation of methylene blue using manganese titanate powder under solar simulated light and neutral conditions at 25 ℃ and pH 7

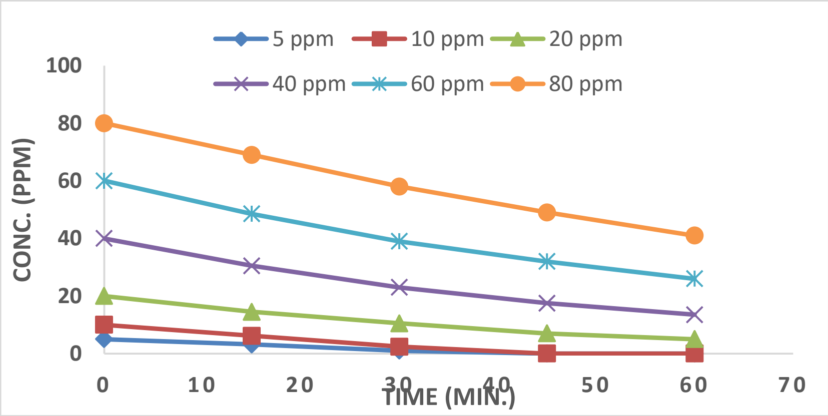

Figure A.22

Photodegradation kinetics of manganese titanate powder catlyst at different amount of methylene blue

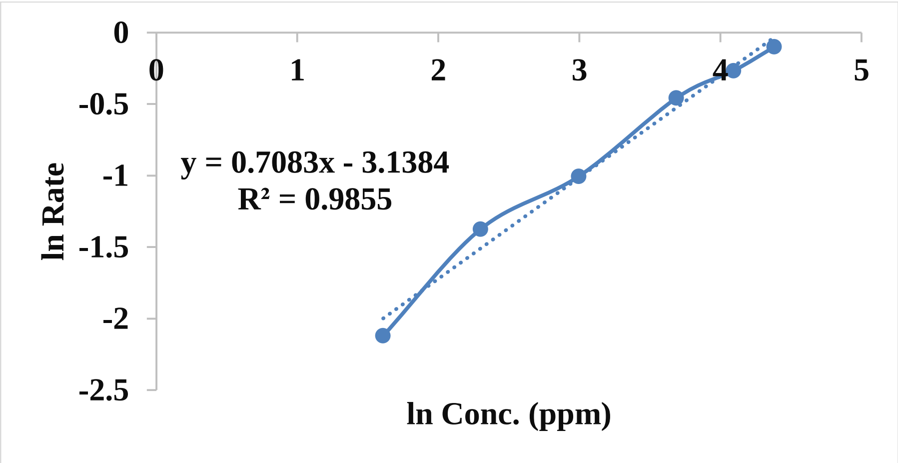

Figure A.23

Effect of loading of manganese titanate on photodegradation of methylene blue under solar simulated light at 25 °C and pH 7

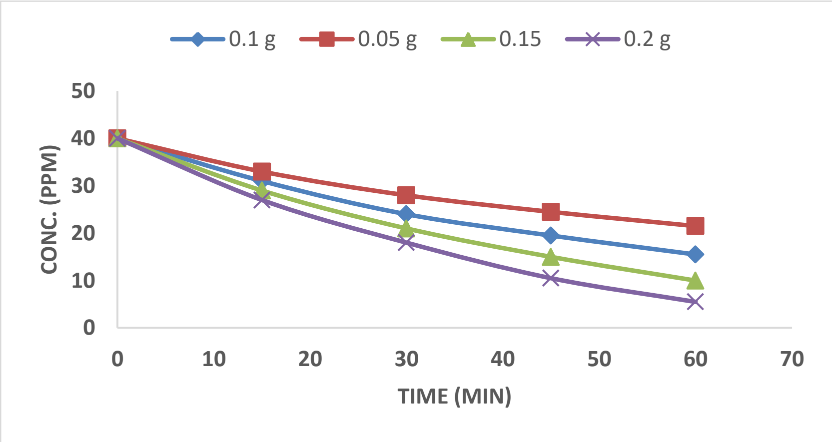

Figure A.24

Photodegradation kinetics at different amount of manganese titanate powder

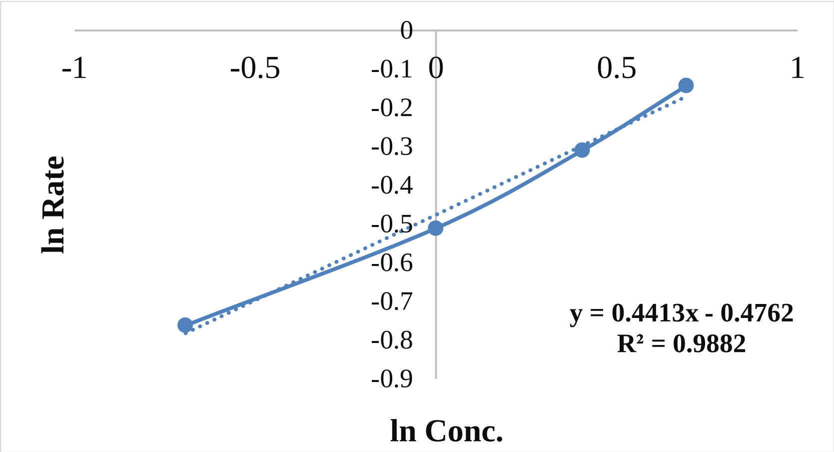

Figure A.25

Effect of pH of methylene blue degradation under solar simulated light using manganese titanate powder

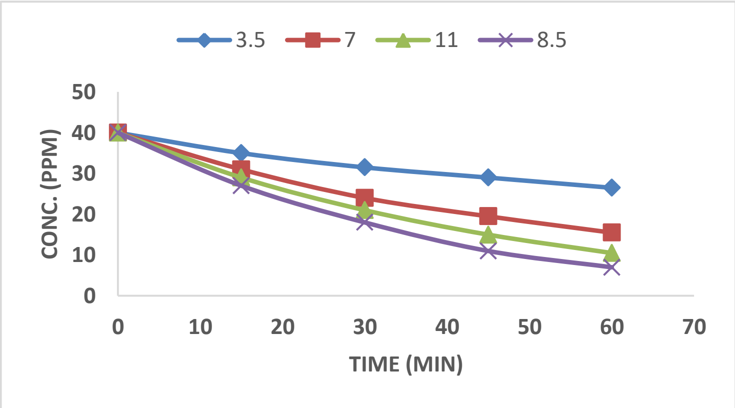

Figure A.26

Effect of contaminant concentration on photodegradation of methylene blue using Manganese titanate films under direct light at 25 ℃ and pH 7

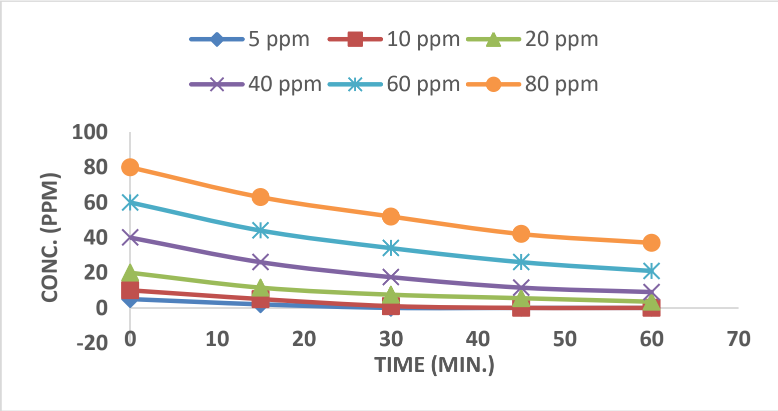

Figure A.27

Photodegradation kinetics of manganese titanate film at different concentration of methylene blue

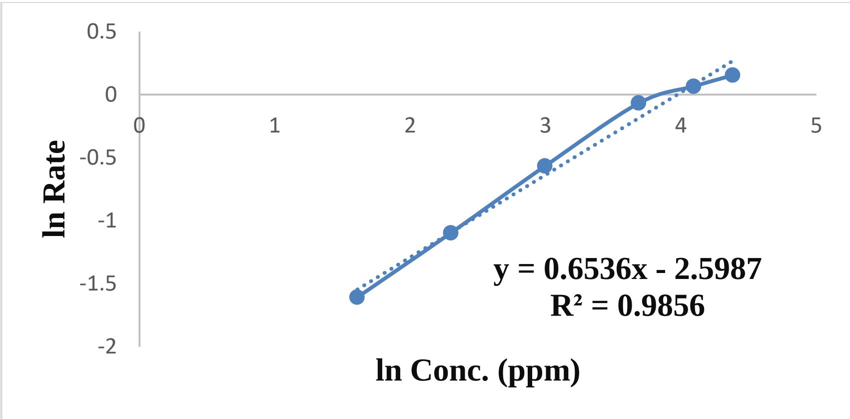

Figure A.28

Effect of layers of manganese titanate film on photodegradation of methylene blue under direct light at 25 ℃ and pH 7

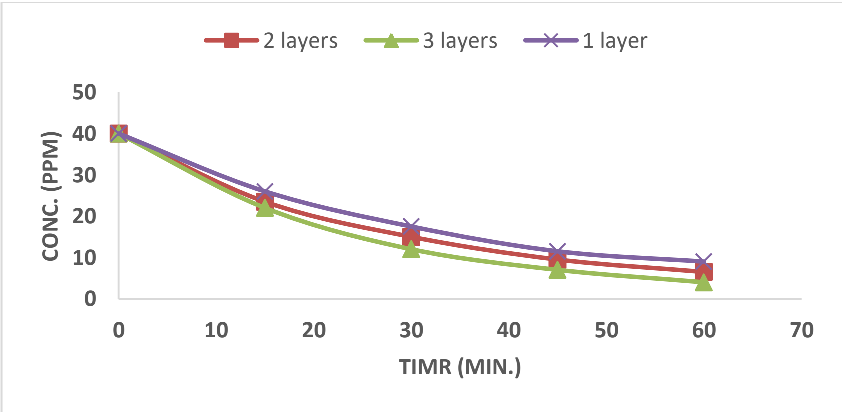

Figure A.29

Effect of pH of methylene blue degradation using manganese titanate film under direct light

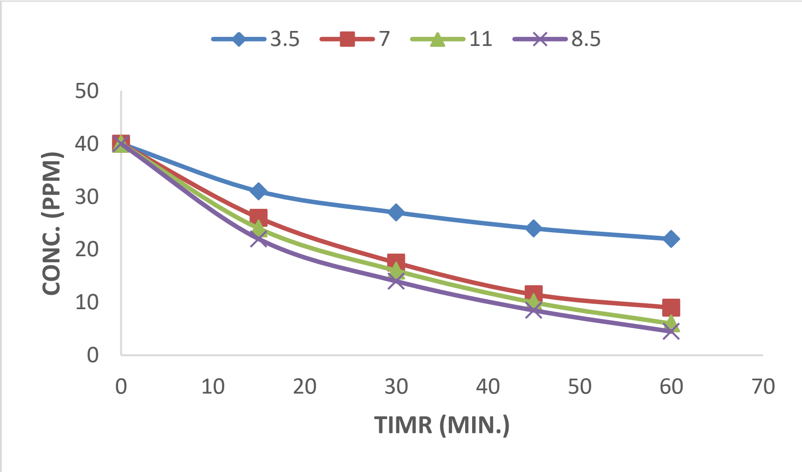

Figure A.30

Manganese titanate powder and film were compared as catalysts for photodegradation of methylene blue at 40 ppm under direct light at 25 ℃ and pH 7

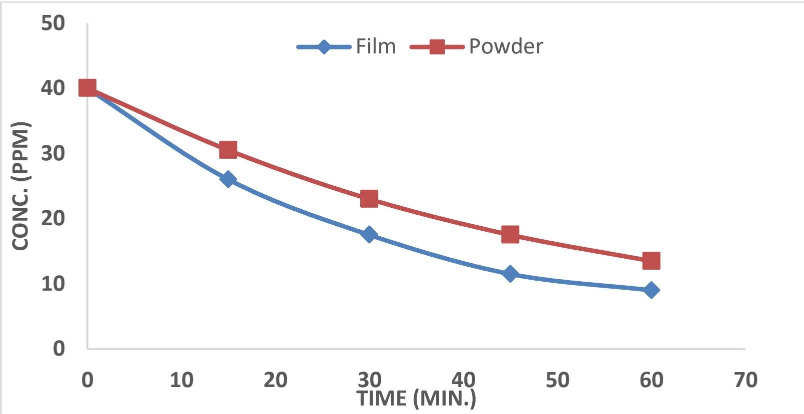

Figure A.31

Photodegradation of perovskite powders and film for longer hours at pH 8.5

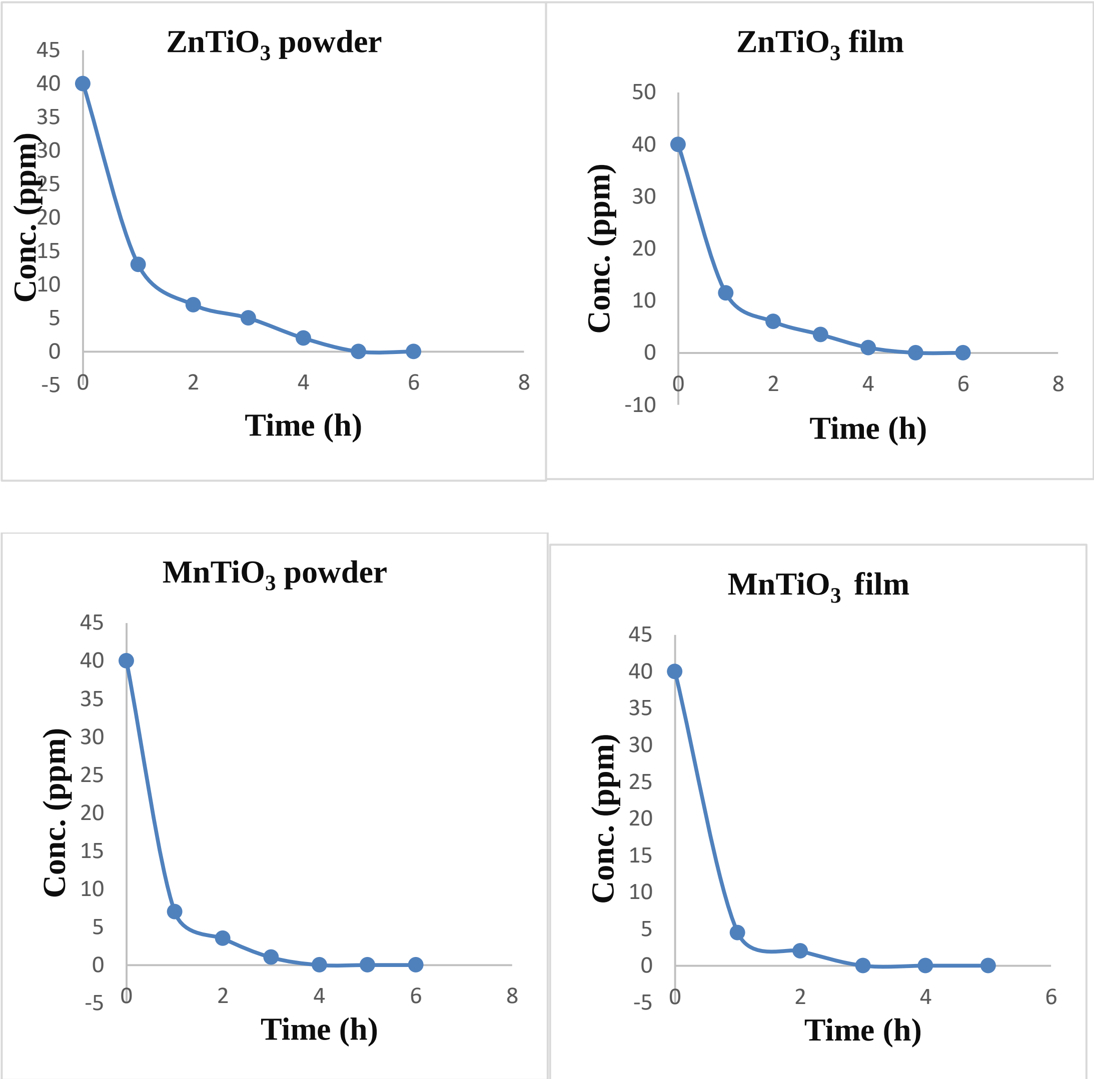

Figure A.32

Methylene blue structural changes with solution pH value. Reproduced based on literature

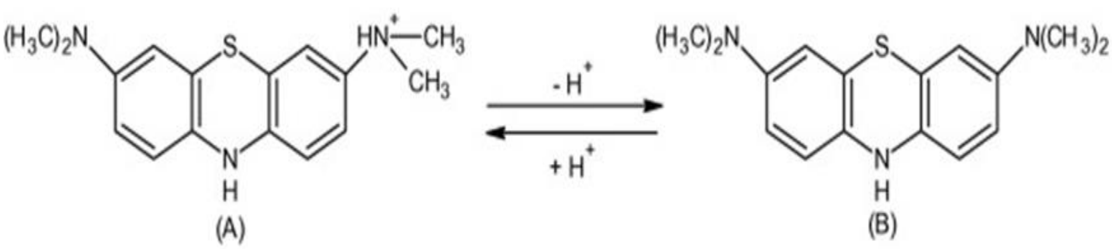

Appendix B

Tables of Study

Table B.1

Effect of perovskite concentration on values of the amount consumed, % degradation, turnover number, turnover frequency and quantum yield for methylene blue degradation after 60 minutes, using manganese titanate film under direct light

Contaminant (ppm)	Degradation %	Amount consumed	T.N	T.F	Q.Y
		(ppm)	$*10^{-3}$	$*10^{-5}$	$*10^{-25}$
5	100	5	0.4	0.7	4.6
10	100	10	0.9	1.5	9.3
20	82.5	16.5	1.4	2.4	15.3
40	77.5	31	2.7	4.5	28.8
60	65	39	3.4	5.6	36.2
80	53.8	43	3.7	6.2	40.0

Table B.2

Effect of perovskite layers on values of amount consumed, % degradation, turnover number, turnover frequency and quantum yield for methylene blue degradation after 60 minutes, using manganese titanate film under simulated light

Catalyst weight	Degradation %	Amount consumed	T.N	T.F	Q.Y
(g)		(ppm)	$*10^{-3}$	$*10^{-5}$	$*10^{-25}$
1 layer	77.5	31	2.7	4.5	28.8
2 layers	83.8	33.5	5.8	9.7	62.2
3 layers	90	36	9.4	15.6	100.2

Table B.3

Effect of pH on values of amount consumed, turnover number, turnover frequency, % degradation and quantum yield for manganese titanate degradation after 60 minutes under direct light using one layer of manganese titanate film

pH	Degradation %	Amount consumed	T.N	T.F	Q.Y
		(ppm)	$*10^{3}$	$*10^{5}$	$*10^{25}$
11	85	34	2.9	4.9	31.6
8.5	75	35.5	3.0	5.1	33.0
7	77.5	31	2.7	4.5	28.8
3.5	45	18	1.6	2.6	16.7

Table B.4

Time needed to end the photodegradation and amount of nitrate ion (ppm)

Perovskite	Time needed for complete photodegradation (h)	Result nitrate ion (ppm)
Zinc titanate powder	5	3.32
Zinc titanate film	4.5	3.4
Manganese titanate powder	3.5	4.34
Manganese titanate film	3	4.5

Appendix C

Certificate of acceptance of the research extracted from the dissertation

Research title: Perovskite Nano-Powder and Nano-Film Catalysts in Mineralization of Aqueous Organic Contaminants through Solar Simulated Radiation

processes

an Open Access Journal by MDPI

CITESCORE 4.7

IMPACT FACTOR 3.5

CERTIFICATE OF PUBLICATION

FEATURE PAPERS

Certificate of publication for the article titled:

Perovskite Nano-Powder and Nano-Film Catalysts in Mineralization of Aqueous Organic Contaminants through Solar Simulated Radiation

Authored by:

Tamara Zorba; Heba Nassar; Muath H. S. Helal; Jeheon Song; Tae Woo Kim; Shehdeh Jodeh; Hikmat S. Hilal

Published in:

Processes **2023**, Volume 11, Issue 8, 2378

MDPI Academic Open Access Publishing since 1996

Basel, November 2023

جــامعـــة النجاح الوطنية

كليـــة الدراســـــات العليـــا

الكترود فلم من مادة البيروفسكايت لتنقية المياه باستخدام الطاقة الشمسية

إعداد

تمارا باسم قاسم زوربا

إشراف

أ. د. حكمت هلال

أ. د. شحدة جودة

قدمت هذه الأطروحة استكمالا لمتطلبات الحصول على درجة الدكتوراه في الكيمياء، من كلية الدراسات العليا، في جامعة النجاح الوطنية، نابلس– فلسطين.

2023

الكترود فلم من مادة البيروفسكايت لتنقية المياه باستخدام الطاقة الشمسية

إعداد

تمارا باسم قاسم زوربا

إشراف

أ. د. حكمت هلال

أ. د. شحدة جودة

الملخص

يعد تلوث المياه أحد المخاطر الصحية العالمية على صحة الناس بما في ذلك الملوثات العضوية. وقد أصبح استصلاح المياه ضروريًا باستخدام طرق آمنة وعملية وبأسعار معقولة، بطرق مختلفة مثل طريقة التحفيز الضوئي. ومن أجل تحقيق هذه الغاية، فقد تم هنا تحضير اثنين من مركبات البيروفسكايت، هما تيتانات المنغنيز ($MnTiO_3$) وتيتانات الزنك ($ZnTiO_3$) كمساحيق نانوية الحجم، ثم تم صنع أفلام رقيقة من كل من المركبين. وتم تشخيص هذه المساحيق بطرق مختلفة منها أشعة اكس، مطيافية الامتصاص الضوئي، مطيافية الانبعاث الضوئي، دراسة السطح وتحليل العناصر، وبعد ذلك تم استخدام المركبين كمحفزات في التحطيم الضوئي الكامل لأزرق ميثيلين (كملوث مشهور) في الماء تحت إشعاعات محاكاة الطاقة الشمسية. ثم تم دراسة تأثير ظروف التفاعل المختلفة على عملية التحلل الضوئي للملوث. ومن أجل حل المشكلة الفنية المتعلقة بصعوبة فصل الحفاز النانوي من الماء بعد معالجته، تم تثبيته كأفلام على سطوح الزجاج. وقد تم دراسة مقارنة كفاءة كل من مادتي البيروفسكايت في شكليها المسحوق والافلام في التفاعلات محصورة الحجم، وتبين أنه في كل من المادتين كان الفيلم له كفاءة أعلى من المسحوق. كما تم استخدام أفلام الحفازين في تفاعلات التدفق المستمر لتنقية الماء وأثبت كل من المادتين كفاءة حفزية عالية. أظهرت النتائج أن المادة الملوثة تم التخلص منها بالكامل في أقل من ست ساعات باستخدام كل من المحفزات المسحوقة والأفلام. كما أظهر $MnTiO_3$ فعالية حفزية أكبر من $ZnTiO_3$

في شكلي المسحوق والفيلم. ولم تختلف طريقة تفاعلات التدفق المستمر في سرعتها عن التفاعلات في الدفعة الواحدة. واعتمادا على النتائج، يمكن معالجة المياه الملوثة بتراكيز مختلفة من أزرق الميثيلين بالمحفزين المذكورين باستخدام الاشعة الشمسية وبالتحديد الجزء الواقع في فوق البنفسجي. كما يمكن استرجاع أفلام الحفازين واعادة استخدامهما دون أي صعوبات فنية أو نقصان بالكفاءة. وتؤكد النتائج إمكانية استخدام محفزات البيروفسكايت في تنقية المياه على نطاق واسع في المستقبل.

الكلمات المفتاحية: تيتانات الزنك، تيتانات المنغنيز، التحلل الضوئي لأزرق الميثيلين، محاكاة الإشعاع الشمسي.